

Dynamic Modeling and Control of a Hybrid Hydronic Heating System

YiTeng, Ma

A thesis in
Department of Building, Civil and Environmental Engineering

Presented in Partial Fulfillment of the Requirements
For the Degree of Master of Applied Science (Building Engineering) at
Concordia University
Montreal, Quebec, Canada

© YiTeng Ma, 2013

CONCORDIA UNIVERSITY

School of Graduate Studies

This is to certify that the thesis prepared by

By: Yi Teng Ma

Entitled: **Dynamic Modeling and Control of a Hybrid Hydronic Heating System**

and submitted in partial fulfillment of the requirements for the degree of

Master of Applied Science (Building Engineering)

complies with the regulations of the University and meets the accepted standards with respect to originality and quality.

Signed by the final examining committee:

_____ Chair
Dr.S.Li

_____ Supervisor
Dr.M.Zaheeruddin

_____ Examiner External (to program)
Dr.M.Y.Chen

_____ Examiner
Dr.S.Li

_____ Examiner
Dr.L.Wang

Approved by _____

Dr. M. Elektorowicz, GPD
Department of Building, Civil and Environmental Engineering

Dr. C. W. Trueman, Interim Dean
Faculty of Engineering and Computer Science

Date _____

ABSTRACT

Dynamic Modeling and Control of a Hybrid Hydronic Heating System

Yiteng Ma

A dynamic model of a hybrid hydronic heating system has been developed. Simulations of the control strategies and the model-based energy analysis for the overall system have been presented in this thesis. The hybrid hydronic system is composed of a conventional natural gas fired boiler hot water heating and a ground source heat pump system. The overall system consists of several components such as a boiler, a heat exchanger, a ground loop heat pump, a ground loop heat exchanger, baseboard heaters, and radiant floor hydraulic piping systems. The system model was described by nonlinear differential equations, which were programmed and solved using MATLAB.

Two control strategies for improving the overall system performance were explored: (i) a conventional PI control, and (ii) an adaptive gain control. The simulation results subject to set-point changes showed that the performance of the adaptive controller is better than the fixed gain PI controller in disturbance rejection and stability.

Energy simulations under three different operating strategies were conducted: (i) a conventional fixed set-point PI control, (ii) an outdoor air temperature reset control, and (iii) an optimal set-point PI control. It was shown that the outdoor temperature reset strategy can save 4.5% and 19.9% energy under cold day and mild day conditions compared to the conventional fixed set-point PI control strategy. In addition, the

implementation of the optimal PI control strategy result in higher energy savings 6.6% and 22% as compared to the base case under cold and mild day conditions, respectively.

ACKNOWLEDGEMENTS

I would like to express my sincere gratitude to Dr. M. Zaheer-Uddin for his invaluable and constant guidance, help, encouragement, sustained interest, and financial support throughout the whole span of this thesis.

My thanks are also to my colleagues, Lianzhong Li, Min Ning and Songchun Li, for their assistance and guidance in my study. I also express my sincere appreciations to the staff in BCEE department.

I would like to dedicate this thesis to my parents, Yanlong Ma, and Xuegang Li, as well as my girl friend, Huirong Lu, for their patience, understanding and support during my whole studies.

TABLE OF CONTENTS

List of Figures.....	x
List of Tables.....	xii
Nomenclature.....	xiii

Chapter 1 Introduction	1
1.1 Introduction	1
1.2 The scope and objectives	2
1.3 The thesis organization	3
Chapter 2 Literature Review	4
2.1 Introduction	4
2.2 Steady state and dynamic models of hydronic heating systems	4
2.2.1 Boiler and heater models.....	4
2.2.2 Heat pump models	5
2.2.3 Ground-coupled heat exchanger models.....	8
2.2.4 Radiant floor heating system models	10
2.3 A review of control strategies for hydronic heating systems.....	13
Chapter 3 Dynamic Models of Hybrid Hydronic Heating System	15
3.1 Introduction	15
3.2 Physical model of the system.....	15
3.3 The formulation of dynamic model	18

3.3.1 Commercial zone model	18
3.3.2 Building enclosure model	20
3.3.3 Baseboard heater model	22
3.3.4 Residential zone model	23
3.3.5 Floor slab model.....	25
3.3.6 Ground loop heat exchanger model	32
3.3.7 Heat pump model	39
3.3.8 Heat exchanger model.....	40
3.3.9 Boiler model.....	41
3.3.10 Heat losses from the water distribution pipe network	41
3.4 Open loop simulations of the system	42
Chapter 4 Proportional-Integral and Adaptive Control of Hybrid Source Hydronic Heating System.....	48
4.1 Introduction	48
4.2 The effects of load disturbances on the residential and commercial zones	52
4.3 Fixed gain PI control of zone air temperatures	54

4.4 Simulation results for the adaptive PI control.....	56
Chapter 5 Control Strategies for Improved Energy Efficiency of Hybrid Hydronic Heating System.....	63
5.1 Introduction	63
5.2 Conventional fixed set-point control strategy	63
5.3 Outside air temperature reset control strategy	65
5.4 Optimal set-point control strategy.....	68
5.5 Energy consumption.....	74
5.6 Summary	77
Chapter 6 Contributions, Conclusions, and Recommendations for Future Research.....	79
6.1 Conclusions and contributions	79
6.1.1 Dynamic modeling of the hybrid source hydronic heating system	79
6.1.2 Adaptive control of hybrid hydronic system	80
6.1.3 Energy simulation under three different control strategies.....	80
6.2 Recommendations for future research	81

References.....82

Appendices86

LIST OF FIGURES

Figure 3.2.1 Commercial and residential floor layout	16
Figure 3.2.2 All boiler heating system layout.....	17
Figure 3.2.3 Hybrid source hydronic heating system layout	18
Figure 3.3.1 Schematic diagram of the reversed return hot water system loop.....	19
Figure 3.3.2 Structure of exterior wall.....	21
Figure 3.3.3 Schematic diagram of the radiant floor heating system loop	23
Figure 3.3.4 Plan view of embedded tube.....	25
Figure 3.3.5 Structure of floor slab	26
Figure 3.3.6 Thermal network analysis for the ground loop heat exchanger describing heat and mass transport processes in a vertical direction	33
Figure 3.3.7 Horizontal cross-section view of the single U-tube	33
Figure 3.4.1 System open loop test at design condition (-15 ° C outside air temperature).....	43
Figure 3.4.2 System open loop test for the heat pump temperature responses at design condition (-15 ° C outside air temperature).....	44
Figure 3.4.3 Supply water temperature of boiler and heat exchanger under different outside air temperature.....	46
Figure 3.4.4 Effect of entering source temperature on COP.....	47
Figure 4.1.1 Schematic diagram of hybrid source hydronic heating system control loop for space heating	49
Figure 4.1.2 Boiler control loop.....	49
Figure 4.1.3 Heat exchanger control loop.....	50
Figure 4.1.4 Heat pump control loop.....	50
Figure 4.1.5 Commercial zone control loop	51
Figure 4.1.6 Residential zone control loop.....	51
Figure 4.2.1 Outdoor air temperature profile.....	53
Figure 4.2.2 Residential and commercial zone air temperature responses with no control	53
Figure 4.3.1 Validation of the constant gain values of PI controllers for the residential and commercial zone temperature control.....	55
Figure 4.4.1 Validation of the adaptive PI controllers for the residential and commercial zone temperature control.....	58
Figure 4.4.2 Comparison of controller responses with adaptive control (a-b) and fixed gain control (c-d) for the residential zone subject to step change in 2 ° C and a outside air temperature profile from -15 ° C to -5 ° C	59

Figure 4.4.3 Comparison of controller responses with adaptive control (a-b) and fixed gain control (c-d) for the residential zone subject to step change in 2 o C and a outside air temperature profile from -5 ° C to 5 ° C.....	60
Figure 4.4.4 Temperature responses of the boiler, heat exchanger, and heat pump control loops for adaptive control	62
Figure 5.2.1 Output responses of residential and commercial zone (fixed set-point control strategy).....	64
Figure 5.2.2 Output responses of boiler and heat exchanger (fixed set-point control strategy).....	65
Figure 5.3.1 Outside temperature reset profile for boiler, heat exchanger and heat pump	66
Figure 5.3.2 Output responses of residential and commercial zone (outside air temperature reset strategy)	67
Figure 5.3.3 Output responses of boiler and heat exchanger (outside air temperature reset strategy).....	67
Figure 5.4.1 Comparison between the simplified aggregated model and the detailed full order model	71
Figure 5.4.2 Optimal set-point temperature profile for boiler, heat exchanger and heat pump	72
Figure 5.4.3 Output responses of residential and commercial zone (optimal control strategy).....	73
Figure 5.4.4 Output responses of boiler and heat exchanger (optimal control strategy) ..	74

LIST OF TABLES

Table 3.1 Physical properties and operating conditions of the radiant floor heating system	32
Table 3.2 Geometrical data, physical properties and operating conditions of the ground loop heat exchanger	39
Table 5.1 Energy comparison of different operating methods (system based) under high heating low demand and low heating load demand conditions	76
Table 5.2 Energy comparison of different operating methods (system based) under high heating low demand and low heating load demand conditions	77

NOMENCLATURE

α	multiplier of the adaptive controller proportional term
A_1	slab area on top of each RFH tube node (m^2)
A_2	slab area on top of each RFH concrete node (m^2)
A_{ex}	heat transfer area of the heat exchanger (m^2)
A_f	net cross-sectional area of the ground loop water node (m^2)
A_g	net cross-sectional area of the grout node (m^2)
A_{si}	net cross-sectional area of the soil node (m^2)
A_{winci}	window area of commercial zone i (m^2)
A_{winri}	window area of residential zone i (m^2)
A_{wnci}	net wall area of commercial zone i (m^2)
A_{wnri}	net wall area of residential zone i (m^2)
a_z	zone heat loss coefficient
c_{air}	specific heat of air ($\text{J}/\text{kg}^\circ\text{C}$)
C_b	thermal capacity of boiler ($\text{J}/^\circ\text{C}$)
C_c	thermal capacity of the water stored in the heat pump condenser ($\text{J}/^\circ\text{C}$)
C_{cc1}	thermal capacity of the RFH concrete node horizontally from the tube for each control volume ($\text{J}/^\circ\text{C}$)
C_{cc2}	thermal capacity of the RFH concrete node vertically from the tube for each control volume ($\text{J}/^\circ\text{C}$)
C_{cc3}	thermal capacity of the RFH concrete node one top of each concrete node in the tube layer for each control volume ($\text{J}/^\circ\text{C}$)
c_{con}	specific heat of slab concrete ($\text{J}/\text{kg}^\circ\text{C}$)
C_e	thermal capacity of the water stored in the heat pump evaporator ($\text{J}/^\circ\text{C}$)
c_{flo}	specific heat of floor covering material ($\text{J}/\text{kg}^\circ\text{C}$)
C_{flo1}	thermal capacity of the floor covering node on top of the tube for each control volume ($\text{J}/^\circ\text{C}$)
C_{flo2}	thermal capacity of the floor covering node on top of the concrete node for each control volume ($\text{J}/^\circ\text{C}$)
C_{fluid}	thermal capacity of the water inside the ground loop for each control volume ($\text{J}/^\circ\text{C}$)
c_g	specific heat of grout ($\text{J}/\text{kg}^\circ\text{C}$)
C_{grout}	thermal capacity of the grout ($\text{J}/^\circ\text{C}$)
C_{h1}	thermal capacity of the water stored in primary side of the heat exchanger ($\text{J}/^\circ\text{C}$)
C_{h2}	thermal capacity of the water stored in secondary side of the heat exchanger ($\text{J}/^\circ\text{C}$)
C_{htri}	thermal capacity of the baseboard heater i ($\text{J}/^\circ\text{C}$)
c_s	specific heat of soil ($\text{J}/\text{kg}^\circ\text{C}$)
C_{soili}	thermal capacity of the soil layer i ($\text{J}/^\circ\text{C}$)

c_w	specific heat of water (J/kg $^{\circ}$ C)
C_w	thermal capacity of the water inside the radiant floor piping for each control volume (J/ $^{\circ}$ C)
C_{wl}	thermal capacity of exterior wall brick layer (J/ $^{\circ}$ C)
C_{zci}	thermal capacity of commercial zone i (J/ $^{\circ}$ C)
C_{zri}	thermal capacity of residential zone j (J/ $^{\circ}$ C)
d_{air}	density of air (kg/m 3)
d_{bore}	borehole diameter (m)
d_{con}	density of slab concrete (kg/m 3)
d_{flo}	density of floor covering material (kg/m 3)
d_g	density of grout (kg/m 3)
$d_{i,g}$	inner diameter of the ground loop tube (m)
$d_{i,r}$	inner diameter of the RFH tube (m)
$d_{o,g}$	outer diameter of the ground loop tube (m)
$d_{o,r}$	outer diameter of the RFH tube (m)
d_{pbore}	borehole depth (m)
d_s	density of soil (kg/m 3)
d_w	density of water (kg/m 3)
e	error
e_b	boiler efficiency (%)
E_{com}	heat pump compressor power (w)
F_{en-p}	Radiation angle factor between the surface node and enclosure
h_v	heating value of fuel (J/kg)
h_w	convection heat transfer coefficient of water inside pipe (w/m 2 $^{\circ}$ C)
k_{ai}	adaptive integral gain
k_{ap}	adaptive proportional gain
k_f	thermal conductivity of the ground loop fluid (w/m $^{\circ}$ C)
k_g	thermal conductivity of the grout (w/m $^{\circ}$ C)
k_i	integral gain
k_o	predictive gain of the outside air temperature
k_p	proportional gain
k_{pipe}	thermal conductivity of the ground loop piping (w/m $^{\circ}$ C)
k_s	thermal conductivity of the soil (w/m $^{\circ}$ C)
k_t	thermal conductivity of the RFH tube (w/m $^{\circ}$ C)
k_w	thermal conductivity of the water (w/m $^{\circ}$ C)
L_{bore}	center to center distance between two boreholes (m)
L_i	length of RFH pipe segment (m)
LMTD	logarithmic mean temperature difference ($^{\circ}$ C)
LMTD $_d$	logarithmic mean temperature difference of heat exchanger at design condition ($^{\circ}$ C)
LMTD $_{ex}$	logarithmic mean temperature difference of heat exchanger ($^{\circ}$ C)

m_{fmax}	maximum flow rate of fuel (kg/s)
m_w	water flow rate (kg/s)
n	factor identified based on heater heat transfer test
N_1	number of bores in each series circuit
N_2	number of bores in each parallel circuit
Q_{bd}	boiler capacity (w)
Q_{hc}	total design heating load of commercial zone (w)
Q_{hczi}	design heating load of commercial zone i (w)
Q_{hr}	total design heating load of residential zone (w)
Q_{hrzi}	design heating load of residential zone i (w)
Q_{intci}	internal heat gain for commercial zone i (w)
$Q_{rad,conv,i}$	radiative/convective heat transfer from radiant floor slab of zone i (w)
Q_{solci}	transmitted solar radiation for commercial zone i (w)
Q_{solri}	transmitted solar radiation for residential zone i (w)
s	shank space between two tubes of ground loop (m)
S_t	interval between RFH tubes (m)
T_b	supply water temperature of boiler (°C)
t_c	Thickness of the floor slab covering layer (m)
T_{c1i}	concrete node temperature of RFH in the tube layer (°C)
T_{c2i}	concrete node temperature of RFH in the concrete layer on top of each tube (°C)
T_{c3i}	concrete node temperature of RFH in the concrete layer on top of the concrete node in the tube layer (°C)
T_{cred}	commercial zone design return water temperature (°C)
T_{cspd}	commercial zone design supply water temperature (°C)
T_{en}	area-average interior surface temperature, excluding the slab surface temperature (°C)
T_{exred}	primary side return water temperature from the heat exchanger at design condition (°C)
T_{exsp}	supply water temperature to the heat exchanger (°C)
T_{exspd}	primary side supply water temperature to the heat exchanger at design condition (°C)
T_{flo1i}	floor covering node temperature on top of each concrete node on top of each tube (°C)
T_{flo2i}	floor covering node temperature on top of each concrete node (°C)
T_{gbi}	grout wall temperature of ground loop of segment i (°C)
T_{gr1i}	grout temperature of ground loop on the down pipe side of segment i (°C)
T_{gr2i}	grout temperature of ground loop on the up pipe side of segment i (°C)
T_{htri}	outlet water temperature of baseboard heater i (°C)
T_{mix}	mix water s temperature to the heat exchanger (°C)
T_o	outside air temperature at operating condition (°C)

T_{od}	outside air temperature at design condition ($^{\circ}\text{C}$)
T_{om}	mean outside air temperature ($^{\circ}\text{C}$)
t_p	thickness of the floor slab concrete layer (m)
T_{r1}	mixed return water temperature from commercial zone 1 & 2 ($^{\circ}\text{C}$)
T_{r2}	mixed return water temperature from commercial zone 1 & 2 & 3 ($^{\circ}\text{C}$)
T_{rb}	return water temperature of boiler ($^{\circ}\text{C}$)
T_{rc}	return water temperature from the commercial zone ($^{\circ}\text{C}$)
T_{rel}	return water temperature from the heat exchanger primary side ($^{\circ}\text{C}$)
T_{rg}	return water temperature from the ground loop ($^{\circ}\text{C}$)
T_{rl}	return water temperature from the heat pump ($^{\circ}\text{C}$)
T_{rr}	return water temperature from the residential zone ($^{\circ}\text{C}$)
T_{rred}	residential zone design return water temperature ($^{\circ}\text{C}$)
T_{rs}	supply water temperature to the ground loop ($^{\circ}\text{C}$)
T_{rspd}	residential zone design supply water temperature ($^{\circ}\text{C}$)
T_{s1i}	floor surface temperature on top of each tube ($^{\circ}\text{C}$)
T_{s2i}	floor surface temperature on top of concrete node ($^{\circ}\text{C}$)
T_{spc}	supply water temperature to the commercial zone ($^{\circ}\text{C}$)
T_{spr}	supply water temperature to the residential zone ($^{\circ}\text{C}$)
T_{wg1i}	down pipe water temperature of ground loop segment i ($^{\circ}\text{C}$)
T_{wg2i}	up pipe water temperature of ground loop segment i ($^{\circ}\text{C}$)
T_{wi}	water node temperature of RFH at section i ($^{\circ}\text{C}$)
T_{wlc_i}	exterior wall nodal temperature of commercial zone i ($^{\circ}\text{C}$)
T_{wlr_i}	exterior wall nodal temperature of residential zone i ($^{\circ}\text{C}$)
T_{wls_i}	exterior wall surface temperature of zone i ($^{\circ}\text{C}$)
T_{zcd}	commercial zone air temperature at design condition ($^{\circ}\text{C}$)
T_{zci}	zone air temperature at commercial zone i ($^{\circ}\text{C}$)
T_{zrd}	residential zone air temperature at design condition ($^{\circ}\text{C}$)
T_{zri}	zone air temperature at residential zone i ($^{\circ}\text{C}$)
U_{bsi}	thermal conductance between the soil node and the grout wall ($\text{w}/\text{m}^{\circ}\text{C}$)
U_{com}	control signal of heat pump compressor
$U_{cond,cc,h}$	thermal conductance between the concrete node in the tube layer and the concrete node in the concrete layer (horizontally) ($\text{w}/^{\circ}\text{C}$)
$U_{cond,cc,v}$	thermal conductance between the concrete node in the tube layer and the concrete node in the concrete layer (vertically) ($\text{w}/^{\circ}\text{C}$)
$U_{cond,cflo1,v}$	thermal conductance between the concrete node on top of the tube node and the floor covering node ($\text{w}/^{\circ}\text{C}$)
$U_{cond,cflo2,v}$	thermal conductance between the concrete node on top of each concrete node in the tube layer and the floor covering node ($\text{w}/^{\circ}\text{C}$)
$U_{cond,flol,v}$	thermal conductance between the floor covering node in the tube layer and the floor surface node ($\text{w}/^{\circ}\text{C}$)
$U_{cond,flo2,v}$	thermal conductance between the floor covering node on top of the concrete

	node and the floor surface node ($w/^\circ\text{C}$)
$U_{\text{cond,wc,h}}$	thermal conductance between the water and the concrete node horizontally from the water node ($w/^\circ\text{C}$)
$U_{\text{cond,wc,v}}$	thermal conductance between the water and the concrete node vertically from the water node ($w/^\circ\text{C}$)
U_{ex}	heat transfer coefficient of heat exchanger ($w/m^2^\circ\text{C}$)
U_f	control signal of gas combustion rate
U_{fg}	thermal conductance between the fluid in the ground loop piping and the grout zones ($w/m^\circ\text{C}$)
$U_{\text{flo,h}}$	thermal conductance between the floor covering nodes ($w/^\circ\text{C}$)
U_{gb}	thermal conductance between the grout wall the grout zones ($w/m^\circ\text{C}$)
U_{gg}	thermal conductance between the grout zones ($w/m^\circ\text{C}$)
U_{htri}	thermal conductance of the baseboard heat i ($w/^\circ\text{C}$)
U_{ssi}	thermal conductance between two connected soil nodes ($w/m^\circ\text{C}$)
U_{w1}	thermal conductance between the wall interior surface and the brick layer node ($w/^\circ\text{C}$)
U_{w2}	thermal conductance between the brick layer node and the exterior surface ($w/^\circ\text{C}$)
u_{wci}	control signal of commercial zone i water flow rate
u_{wri}	control signal of residential zone i water flow rate
U_{win}	thermal conductance of window ($w/^\circ\text{C}$)
z_1	distance between vertical nodes of ground loop heat exchanger ($z < 10\text{m}$) (m)
z_2	distance between vertical nodes of ground loop heat exchanger ($10\text{m} < z < 75\text{m}$) (m)
β	multiplier of the adaptive controller integral term
γ	weighting factor of the residential zone thermal comfort to the energy consumption
φ	weighting factor of the commercial zone thermal comfort to the energy consumption

Subscripts

agg	referring to aggregated
air	referring to air
b	referring to boiler or building
c	referring to commercial, concrete or condenser
com	referring to compressor
conv	referring to convective
cond	referring to conductive
d	referring to design condition
e	referring to evaporator

eq, equ	referring to equality constraint
ex	referring to heat exchanger
f	referring to fuel or fluid
flo	referring to floor
g	referring to grout
h	referring to horizontal
htr	referring to terminal heater
i	referring to sequent number or number of heated zones
inci	referring to incident solar radiation
ins	referring to insulation
int	referring to internal load
pv	referring to present value
r	referring to residential
rad	referring to radiative
re	referring to return
s	referring to surface
s, soil	referring to soil
sol	referring to solar
sp, set	referring to supply, set-point
t	referring to tube
v	referring to vertical
Vol	referring to volume
w	referring to water
win	referring to window
wls	referring to wall surface
wn, wl	referring to wall

Abbreviations

ACH	air change per hour
ASHRAE	American society of heating, refrigerating and air-conditioning engineers
COP	coefficient of performance
HVAC	heating, ventilating, and air conditioning
OLT	open loop test
PI	proportional plus integral controller

Chapter 1 Introduction

1.1 Introduction

In recent days, energy efficiency and sustainability have dominated the research in the field of design and operation of HVAC systems. To this end, there is a growing awareness of the influence the building HVAC system operation on the energy consumption. Most of the heating, cooling, and ventilation systems have optimal range for satisfactory and economical operation subject to their capacity constraints. To a large extent, a single HVAC system may not be adequate to meet all requirements of a multi-functional building to perform in the most efficient and economical manner. Therefore, it is more appealing to use a decentralized hybrid system approach such that the overall integrated system can operate in a more efficiency way.

In the past few decades, more environmental friendly way to achieve heating, cooling, and ventilation has been explored and emphasized in practical applications. Hence, systems that utilize geothermal, solar, wind, or other means of green energy, are increasingly popular in the context of broader awareness of sustainable building energy technologies.

To this end, a hybrid hydronic space heating system for a multi-functional building is proposed in this thesis to maintain desired zone air temperatures, while minimizing the energy consumption. A ground loop heat pump system is integrated into an existing conventional hot water heating natural gas fired boiler system. As such, hot water can be

partially or completely supplied by the ground source heat pump system so that the boiler energy consumption can be minimized. The interactions of combined systems are examined and evaluated in terms of system performance and temperature control.

1.2 The scope and objectives

The main focus of this thesis is to develop dynamic models of a hybrid hydronic heating system, so that the system operation and control can be performed in a realistic and energy-efficient manner.

The main objectives of the study are as follows:

- 1) To design a hybrid hydronic heating system for a multi-functional building based on practical guidelines and steady state methods.
- 2) To develop dynamic models for each system component, including a boiler, a heat exchanger, a ground loop heat pump, a ground loop heat exchanger, baseboard heaters, and radiant floor hydraulic piping systems. The dynamic models are used to analyze and simulate the system responses, under various operating conditions.
- 3) To develop control strategies to maintain desired zone air temperatures, while improving the overall energy efficiency of the system.
- 4) To obtain optimal set-points of the system by formulating and solving a multi-variable constraint optimization problem to minimize energy consumption.
- 5) Conduct several energy simulations of the system under different control strategies to evaluate the potential energy savings.

1.3 The thesis organization

The thesis is organized into several chapters. In Chapter 2, a literature review is presented. In Chapter 3, the dynamic models of hybrid hybronic heating system are developed and the open loop simulation results are presented. In Chapter 4, control strategies, including a conventional PI control and an adaptive PI control, are developed. Simulation results are presented to show the performance and control strategies under variable load conditions. In Chapter 5, an energy based analysis for each operating strategy is presented. Conclusions are given in Chapter 6.

Chapter 2 Literature Review

2.1 Introduction

A hybrid hydronic heating system consists of several components, such as a boiler, a heat exchanger, a ground loop heat pump, a ground loop heat exchanger, baseboard heaters, and piping systems. The modeling aspects of the system were studied by many researchers. A literature review of steady state and dynamic models will be given first. Also, the hydronic heating system operation, control strategies and controller design methods published in the literature are reviewed and presented in the following sections.

2.2 Steady state and dynamic models of hydronic heating system

2.2.1 Boiler and heater models

Zaheer-uddin and Monastiriakos (1998) proposed a hydronic heating system model, which consisted of models for a boiler, baseboard terminal units, a domestic hot water heat exchanger and an environmental zone. Nonlinear coupled differential equations were utilized to develop the model. Simulation results were compared with the field measured data. It was shown that the designed controllers are able to maintain the boiler, zone and DHW temperatures close to their respective set-points when the space heating and DHW loads are subjected to step changes. A load tracking set-point control strategy was developed and validated and it was shown that the boiler temperature when regulated as a function of outdoor air temperature result in better zone temperature control.

Liao and Parand (2002) developed a dynamic model of commercial hot water boilers that was integrated with other heating system component models for optimization of boiler control in central heating systems. The mathematical model included of six major components, a burner, a flame tunnel, an inner shell separating the flame and the water mass, a water channel where water is heated, an outer shell wrapped with an insulation layer. The dynamics of the inner shell, water node, outer shell, and the insulation layer were modeled and evaluated by the thermodynamic equations and energy conservation law. The results showed that the model can accurately simulate the dynamic performance of the targeted boilers.

Li and Zaheer-uddin (2010) proposed a dynamic model of an indirect district heating (IDH) system. The dynamic model consists of sub-system models such as a boiler, a pipe network, a heat exchanger, terminal heaters and a zone model. The simulation results showed that the overall efficiency of the IDH system is 78.7% and it was also shown that the two highest heat loss components were the boiler heat losses (8.7%) and the secondary water makeup loss (6.1%) in the system.

2.2.2 Heat pump models

A number of heat pump models have been proposed by researchers over the years ranging from detailed deterministic models to simple curve-fit models. The detailed deterministic model usually requires numerous unavailable and uncertain inputs and a detailed analysis based on thermodynamic laws and heat transfer relations applied to

individual components. On the other hand, a curve-fit model treats the heat pump as a black box and the system performance curve is predicted by fitting a polynomial function to the performance data extracted from the manufactures' catalog.

Cecchini and Marchal (1991) proposed a computer program for simulating refrigeration and air-conditioning equipment performance. The simulation model was based on thermodynamic cycles and experimental data from equipment testing. Some of the parameters, such as saturation pressures in evaporator and condenser, superheating and subcooling, which are usually not available in manufactures' catalogs, were also used from experimental data.

Stefanuk et al. (1992) developed a superheat-controlled water-to-water heat pump model, which was derived from mass, energy, momentum balance as well as fundamental correlations of heat transfer. Parameters that describe the behavior of the individual components were assumed to be available for model prediction, such as the relationship among mass flow rate, input electrical power, evaporation temperature and the compressor discharge pressure, which are normally not available in the heat pump manufacturers' catalogs. Results for the evaporating and condensing pressures, the heat transfer rates in the evaporator and the condenser, and the COP of the heat pump from the model predictions were compared with experimental measurements. Except for a few points with errors beyond $\pm 10\%$, most of the results were in an acceptable range.

Jin and Spitler (2002) developed a parameter estimation based model for a water-to-water reciprocating vapor compression heat pump. The model was developed from the basic thermodynamic principles and heat transfer relations and it is suitable for use in building energy analysis and HVAC simulation programs. The model included several parameters that were estimated from manufactures' catalog by applying a multi-variable curve-fit algorithm. The modeling and validation results showed that the physically based model representation of the heat pump aids in achieving a better match of the catalog data and as well as lends itself to some extrapolation beyond the catalog data. As compared to more detailed deterministic models, the estimated models do not require internally measured data which are usually unavailable.

Tang (2003) developed a curve-fit water-to-water heat pump model in his thesis. The generalized least square method was applied to generate a set of performance coefficients from the catalog data at indicated reference conditions. The following variables that affected the heat pump performance were chosen: load side inlet water temperature, source side inlet water temperature, source side water flow rate and load side water flow rate. The governing equations for the heating mode are derived. These are:

$$\frac{Q_h}{Q_{h,ref}} = D1 + D2 \frac{T_{L,in}}{T_{ref}} + D3 \frac{T_{S,in}}{T_{ref}} + D4 \frac{V_L}{V_{L,ref}} + D5 \frac{V_S}{V_{S,ref}}$$

$$\frac{Power_h}{Power_{h,ref}} = E1 + E2 \frac{T_{L,in}}{T_{ref}} + E3 \frac{T_{S,in}}{T_{ref}} + E4 \frac{V_L}{V_{L,ref}} + E5 \frac{V_S}{V_{S,ref}}$$

$$\frac{Q_{source,c}}{Q_{source,c,ref}} = F1 + F2 \frac{T_{L,in}}{T_{ref}} + F3 \frac{T_{S,in}}{T_{ref}} + F4 \frac{V_L}{V_{L,ref}} + F5 \frac{V_S}{V_{S,ref}}$$

The validation results showed that the curve-fit water-to-water heat pump model performs adequately well compared to the catalog data with RMS error less than 7%, and it is more robust and requires less computation time than the parameter estimation model.

2.2.3 Ground-coupled heat exchanger models

The design and modeling of ground heat exchangers are complicated by a variety of factors such as geological formations and properties that affect thermal performance.

The earliest approach to calculating the thermal transport around a heat exchange pipe in the ground is the Kelvin's line-source theory (1882). It assumed that the ground is an infinite medium, and heat conduction process is one-dimensional because the length of the vertical ground heat exchanger is much greater than its diameter.

Carslaw and Jaeger (1947) developed a cylindrical heat source solution for a constant heat transfer rate. In the cylindrical source model, the borehole is assumed as an infinite cylinder surrounded by homogeneous medium with constant properties.

Ingersoll and Zobel (1954) proposed a steady-state heat transfer equation to predict the shorter term variations. The model is also referred to as a line source model, which assumes that heat transfer takes place from an infinite long line source or sink in an infinite medium. Kavanaugh (1985) adjusted the method to account for the U-bend arrangement and hourly heat rate variations. Other design modeling alternatives were described by Eskilson (1987), Morrison (1997), and Spitler (2000).

Bernier et al. (2004) proposed a cylindrical heat source model for the vertical ground loop heat exchanger that aggregates heating or/and cooling loads and takes into account the thermal interactions among surrounding boreholes. This model was also referred to as multiple-load aggregation algorithm (MLAA).

Daniel E. Fisher et al (2005) presented a ground source heat pump system model that is implemented in the whole building annual energy simulation program EnergyPlus. Simplified models of heat exchanger and expansion device components and a more detailed compressor model were proposed and validated. Multi-variable parameter estimation methods have been used to find model parameter values from manufacturers' catalogue data. The results showed that the model is able to reproduce the manufactures' catalogue data within a +/-10% error bound. Compared to deterministic and curve-fit models, it has the advantage that no detailed component data or measurements are required and the extrapolation over a wide range of operating conditions is feasible.

Georgios Florides and Soteris Kalogirou (2007) did a review on ground heat exchangers regarding systems, models and their applications. Various system types were described and compared for their efficiencies, performance under different operating conditions, as well as the modeling metrologies.

Yujin Nam, Ryozo Ooka, and Suckho Hwang (2008) developed a numerical model that combines a heat transport model with ground water flow and a heat exchanger model. The proposed model was used to predict the heat exchange rate for an actual office

building in Japan. Simulation results using the developed prediction model were compared with the experimental results, and a good match was reported.

Bauer, Heidemann, and Diersch (2011) proposed a transient 3D analysis of a borehole heat exchanger model. The model was based on thermal resistance and capacity approaches, considering the transient effects of heat and mass transports inside the borehole. The model was used to conduct a three-dimensional numerical simulation of U-tube borehole heat exchangers. The results showed that the proposed model can provide accurate results while substantially reducing the number of nodes and the computation time.

2.2.4 Radiant floor heating system models

Radiant floor heating systems use pipes that are embedded into a concrete floor and thus the circulating hot water inside the pipes warms up the surrounding concrete structure, which, in turn, directly radiates heat into the space. Several benefits of radiant floor heating systems have been shown. Such systems give better thermal comfort, produce less noise, can operate with low-temperature water, and often use less energy than other types of heating systems. Furthermore, dust accumulation and stratification problems that may occur with air handling system and baseboard heating system are not problems with radiant floor heating.

Due to the significant advantage over conventional heating systems, several researchers have studied on radiant floor heating systems. Cho and Zaheer-uddin (1999) conducted

an experimental study to comparatively evaluate the performances of two different control schemes for the radiant floor heating systems. Those two control schemes are conventional on-off control and two parameter switching control (TPSC). The TPSC showed a better performance in controlling the indoor air temperature.

Zaheer-uddin and Zhang (2002) developed a dynamic model and proposed two control strategies: a multistage on-off control and an augmented constant gain control (ACGC) for improving the temperature regulation of a radiant floor heating system. Simulation results showed that by staging the control action in multiple steps, the temperature regulation of RFH systems was significantly improved compared to the on-off control. The ACGC strategy eliminates the use of floor slab temperature sensor. Also, ACGC strategy showed better zone temperature control and robustness compared to the conventional proportional control.

Sattari and Farhanieh (2006) presented a parametric study on radiant floor heating system performance. In their paper, the effects of design parameters, such as type of pipe, diameter, material, number of pipes, thickness, and the floor covering on performance of a typical radiant floor heating system were investigated using finite element modeling method. The simulation results showed that the type and thickness of the floor cover play a more crucial role than the number, type and diameter of pipes on the thermal performance of the floor heating system.

Li (2010) developed a dynamic model for a radiant floor heating system which predicted the mean zone air temperature, the water temperature distribution, the temperature distribution in floor slab and slab surface temperature under design and off design conditions. By applying single zone and multi-zone analysis, the simulation results were presented to show that the maximum surface temperature difference in RFH system is about 4 ° C, and, the maximum variation in air temperature in the zone can reach as much as 1.6 ° C. The simulation results from the multi-zone model also showed that increasing the number of water tubes and increasing the water mass flow rate can compensate for the high heat loss rate in the zone. Different control strategies, such as conventional PI control, predictive control, and optimal control were developed and compared for improving the performance of RFH systems. The simulation results showed that the optimal PI control strategy not only has the best zone air temperature regulation, but also it has the greatest energy efficiency. It was showed that the predictive control strategy is easier to implement compared to optimal control strategy.

Chae et al. (2011) investigated the thermal performance enhancement of the hydronic radiant floor heating system by exploring tube shape improvement. Both analytical and detailed CFD simulations were conducted to assess the impact of each tube design parameter. Other performance indicators, such as the floor surface temperature distribution, the return hot water temperature, and the actual heating supply requirement of the radiant floor system were also investigated under both steady-state and transient

conditions. The conclusions drawn by the authors stated that radiant floor tube fin thickness, the number of fins, and the tube thermal conductivity refinements have significant influence on thermal performance enhancement. The heating energy consumption was significantly reduced by selecting suitable tube shape geometry.

2.3 A review of control strategies for hydronic heating systems

Zaheer-uddin (1993) proposed an adaptive control method for the design of temperature controllers for intelligent buildings. The linear models of the systems were used to design controllers for VAV-HVAC systems. It was shown that by a proper choice of the adaptation rate, the output response of the VAV system can be improved.

Chen (2002) described an improved algorithm for generalized predictive control (GPC) and applied it to a radiant floor heating system in a full-scale outdoor test-room. The performance of the floor heating system controlled by on-off and PI controllers was also evaluated and compared with GPC control through computer simulations. The results demonstrated that the GPC controller was superior to the other two in terms of response speed, minimum offset and on-off cycling frequency.

Singh et al (2000) proposed an adaptive control strategy for multivariable thermal processes in HVAC systems. A two zone fan-coil heating system is considered and simulated by using a nonlinear model. A multivariable adaptive controller based on linear quadratic regulator theory was designed. The simulation results showed that the adaptive controller was able to reject the effects of both static and dynamic disturbances rapidly,

and the maximum percentage overshoot in zone temperature was found to be within acceptable limits. The controller also showed robust control could handle unmodelled dynamics and system nonlinearities.

Fatemeh et al (2011) studied unstable oscillatory behavior of the thermostatic radiator valves during the partial load operating conditions as they were designed for full load condition. To achieve a balance between stability and performance for radiator control, they presented a linear parameter varying model of the thermostatic radiator valve (TRV) as a function of operating flow rate, room temperature and the radiator specifications so that the TRV controller can be adaptive with the operating conditions. The simulation results showed that the designed controller based on the LPV model performed satisfactorily and remained stable in the whole operating conditions.

From the literature review, it is noted that most systems are related to stand-alone HVAC systems. On the other hand, very little work has been done on the integration of multiple HVAC systems. Furthermore, much less work has been done on the integration of conventional hot water heating system and ground source heat pump systems.

To this end, the major objective of this thesis is to model an integrated hot water and ground source heat pump system and to develop improved control strategies to optimize energy efficiency of the overall system.

Chapter 3 Dynamic Models of Hybrid Hydronic Heating System

3.1 Introduction

In this chapter, dynamic models of a hybrid hydronic heating system are developed. Firstly, the system layout and the nodal arrangement of the model are described. Then, dynamic models are developed for each component, including zone air, building enclosure, baseboard heaters, radiant floor piping, ground source heat exchanger, heat pump, heat exchanger, and the boiler. Finally, open loop tests are conducted to show the dynamic response characteristics of the system at design condition.

3.2 Physical model of the system

As shown in Figure 3.2.1, a typical multi-functional two-storey building is considered in this thesis. The first floor and the second floor are used for commercial and residential application respectively. The commercial floor consists of four zones and it is designed to be served by baseboard heaters. The residential floor consists of four apartments, and each apartment has four rooms. Radiant floor heating system is installed in each of the residential spaces.

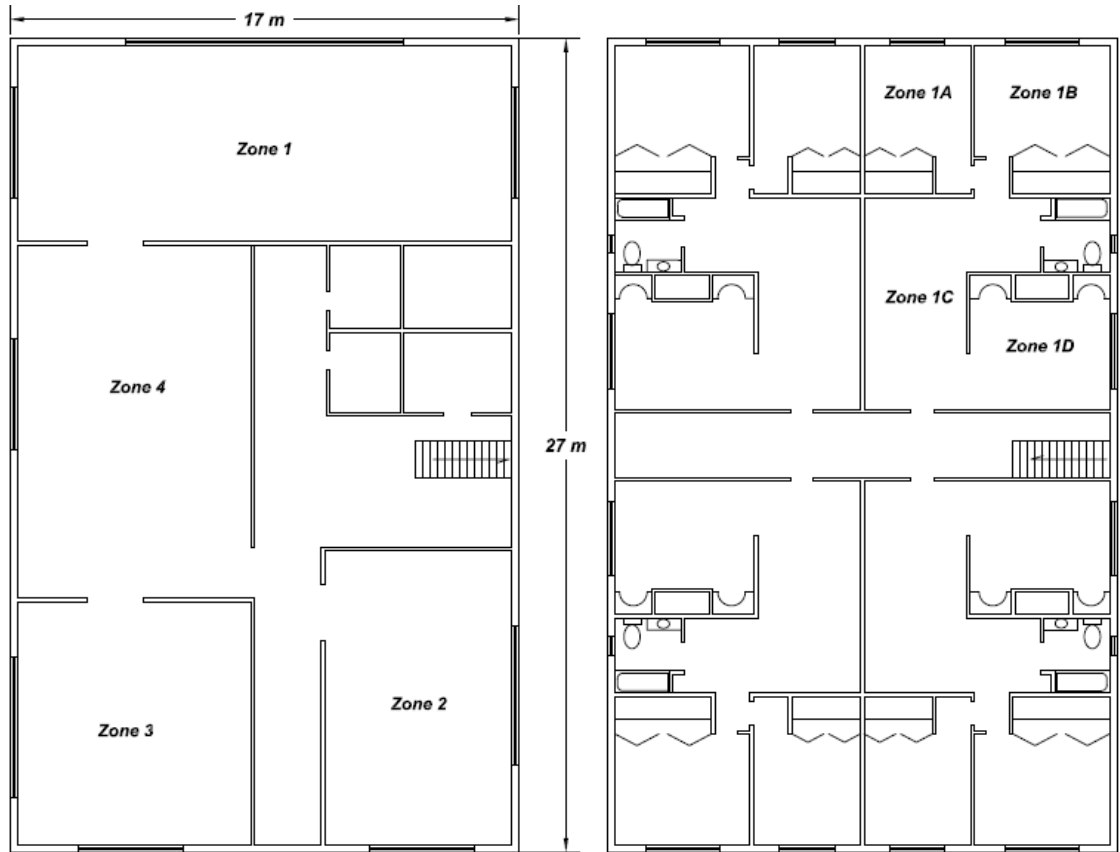


Figure 3.2.1 Commercial and residential floor layout

The schematic diagrams of two systems are shown in Figure 3.2.2 and Figure 3.2.3, respectively. The base case system is a conventional all boiler system that all the hot water supply is from the boiler located in a central plant. High temperature water can be used directly to heat up the commercial floor by circulating hot water through the baseboard heater units. For residential zones where lower temperature water is required for the radiant floor heating (RFH), a heat exchanger is applied to regulate the supply water temperature to the RFH system.

However, to use high-quality heat (boiler source) for low-quality energy demand system (radiant floor space heating) is not desirable because of the low exergy efficiency. Therefore, to upgrade and make the system sustainable, it is proposed to add a ground-source heat pump system to the conventional hot water boiler heating system. Thus the overall system is a hybrid hydronic heating system which is flexible to provide high temperature and medium temperature hot water as needed in the baseboard and RFH systems respectively. As such, low temperature water can be supplied, partially or completely, by the suitable sources at desirable quality levels.

The schematic layout of the above two systems are shown in Figure 3.2.2 and Figure 3.2.3, respectively.

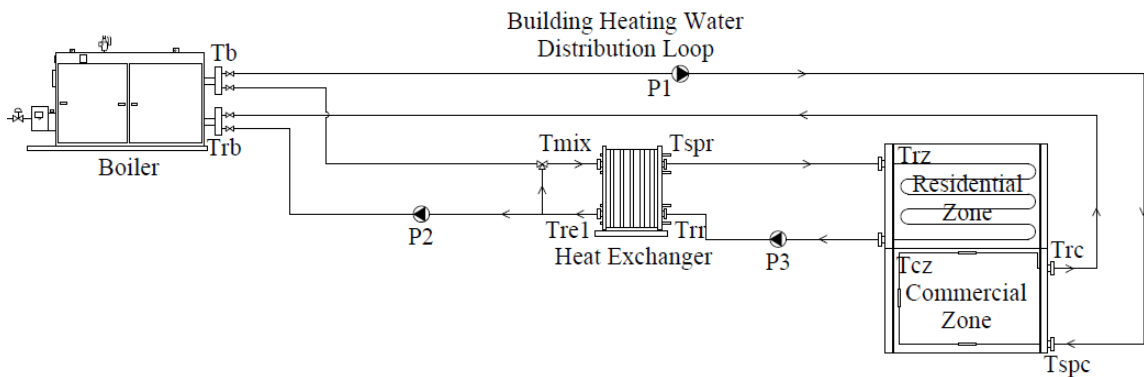


Figure 3.2.2 All boiler heating system layout

Figure 3.2.2 represents a conventional all boiler heating system. The boiler is located in a central plant and hot water is supplied through an underground distribution loop.

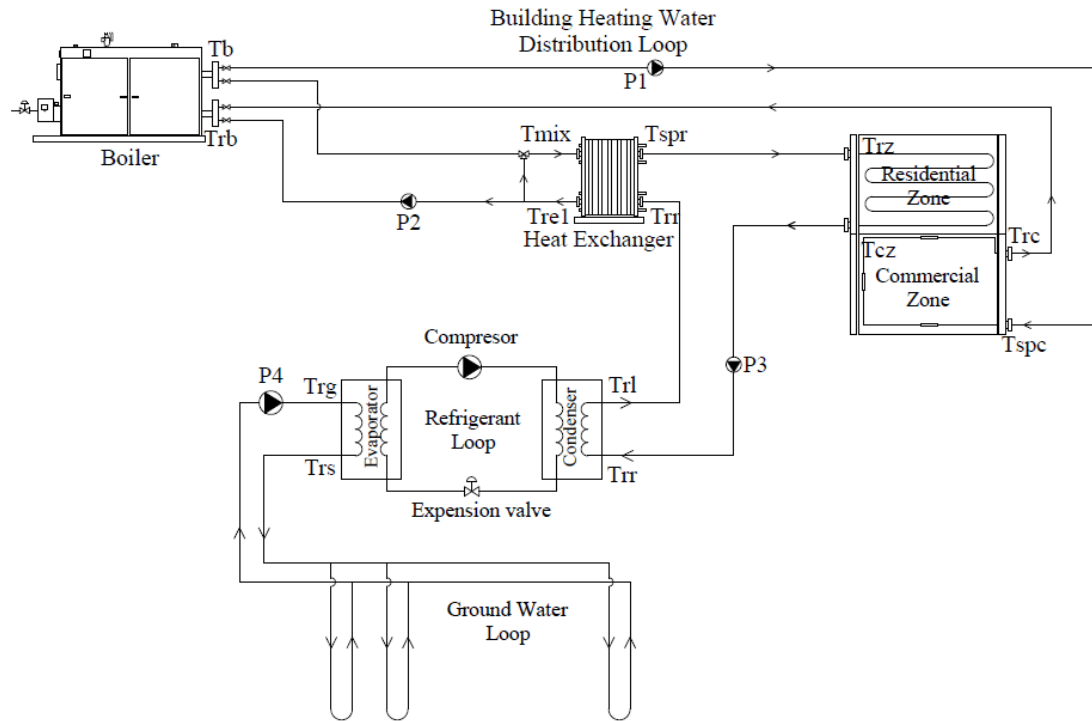


Figure 3.2.3 Hybrid hydronic heating system layout

The system design and equipment selection consist of (1) heating load estimation, (2) radiant floor heating system sizing, (3) Baseboard heater sizing, (4) Ground loop heat exchanger sizing, (4) Heat pump selection, (5) Heat exchanger sizing, and (6) Boiler selection. Steady state design method was used to determine the design capacity. The summary of calculations is presented in Appendix-A.

3.3 The formulation of a dynamic model

3.3.1 Commercial zone model

Figure 3.3.1 shows a schematic diagram of the piping system and the baseboards installed in each of the four commercial zones of the building. To develop the commercial zone

model, an energy balance approach was used. The equations 3.1 to 3.4 describe the model.

These equations state that the net energy stored in the zone air is equal to the heat output from the baseboard heater units, the solar radiation and the internal heat gain minus the heat losses from the building enclosure and infiltration.

Note that there are four commercial zones and the zone temperatures are identified by T_{zc1} , T_{zc2} , T_{zc3} , T_{zc4} , respectively.

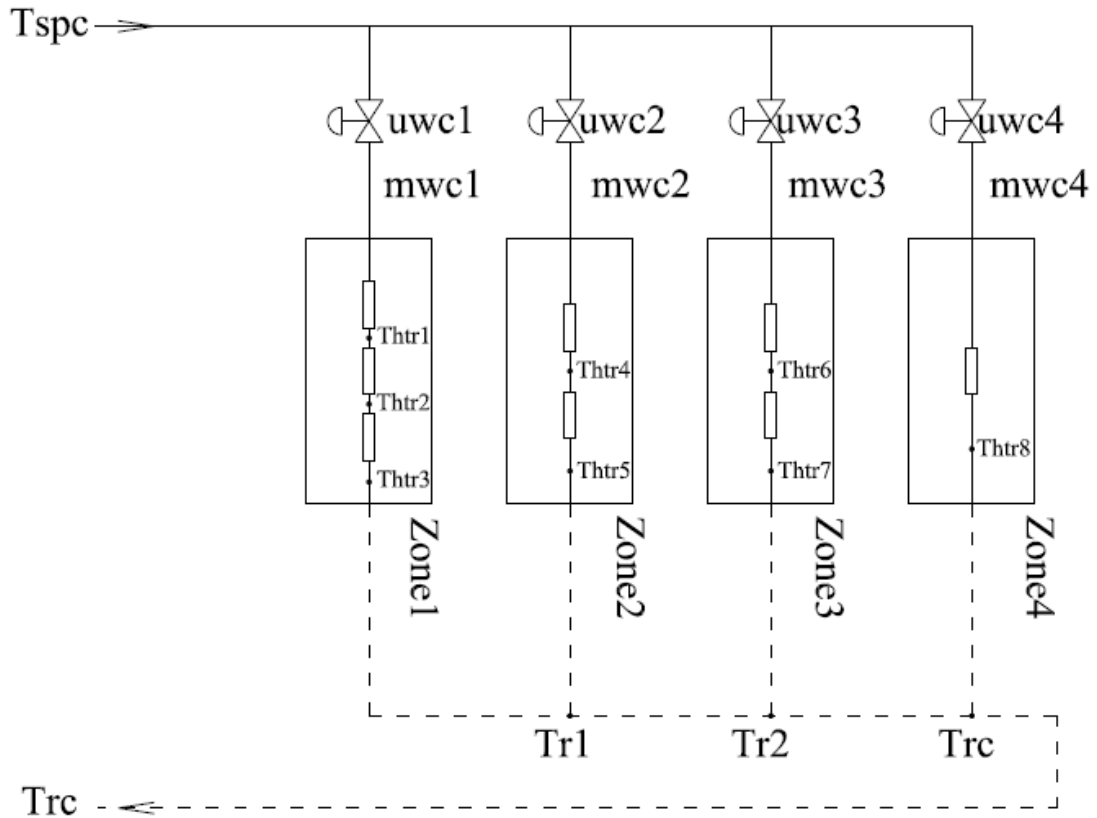


Figure 3.3.1 Schematic diagram of the reversed return hot water system loop

$$C_{zc1} \frac{d(T_{zc1})}{dt} = c_w m_{wc1} (T_{spc} - T_{htr3}) - A_{wincl} U_{win} (T_{zc1} - T_o) - A_{wncl} U_{wl} (T_{zc1} - T_{wlc1}) - \frac{ACH \times Vol_{c1} \times c_{air} \rho_{air} (T_{zc1} - T_o)}{3600} + Q_{solc1} + Q_{intc1} \quad (3.1)$$

$$C_{zc2} \frac{d(T_{zc2})}{dt} = c_w m_{wc2} (T_{spc} - T_{htr5}) - A_{winc2} U_{win} (T_{zc2} - T_o) - A_{wncl} U_{wl} (T_{zc2} - T_{wlc2}) - \frac{ACH \times Vol_{c2} \times c_{air} \rho_{air} (T_{zc2} - T_o)}{3600} + Q_{solc2} + Q_{intc2} \quad (3.2)$$

$$C_{zc3} \frac{d(T_{zc3})}{dt} = c_w m_{wc3} (T_{spc} - T_{htr7}) - A_{winc3} U_{win} (T_{zc3} - T_o) - A_{wncl} U_{wl} (T_{zc3} - T_{wlc3}) - \frac{ACH \times Vol_{c3} \times c_{air} \rho_{air} (T_{zc3} - T_o)}{3600} + Q_{solc3} + Q_{intc3} \quad (3.3)$$

$$C_{zc4} \frac{d(T_{zc4})}{dt} = c_w m_{wc4} (T_{spc} - T_{htr8}) - A_{winc4} U_{win} (T_{zc4} - T_o) - A_{wncl} U_{wl} (T_{zc4} - T_{wlc4}) - \frac{ACH \times Vol_{c4} \times c_{air} \rho_{air} (T_{zc4} - T_o)}{3600} + Q_{solc4} + Q_{intc4} \quad (3.4)$$

$$m_{wc1} = u_{wc1} \cdot m_{wc1d} \quad (3.5)$$

$$m_{wc2} = u_{wc2} \cdot m_{wc2d} \quad (3.6)$$

$$m_{wc3} = u_{wc3} \cdot m_{wc3d} \quad (3.7)$$

$$m_{wc4} = u_{wc4} \cdot m_{wc4d} \quad (3.8)$$

3.3.2 Building enclosure model

A sectional view of the wall assembly is shown in Figure 3.3.2, and a wall temperature model was derived. The wall assembly consists of a 100 mm face brick, an air gap, a 100 mm insulation layer, another air gap, and a 13 mm gypsum board.

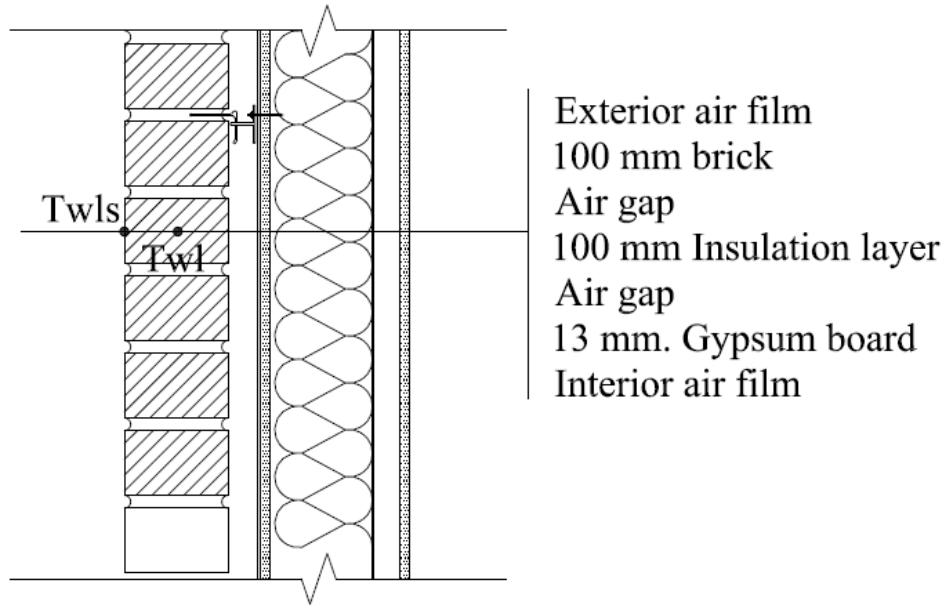


Figure 3.3.2 Structure of exterior wall

To simplify the model, uniform temperature in the wall assembly is used for the heat transfer analysis. Therefore, the heat transfer process through the wall section can be simply considered as one-dimensional problem. Two nodes are used for the heat transfer analysis: one is located in the outside brick layer, and the other is located on the exterior surface. Based on the energy conservation analysis at each node, the temperature equation for each node can be described as:

$$C_{wl} \frac{d(T_{wl})}{dt} = A_{wn} U_{w1} (T_z - T_{wl}) - A_{wn} U_{w2} (T_{wl} - T_{wls}) \quad (3.9)$$

$$T_{wls} = \frac{U_{w2} T_{wl} + h_o T_o + Q_{inci}}{U_{w2} + h_o} \quad (3.10)$$

The symbols used in the equations are described in the nomenclature.

3.3.3 Baseboard heater model

By applying the energy balance principle, an equation describing heat transfer processes in the heater was developed. The models are described by equations 3.11 to 3.18.

The following equations state that the net energy stored in the water inside of the heater tube in each zone is equal to the heat supplied from the hot water minus the heat emission from the outside surface of the heater(s) to the zone air.

$$C_{htr1} \frac{d(T_{htr1})}{dt} = c_w m_{wc1} (T_{spc} - T_{htr1}) - U_{htr1} \left(\frac{T_{spc} + T_{htr1}}{2} - T_{zc1} \right)^{1+n} \quad (3.11)$$

$$C_{htr2} \frac{d(T_{htr2})}{dt} = c_w m_{wc1} (T_{htr1} - T_{htr2}) - U_{htr2} \left(\frac{T_{htr1} + T_{htr2}}{2} - T_{zc1} \right)^{1+n} \quad (3.12)$$

$$C_{htr3} \frac{d(T_{htr3})}{dt} = c_w m_{wc1} (T_{htr2} - T_{htr3}) - U_{htr3} \left(\frac{T_{htr2} + T_{htr3}}{2} - T_{zc1} \right)^{1+n} \quad (3.13)$$

$$C_{htr4} \frac{d(T_{htr4})}{dt} = c_w m_{wc2} (T_{spc} - T_{htr4}) - U_{htr4} \left(\frac{T_{spc} + T_{htr4}}{2} - T_{zc2} \right)^{1+n} \quad (3.14)$$

$$C_{htr5} \frac{d(T_{htr5})}{dt} = c_w m_{wc2} (T_{htr4} - T_{htr5}) - U_{htr5} \left(\frac{T_{htr4} + T_{htr5}}{2} - T_{zc2} \right)^{1+n} \quad (3.15)$$

$$C_{htr6} \frac{d(T_{htr6})}{dt} = c_w m_{wc3} (T_{spc} - T_{htr6}) - U_{htr6} \left(\frac{T_{spc} + T_{htr6}}{2} - T_{zc3} \right)^{1+n} \quad (3.16)$$

$$C_{htr7} \frac{d(T_{htr7})}{dt} = c_w m_{wc3} (T_{htr6} - T_{htr7}) - U_{htr7} \left(\frac{T_{htr6} + T_{htr7}}{2} - T_{zc3} \right)^{1+n} \quad (3.17)$$

$$C_{htr8} \frac{d(T_{htr8})}{dt} = c_w m_{wc4} (T_{spc} - T_{htr8}) - U_{htr8} \left(\frac{T_{spc} + T_{htr8}}{2} - T_{zc4} \right)^{1+n} \quad (3.18)$$

$$T_{r1} = \frac{(T_{htr3} m_{w1} + T_{htr5} m_{w2})}{m_{w1} + m_{w2}} \quad (3.19)$$

$$T_{r2} = \frac{T_{r1} \cdot (m_{w1} + m_{w2}) + T_{hr7} m_{w3}}{m_{w1} + m_{w2} + m_{w3}} \quad (3.20)$$

$$T_{rc} = \frac{T_{r2} \cdot (m_{w1} + m_{w2} + m_{w3}) + T_{hr8} m_{w4}}{m_{w1} + m_{w2} + m_{w3} + m_{w4}} \quad (3.21)$$

3.3.4 Residential zone model

Figure 3.3.3 shows a schematic diagram of the RFH system installed in each of the four residential zones of the building. A model for predicting the zone air temperature of each zone was formulated by assuming that the zone air temperature is uniformly distributed throughout the zone. Equations 3.22 to 3.25 state that the net energy stored in the zone air is equal to the heat output from the radiant floor panel, the solar radiation and the internal heat gain minus the heat losses from the building enclosure and infiltration.

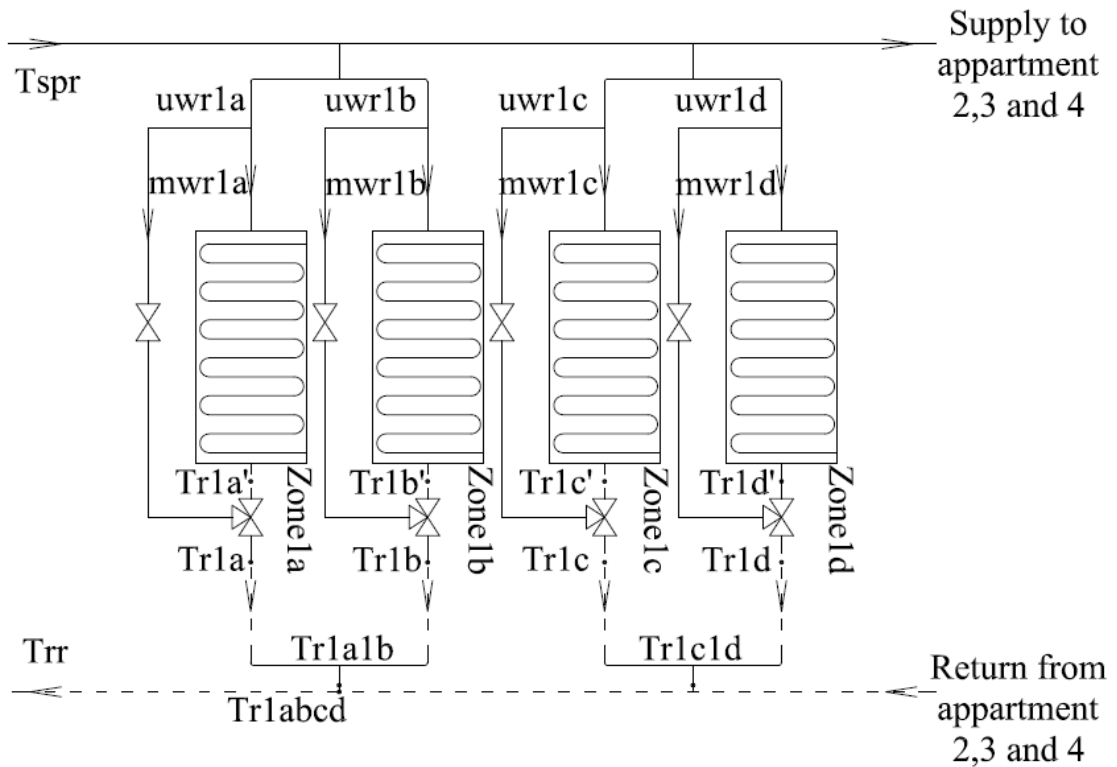


Figure 3.3.3 Schematic diagram of the radiant floor heating system loop

$$C_{zr1a} \frac{d(T_{zr1a})}{dt} = Q_{rad,conv,1a} - A_{winr1a} U_{win} (T_{zr1a} - T_o) - A_{wnr1a} U_{wl} (T_{zr1a} - T_{wlr1a}) - \frac{ACH \times Vol_{1a} \times c_{air} \rho_{air} (T_{zr1a} - T_o)}{3600} + Q_{solr1a} \quad (3.22)$$

$$C_{zr1b} \frac{d(T_{zr1b})}{dt} = Q_{rad,conv,1b} - A_{winr1b} U_{win} (T_{zr1b} - T_o) - A_{wnr1b} U_{wl} (T_{zr1b} - T_{wlr1b}) - \frac{ACH \times Vol_{1b} \times c_{air} \rho_{air} (T_{zr1b} - T_o)}{3600} + Q_{solr1b} \quad (3.23)$$

$$C_{zr1c} \frac{d(T_{zr1c})}{dt} = Q_{rad,conv,1c} - A_{winr1c} U_{win} (T_{zr1c} - T_o) - A_{wnr1c} U_{wl} (T_{zr1c} - T_{wlr1c}) - \frac{ACH \times Vol_{1c} \times c_{air} \rho_{air} (T_{zr1c} - T_o)}{3600} + Q_{solr1c} \quad (3.24)$$

$$C_{zr1d} \frac{d(T_{zr1d})}{dt} = Q_{rad,conv,1d} - A_{winr1d} U_{win} (T_{zr1d} - T_o) - A_{wnr1d} U_{wl} (T_{zr1d} - T_{wlr1d}) - \frac{ACH \times Vol_{1d} \times c_{air} \rho_{air} (T_{zr1d} - T_o)}{3600} + Q_{solr1d} \quad (3.25)$$

$$T_{r1a} = \frac{(u_{wrla} \cdot m_{wrlad} \cdot T_{r1a} + (1 - u_{wrla}) \cdot m_{wrlad} \cdot T_{spr})}{u_{wrla} \cdot m_{wrlad} + (1 - u_{wrla}) \cdot m_{wrlad}} \quad (3.26)$$

$$T_{r1b} = \frac{(u_{wrlb} \cdot m_{wrlbd} \cdot T_{r1b} + (1 - u_{wrlb}) \cdot m_{wrlbd} \cdot T_{spr})}{u_{wrlb} \cdot m_{wrlbd} + (1 - u_{wrlb}) \cdot m_{wrlbd}} \quad (3.27)$$

$$T_{r1ab} = \frac{(m_{wrlad} \cdot T_{r1a} + m_{wrlbd} \cdot T_{r1b})}{m_{wrlad} + m_{wrlbd}} \quad (3.28)$$

$$T_{r1c} = \frac{(u_{wrlc} \cdot m_{wrlcd} \cdot T_{r1c} + (1 - u_{wrlc}) \cdot m_{wrlcd} \cdot T_{spr})}{u_{wrlc} \cdot m_{wrlcd} + (1 - u_{wrlc}) \cdot m_{wrlcd}} \quad (3.29)$$

$$T_{r1d} = \frac{(u_{wrl d} \cdot m_{wrl d d} \cdot T_{r1 d} + (1 - u_{wrl d}) \cdot m_{wrl d d} \cdot T_{spr})}{u_{wrl d} \cdot m_{wrl d d} + (1 - u_{wrl d}) \cdot m_{wrl d d}} \quad (3.30)$$

$$T_{r1c1d} = \frac{(m_{wrlcd} \cdot T_{r1c} + m_{wrl d d} \cdot T_{r1d})}{m_{wrlcd} + m_{wrl d d}} \quad (3.31)$$

$$T_{r1abcd} = \frac{(m_{wrlad} + m_{wrlbd}) \cdot T_{r1ab} + (m_{wrlcd} + m_{wrl d d}) \cdot T_{r1c1d}}{m_{wrlad} + m_{wrlbd} + m_{wrlcd} + m_{wrl d d}} \quad (3.32)$$

3.3.5 Floor slab model

The plan view of the radiant floor heating panel is shown in the Figure 3.3.4. Since the specific heat of water is higher than that of the concrete, the temperature gradient in the direction of the hot water pipes is negligible compared to that in the direction perpendicular to the RFH pipes. Also, as the hot water pipes are equally spaced, it can be assumed that the same unit section is symmetrically repeating.

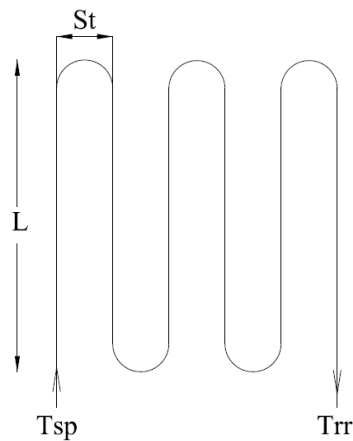


Figure 3.3.4 Plan view of embedded tube

A typical floor slab structure is shown in Figure 3.3.5. The heat transfer from the water circulated in the radiant floor piping to the slab surface is considered as two-dimensional heat flow: horizontal heat flux from the water node to the nearby concrete nodes, and vertical heat flux from water node as well as the concrete nodes in the tube layer to the upper layer. It is also assumed that the concrete nodes on both sides of each tube node are of the same condition.

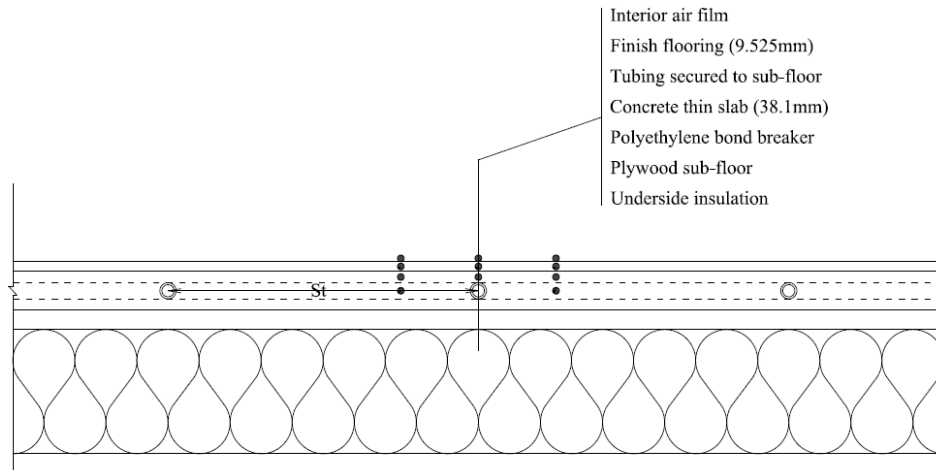


Figure 3.3.5 Structure of floor slab

1. Water node

The equation describing the water temperature in the tube is given by:

$$C_w \frac{d(T_{w,i})}{dt} = c_w m_{wr} (T_{spr} - T_{w,i}) - 2U_{cond,wc,h} (T_{w,i} - T_{c1,i}) - U_{cond,wc,v} (T_{w,i} - T_{c2,i}) \quad (3.33)$$

2. Concrete node horizontally from the tube

The equation describing the concrete node temperature horizontally from the tube is given by:

$$C_{cc1} \frac{d(T_{c1,i})}{dt} = 2U_{cond,wc,h} (T_{w,i} - T_{c1,i}) - U_{cond,cc,v} (T_{c1,i} - T_{c3,i}) \quad (3.34)$$

3. Concrete node on top of each tube

The equation describing the concrete node temperature on top of each tube is given by:

$$C_{cc2} \frac{d(T_{c2,i})}{dt} = U_{cond,wc,v} (T_{w,i} - T_{c2,i}) - 2U_{cond,cc,h} (T_{c2,i} - T_{c3,i}) - U_{cond,cflo1,v} (T_{c2,i} - T_{flo1,i}) \quad (3.35)$$

4. Concrete node on top of each concrete node horizontally from the tube

The equation describing the concrete node temperature on top of each concrete node horizontally from the tube is given by:

$$C_{cc3} \frac{d(T_{c3,i})}{dt} = 2U_{cond,cc,h} (T_{c2,i} - T_{c3,i}) + U_{cond,cc,v} (T_{c1,i} - T_{c3,i}) - U_{cond,cflo2,v} (T_{c3,i} - T_{flo2,i}) \quad (3.36)$$

5. Floor covering node on top of each tube

The equation describing the floor covering node temperature on top of each tube is given by:

$$C_{flo1} \frac{d(T_{flo1,i})}{dt} = U_{cond,cflo1,v} (T_{c2,i} - T_{flo1,i}) - 2U_{flo,h} (T_{flo1,i} - T_{flo2,i}) - U_{cond,flo1,v} (T_{flo1,i} - T_{s1,i}) \quad (3.37)$$

6. Floor covering node on top of each concrete node horizontally from the tube

The equation describing the floor covering node temperature on top of each concrete node horizontally from the tube is given by

$$C_{flo2} \frac{d(T_{flo2,i})}{dt} = U_{cond,cflo2,v} (T_{c3,i} - T_{flo2,i}) + 2U_{flo,h} (T_{flo1,i} - T_{flo2,i}) - U_{cond,flo2,v} (T_{flo2,i} - T_{s2,i}) \quad (3.38)$$

7. Floor surface node on top of each tube

The equation describing the floor surface node temperature on top of each tube is given by:

$$T_{s1,i} = T_{flo1,i} - \left(\frac{q_{r1,i}}{U_{cond,flo1,v}} \right) - \left(\frac{q_{c1,i}}{U_{cond,flo1,v}} \right) \quad (3.39)$$

8. Floor surface node on top of each concrete node horizontally from the tube

The equation describing the floor surface node temperature on top of concrete node horizontally from the tube is given by:

$$T_{s2,i} = T_{flo2,i} - \left(\frac{q_{r2,i}}{U_{cond,flo2,v}} \right) - \left(\frac{q_{c2,i}}{U_{cond,flo2,v}} \right) \quad (3.40)$$

9. Heat transfer due to radiation and convection from the floor surface on top of each tube

$$q_{r1,i} = 5 \times 10^{-8} F_{en-p} A_1 ((T_{s1,i} + 273)^4 - (T_{en} + 273)^4) \quad (3.41)$$

$$q_{c1,i} = 2.17 A_1 (T_{s1,i} - T_z)^{1.31} \quad (3.42)$$

10. Heat transfer due to radiation and convection from the floor surface on top of each concrete node horizontally from the tube

$$q_{r2,i} = 5 \times 10^{-8} F_{en-p} A_2 ((T_{s2,i} + 273)^4 - (T_{en} + 273)^4) \quad (3.43)$$

$$q_{c2,i} = 2.17 A_2 (T_{s2,i} - T_z)^{1.31} \quad (3.44)$$

11. Radiative and convective heat transfer from radiant floor slab to the zone air

$$Q_{rad,conv} = \sum_{i=1}^n (q_{r1,i} + q_{c1,i} + q_{r2,i} + q_{c2,i}) \quad (3.45)$$

The properties of the materials in the radiant floor system and the symbols used in the equations 3.33-3.45 are listed in the following Table 3.1.

Symbol	Description	Value or formula
$d_{flo}c_{flo}$ [J/(m ³ ° C)]	Density*specific heat capacity of floor covering material	8400
$d_{con}c_{con}$ [J/(m ³ ° C)]	Density*specific heat capacity of slab concrete	1.8*10 ⁶
Pr_w [-]	Prandtl number of the water	4.34
ν_w [m ² s ⁻¹]	Kinematic viscosity of water	0.658*10 ⁻⁶
k_w [W/(m ° C)]	Thermal conductivity of the water	0.649
k_t [W/(m ° C)]	Thermal conductivity of the tube	0.38
Re_w [-]	Reynolds number of the water	$Re_w = \frac{V_w \cdot d_{i,r}}{\nu_w}$
Nu_w [-]	Nusselt number of the water	if $Re_w < 2300$ $Nu_w = 4.36$ else if $Re_w \geq 2300$ & $Re_w < 10000$ $f_r = (0.79 \cdot \ln Re_w - 1.64)^{-2}$ $Nu_w = \frac{(\frac{f_r}{8} \cdot Re_w \cdot Pr_w)}{1.07 + 12.7 \cdot (\frac{f_r}{8})^{0.5} \cdot (Pr_w^{0.67} - 1)}$ else $Re_w \geq 10000$ $Nu_w = 0.023 \cdot Re_w^{0.8} \cdot Pr_w^{0.3}$
$R_{cond,t}$ [° C/W]	Thermal resistance of the tube wall	$R_{cond,t} = \frac{\ln(\frac{d_{o,r}}{d_{i,r}})}{2 \cdot \pi \cdot k_t \cdot L}$
$R_{conv,w}$ [° C/W]	Thermal resistance between water and tube wall due to convection	$R_{conv,w} = \frac{1}{Nu_w \cdot k_w \cdot \pi \cdot L}$
$R_{cond,tc,v}$ [° C/W]	Thermal resistance between the tube wall and the concrete node vertically from the tube wall	$R_{cond,tc,v} = \frac{0.25 \cdot t_p - 0.5 \cdot d_{o,r}}{k_p \cdot L \cdot d_{o,r}}$

$R_{cond,wc,h}$ [$^{\circ}$ C/W]	Thermal resistance between the water and the concrete node horizontally from the water node	$R_{cond,wc,h} = R_{conv,w} + R_{cond,t} + R_{cond,tc,h}$
$R_{cond,wc,v}$ [$^{\circ}$ C/W]	Thermal resistance between the water and the concrete node vertically from the water node	$R_{cond,wc,h} = R_{conv,w} + R_{cond,t} + R_{cond,tc,v}$
$U_{cond,wc,h}$ [W/ $^{\circ}$ C]	Thermal conductance between the water and the concrete node horizontally from the water node	$U_{cond,wc,h} = \frac{1}{R_{cond,wc,h}}$
$U_{cond,wc,v}$ [W/ $^{\circ}$ C]	Thermal conductance between the water and the concrete node vertically from the water node	$U_{cond,wc,v} = \frac{1}{R_{cond,wc,v}}$
$R_{cond,cc,v}$ [$^{\circ}$ C/W]	Thermal resistance between the concrete node in the tube layer and the concrete node in the concrete layer (vertically)	$R_{cond,cc,v} = \frac{0.25 \cdot t_p}{k_p \cdot L \cdot 0.5 \cdot (S_t - d_{o,r})}$
$R_{cond,cc,h}$ [$^{\circ}$ C/W]	Thermal resistance between the concrete node in the tube layer and the concrete node in the concrete layer (horizontally)	$R_{cond,cc,h} = \frac{0.25 \cdot S_t}{k_p \cdot L \cdot 0.5 \cdot (t_p - d_{o,r})}$
$U_{cond,cc,v}$ [W/ $^{\circ}$ C]	Thermal conductance between the concrete node in the tube layer and the concrete node in the concrete layer (vertically)	$R_{cond,cc,v} = \frac{1}{R_{cond,cc,v}}$
$U_{cond,cc,h}$ [W/ $^{\circ}$ C]	Thermal conductance between the concrete node in the tube layer and the concrete node in the concrete layer (horizontally)	$R_{cond,cc,h} = \frac{1}{R_{cond,cc,h}}$
$R_{cond,cflo1,v}$ [$^{\circ}$ C/W]	Thermal resistance between the concrete node on top of the tube node and the floor covering node	$R_{cond,cflo1,v} = \frac{0.25 \cdot t_p - 0.25 \cdot d_{o,r}}{k_p \cdot L \cdot d_{o,r}} + \frac{0.25 \cdot t_c}{k_c \cdot L \cdot d_{o,r}}$
$R_{cond,cflo2,v}$ [$^{\circ}$ C/W]	Thermal resistance between the concrete node on top of each concrete node in the tube layer and the floor covering node	$R_{cond,cflo2,v} = \frac{0.25 \cdot t_p - 0.25 \cdot d_{o,r}}{k_p \cdot L \cdot 0.5 \cdot (S_t - d_{o,r})} + \frac{0.25 \cdot t_c}{k_c \cdot L \cdot (S_t - d_{o,r})}$

$U_{cond,cflo1,v}$ [W/°C]	Thermal conductance between the concrete node on top of the tube node and the floor covering node	$U_{cond,cflo1,v} = \frac{1}{R_{cond,cflo1,v}}$
$U_{cond,cflo2,v}$ [W/°C]	Thermal conductance between the concrete node on top of each concrete node in the tube layer and the floor covering node	$U_{cond,cflo2,v} = \frac{1}{R_{cond,cflo2,v}}$
$R_{flo,h}$ [°C/W]	Thermal resistance between the floor covering nodes	$R_{flo,h} = \frac{0.25 \cdot S_t}{k_c \cdot L \cdot t_c}$
$U_{flo,h}$ [W/°C]	Thermal conductance between the floor covering nodes	$U_{flo,h} = \frac{1}{R_{flo,h}}$
$R_{cond,flo1,v}$ [°C/W]	Thermal resistance between the floor covering node in the tube layer and the floor surface node	$R_{cond,flo1,v} = \frac{0.5 \cdot t_c}{k_c \cdot L \cdot d_{o,r}}$
$R_{cond,flo2,v}$ [°C/W]	Thermal resistance between the floor covering node on top of the concrete node and the floor surface node	$R_{cond,flo2,v} = \frac{0.5 \cdot t_c}{k_c \cdot L \cdot 0.5 \cdot (S_t - d_{o,r})}$
$U_{cond,flo1,v}$ [W/°C]	Thermal conductance between the floor covering node in the tube layer and the floor surface node	$U_{cond,flo1,v} = \frac{1}{R_{cond,flo1,v}}$
$U_{cond,flo2,v}$ [W/°C]	Thermal conductance between the floor covering node on top of the concrete node and the floor surface node	$U_{cond,flo2,v} = \frac{1}{R_{cond,flo2,v}}$
C_w [J/°C]	Thermal capacitance of the water inside the radiant floor piping for each control volume	$C_w = \pi \cdot \frac{d_{i,r}^2}{4} \cdot L \cdot d_w \cdot c_w$
C_{ccl} [J/°C]	Thermal capacitance of the concrete node horizontally from the tube for each control volume	$C_{ccl} = \frac{(S_t - d_{o,r})}{2} \cdot d_{o,r} \cdot L \cdot d_{con} \cdot c_{con}$

$C_{cc2} [J/^{\circ} C]$	Thermal capacitance of the concrete node vertically from the tube for each control volume	$C_{cc2} = \frac{(t_p - d_{o,r})}{2} \cdot d_{o,r} \cdot L \cdot d_{con} \cdot c_{con}$
$C_{cc3} [J/^{\circ} C]$	Thermal capacitance of the concrete node on top of each concrete node in the tube layer for each control volume	$C_{cc3} = \frac{(t_p - d_{o,r})}{2} \cdot \frac{(S_t - d_{o,r})}{2} \cdot L \cdot d_{con} \cdot c_{con}$
$C_{flo1} [J/^{\circ} C]$	Thermal capacitance of the floor covering node on top of the tube for each control volume	$C_{flo1} = d_{o,r} \cdot t_c \cdot L \cdot d_{flo} \cdot c_{flo}$
$C_{flo2} [J/^{\circ} C]$	Thermal capacitance of the floor covering node on top of the concrete node for each control volume	$C_{flo2} = \frac{(S_t - d_{o,r})}{2} \cdot L \cdot d_{flo} \cdot c_{flo}$

Table 3.1 Physical properties and operating conditions of the radiant floor heating system

3.3.6 Ground loop heat exchanger model

A three-dimensional numerical simulation model for U-tube borehole heat exchanger is presented. The transient effects of heat transports inside the ground coupled heat exchanger are considered by analyzing each thermal capacity of borehole components: water inside the ground buried tubes, grouting material, and surrounding soil.

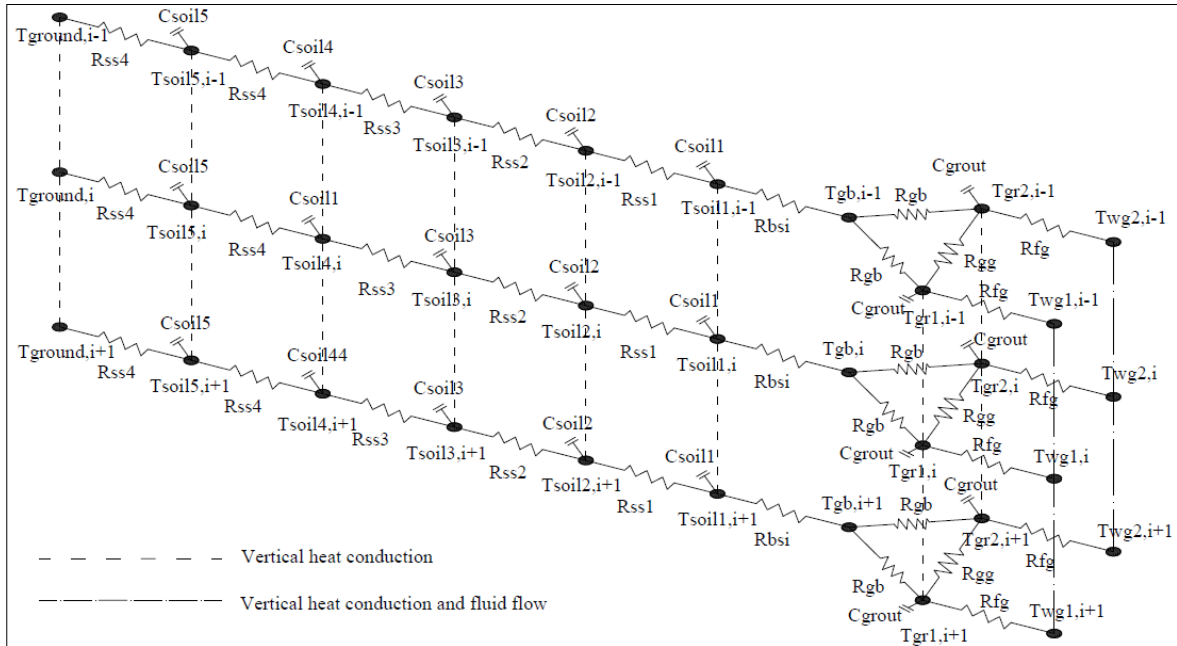


Figure 3.3.6 Thermal network analysis for the ground loop heat exchanger describing heat and mass transport processes in a vertical direction

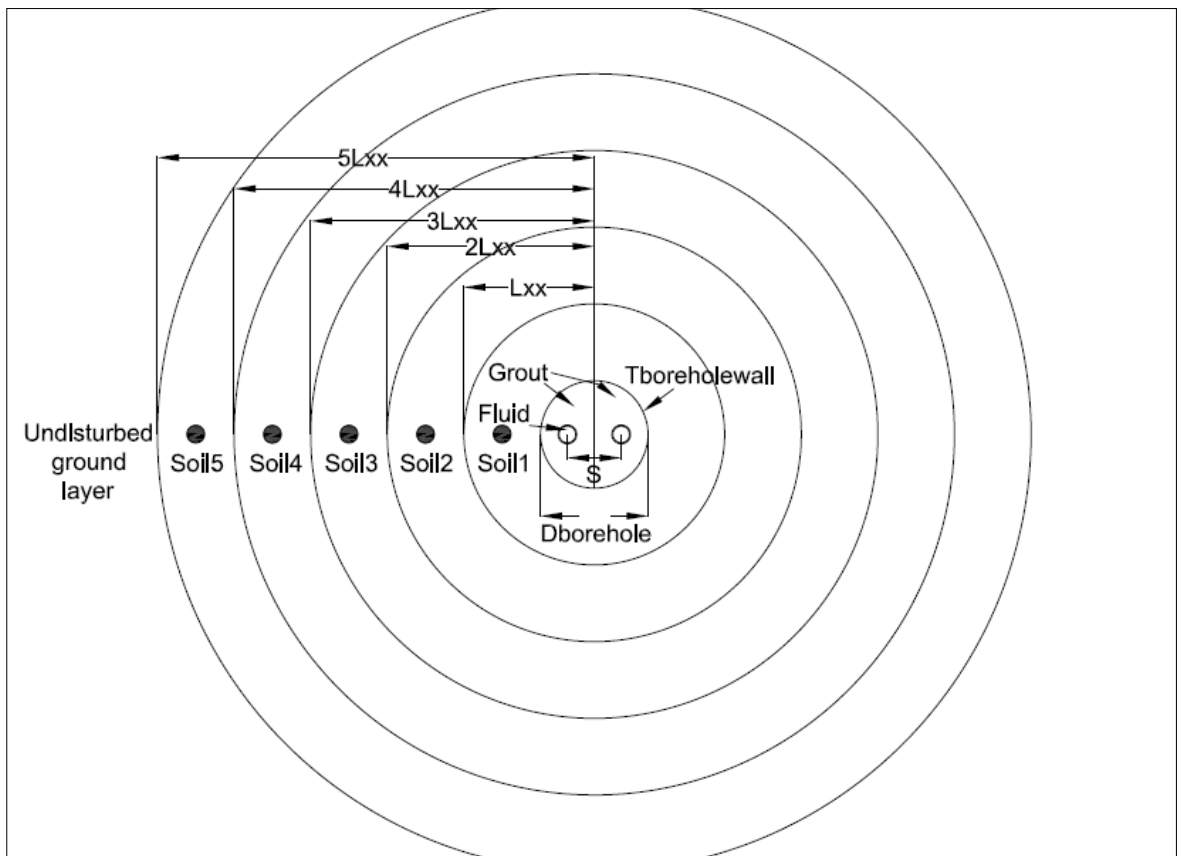


Figure 3.3.7 Horizontal cross-section view of the single U-tube

1. Fluid node inside the tube

The heat and mass transports inside the U-tube are considered by the force convection from the moving fluid, and the conduction from/to the connected grout node. In the meantime, the conduction between fluid nodes is also considered since slow water mass flow rate inside the tube is considered. While moving along the tubes, the grout nodes transfer heat to the fluid:

$$C_{fluid} \frac{d(T_{wg1,i})}{dt} = c_w m_{wg} (T_{wg1,i-1} - T_{wg1,i}) + \frac{k_f A_f (T_{wg1,i+1} - 2T_{wg1,i} + T_{wg1,i-1})}{\Delta z} + U_{fg} \Delta z (T_{gr1,i} - T_{wg1,i}) \quad (3.46)$$

$$C_{fluid} \frac{d(T_{wg2,i})}{dt} = c_w m_{wg} (T_{wg2,i-1} - T_{wg2,i}) + \frac{k_f A_f (T_{wg2,i+1} - 2T_{wg2,i} + T_{wg2,i-1})}{\Delta z} + U_{fg} \Delta z (T_{gr2,i} - T_{wg2,i}) \quad (3.47)$$

The symbols used in the equations are described in the nomenclature.

2. Grout node

In each layer, the grout nodes are connected to each other, to the borehole wall, and to the fluid nodes inside the tubes. The heat transfer equations for the grout nodes can be described:

$$C_{grout} \frac{d(T_{gr1,i})}{dt} = U_{gb} dz (T_{gb,i} - T_{gr1,i}) + \frac{k_g A_g (T_{gr1,i+1} - 2T_{gr1,i} + T_{gr1,i-1})}{\Delta z} + U_{gg} \Delta z (T_{gr2,i} - T_{gr1,i}) + U_{fg} \Delta z (T_{wg1,i} - T_{gr1,i}) \quad (3.48)$$

$$C_{grout} \frac{d(T_{gr2,i})}{dt} = U_{gb} \Delta z (T_{gb,i} - T_{gr2,i}) + \frac{k_g A_g (T_{gr2,i+1} - 2T_{gr2,i} + T_{gr2,i-1})}{\Delta z} + U_{gg} \Delta z (T_{gr1,i} - T_{gr2,i}) + U_{fg} \Delta z (T_{wg2,i} - T_{gr2,i}) \quad (3.49)$$

3. Grout wall node

The borehole wall nodes are considered as nodes without volume. Therefore, a steady-state analysis for the grout wall nodes is proposed:

$$T_{gb,i} = \frac{U_{bsi} T_{soil1,i} + U_{gb} (T_{gr1,i} + T_{gr2,i})}{U_{bsi} + 2U_{gb}} \quad (3.50)$$

4. Soil node

The soil layer is divided as 5 sub-layers, and the end nodes connected with the last soil layer nodes are considered as the undisturbed ground temperature. The heat transfer among soil nodes occur by heat conduction. Since the heat transport in the soil is always considered transient, the transport equations for the soil node are:

$$C_{soil1} \frac{d(T_{soil1,i})}{dt} = U_{ss1} \Delta z (T_{soil2,i} - T_{soil1,i}) + U_{bsi} \Delta z (T_{gb,i} - T_{soil1,i}) + \frac{k_s A_{s1} (T_{soil1,i+1} - 2T_{soil1,i} + T_{soil1,i-1})}{\Delta z} \quad (3.51)$$

$$C_{soil2} \frac{d(T_{soil2,i})}{dt} = U_{ss2} \Delta z (T_{soil3,i} - T_{soil2,i}) + U_{ss1} \Delta z (T_{soil1,i} - T_{soil2,i}) + \frac{k_s A_{s2} (T_{soil2,i+1} - 2T_{soil2,i} + T_{soil2,i-1})}{\Delta z} \quad (3.52)$$

$$C_{soil3} \frac{d(T_{soil3,i})}{dt} = U_{ss3} \Delta z (T_{soil4,i} - T_{soil3,i}) + U_{ss2} \Delta z (T_{soil2,i} - T_{soil3,i}) + \frac{k_s A_{s3} (T_{soil3,i+1} - 2T_{soil3,i} + T_{soil3,i-1})}{\Delta z} \quad (3.53)$$

$$C_{soil4} \frac{d(T_{soil4,i})}{dt} = U_{ss4} \Delta z (T_{soil5,i} - T_{soil4,i}) + U_{ss3} \Delta z (T_{soil3,i} - T_{soil4,i}) + \frac{k_s A_{s4} (T_{soil4,i+1} - 2T_{soil4,i} + T_{soil4,i-1})}{\Delta z} \quad (3.54)$$

$$C_{soil5} \frac{d(T_{soil5,i})}{dt} = U_{ss4} \Delta z (T_{groundi} - T_{soil5,i}) + U_{ss4} \Delta z (T_{soil4,i} - T_{soil5,i}) + \frac{k_s A_{s5} (T_{soil5,i+1} - 2T_{soil5,i} + T_{soil5,i-1})}{\Delta z} \quad (3.55)$$

The parameters of the ground loop model and equations used to determine the parameters are described in the following Table 3.2.

Symbol	Description	Value or formula
m_{wg} [kg/s]	Ground loop water mass flow rate	0.24
Physical properties		
k_f [W/(m° C)]	Thermal conductivity of the ground loop fluid	0.568
A_f [m ²]	Cross-sectional area of the fluid node	$A_f = \pi \cdot \frac{d_{i,g}^2}{4}$
Pr_{fluid} [-]	Prandtl number of the ground loop fluid	11.4
ν_{fluid} [m ² s ⁻¹]	Kinematic viscosity of ground loop fluid	1.535*10 ⁻⁶
Re_{fluid} [-]	Reynolds number of the ground loop fluid	$Re_{fluid} = \frac{V_{wg} \cdot d_{i,g}}{\nu_{fluid}}$
Nu_{fluid} [-]	Nusselt number of the ground loop fluid	if $Re_{fluid} < 2300$ $Nu_{fluid} = 4.36$ else if $Re_{fluid} \geq 2300$ & $Re_{fluid} < 10000$ $f_g = (0.79 \cdot \ln Re_{fluid} - 1.64)^{-2}$

		$Nu_{fluid} = \frac{\left(\frac{f_g}{8} \cdot Re_{fluid} \cdot Pr_{fluid}\right)}{1.07 + 12.7 \cdot \left(\frac{f_g}{8}\right)^{0.5} \cdot (Pr_{fluid}^{0.67} - 1)}$ <p>else $Re_{fluid} \geq 10000$</p> $Nu_{fluid} = 0.023 \cdot Re_{fluid}^{0.8} \cdot Pr_{fluid}^{0.3}$
$C_{fluid} [J/^\circ C]$	Thermal capacitance of the fluid node	$C_{fluid} = A_f \cdot dz \cdot d_w \cdot c_w$
$k_g [W/(m^\circ C)]$	Thermal conductivity of the grout	2.4
$d_g c_g [J/(m^3 \circ C)]$	Density*specific heat capacity of grout	$2.19 \cdot 10^6$
$A_g [m^2]$	Cross-sectional area of the grout node	$A_g = \frac{\pi}{4} \cdot \left(\frac{D_{bore}^2}{2} - d_{o,g}^2\right)$
$C_{grout} [J/^\circ C]$	Thermal capacitance of the grout node	$C_{grout} = d_g c_g \cdot \frac{\pi}{4} \cdot \left(\frac{D_{bore}^2}{2} - d_{o,g}^2\right) \cdot dz$
$k_s [W/(m^\circ C)]$	Thermal conductivity of the soil	2.2
$d_s c_s [J/(m^3 \circ C)]$	Density*specific heat capacity of soil	$2.21 \cdot 10^6$
$A_{s1} [m^2]$	Cross-sectional area of the soil node 1	$A_{s1} = \pi \cdot L_{xx}^2 - \pi \cdot \frac{D_{bore}^2}{4}$
$A_{s2} [m^2]$	Cross-sectional area of the soil node 2	$A_{s2} = \pi \cdot (2 \cdot L_{xx})^2 - \pi \cdot L_{xx}^2$
$A_{s3} [m^2]$	Cross-sectional area of the soil node 3	$A_{s3} = \pi \cdot (3 \cdot L_{xx})^2 - \pi \cdot (2 \cdot L_{xx})^2$
$A_{s4} [m^2]$	Cross-sectional area of the soil node 4	$A_{s4} = \pi \cdot (4 \cdot L_{xx})^2 - \pi \cdot (3 \cdot L_{xx})^2$
$A_{s5} [m^2]$	Cross-sectional area of the soil node 5	$A_{s5} = \pi \cdot (5 \cdot L_{xx})^2 - \pi \cdot (4 \cdot L_{xx})^2$
$C_{soil1} [J/^\circ C]$	Thermal capacitance of the soil node 1	$C_{soil,1} = \left(\pi \cdot L_{xx}^2 - \pi \cdot \frac{D_{bore}^2}{4}\right) \cdot dz \cdot d_s c_s$
$C_{soil2} [J/^\circ C]$	Thermal capacitance of the soil node 2	$C_{soil,2} = \left(\pi \cdot (2 \cdot L_{xx})^2 - \pi \cdot L_{xx}^2\right) \cdot dz \cdot d_s c_s$

C_{soil3} [J/°C]	Thermal capacitance of the soil node 3	$C_{soil,3} = (\pi \cdot (3 \cdot L_{xx})^2 - \pi \cdot (2 \cdot L_{xx})^2) \cdot dz \cdot d_s c_s$
C_{soil4} [J/°C]	Thermal capacitance of the soil node 4	$C_{soil,4} = (\pi \cdot (4 \cdot L_{xx})^2 - \pi \cdot (3 \cdot L_{xx})^2) \cdot dz \cdot d_s c_s$
C_{soil5} [J/°C]	Thermal capacitance of the soil node 5	$C_{soil,5} = (\pi \cdot (5 \cdot L_{xx})^2 - \pi \cdot (4 \cdot L_{xx})^2) \cdot dz \cdot d_s c_s$
R_{conv} [mK W ⁻¹]	Thermal resistance between water and tube wall due to convection	$R_{conv} = \frac{1}{Nu_{fluid} \cdot k_f \cdot \pi}$
k_{pipe} [W/(m°C)]	Thermal conductivity of the pipe	0.38
$R_{cond,1}$ [m°C/W]	Thermal resistance of the tube wall	$R_{cond,1} = \frac{\ln(\frac{d_{o,g}}{d_{i,g}})}{2 \cdot \pi \cdot k_{pipe}}$
$R_{cond,2}$ [m°C/W]	Thermal resistance between the tube wall and the grout zone	$R_{cond,2} = L_g \cdot R_g$
R_{fg} [m°C/W]	Thermal resistance between the fluid in the pipes and the grout zones	$R_{fg} = R_{conv} + R_{cond,1} + R_{cond,2}$
R_g [m°C/W]	Thermal resistance between the outer wall of one tube and the borehole wall gaining from two-dimensional heat conduction analysis and borehole geometry	$R_g = \frac{\operatorname{ar\,cosh}(\frac{D_{bore}^2 + d_{o,g}^2 - s^2}{2 \cdot \pi \cdot d_{o,g}})}{2 \cdot \pi \cdot k_g} \times (1.601 - 0.888 \cdot \frac{s}{d_b})$
R_{ar} [m°C/W]	Thermal resistance between the outer walls of two tubes	$R_{ar} = \frac{\operatorname{ar\,cosh}(\frac{2 \cdot s^2 - d_{o,g}^2}{d_{o,g}^2})}{2 \cdot \pi \cdot k_g}$
L_g [-]	The value L_g determines how the thermal resistance between the outer wall of one tube and the borehole wall R_g is divided	$L_g = \frac{\ln(\frac{\sqrt{D_{bore}^2 + 2 \cdot d_{o,g}^2}}{2 \cdot d_{o,g}})}{\ln(\frac{D_{bore}}{\sqrt{2} \cdot d_{o,g}})}$
R_{gb} [m°C/W]	Thermal resistance between the grout zones and the borehole wall	$R_{gb} = (1 - L_g) \cdot R_g$

R_{gg} [$m^{\circ} C/W$]	Thermal resistance between two grout zones	$R_{gg} = \frac{2 \cdot R_{gb} \cdot (R_{ar} - 2 \cdot L_g \cdot R_g)}{2 \cdot R_{gb} - R_{ar} + 2 \cdot L_g \cdot R_g}$
R_{bsi} [$m^{\circ} C/W$]	Thermal resistance between the soil node1 and the grout wall	$R_{bsi} = \frac{\log\left(\frac{\left(\frac{L_{bore}}{4}\right)}{\left(\frac{D_{bore}}{2}\right)}\right)}{2 \cdot \pi \cdot k_s}$
R_{ss1} [$m^{\circ} C/W$]	Thermal resistance between soil node1 and soil node2	$R_{ss1} = \frac{\log\left(\frac{1.5 \cdot L_{xx}}{\frac{L_{xx}}{2} + \frac{D_{bore}}{4}}\right)}{2 \cdot \pi \cdot k_s}$
R_{ss2} [$m^{\circ} C/W$]	Thermal resistance between soil node2 and soil node3	$R_{ss2} = \frac{\log\left(\frac{2.5 \cdot L_{xx}}{1.5 \cdot L_{xx}}\right)}{2 \cdot \pi \cdot k_s}$
R_{ss3} [$m^{\circ} C/W$]	Thermal resistance between soil node3 and soil node4	$R_{ss3} = \frac{\log\left(\frac{3.5 \cdot L_{xx}}{2.5 \cdot L_{xx}}\right)}{2 \cdot \pi \cdot k_s}$
R_{ss4} [$m^{\circ} C/W$]	Thermal resistance between soil node4 and soil node5	$R_{ss4} = \frac{\log\left(\frac{4.5 \cdot L_{xx}}{3.5 \cdot L_{xx}}\right)}{2 \cdot \pi \cdot k_s}$

Table 3.2 Geometrical data, physical properties and operating conditions of the ground loop heat exchanger

3.3.7 Heat pump model

A water-to-water heat pump is modeled based on its two major components: evaporator and condenser, and an equation-fit COP model is utilized to connect the two. The energy balance equation of the heat pump can be described as:

1. Evaporator model

$$C_e \frac{d(T_{is})}{dt} = m_{wg} c_w (T_{ig} - T_{is}) - U_{com} E_{com} (COP - 1) \quad (3.56)$$

2. Condenser model

$$C_c \frac{d(T_{rl})}{dt} = U_{com} E_{com} COP - m_{wr} c_w (T_{rl} - T_{rr}) \quad (3.57)$$

3. COP model (R410a refrigerant)

The COP model is based on the polynomial curve-fit to the manufacture's data. The data used is listed in the Appendix-B.

$$COP = \frac{E_{cond}}{E_{com}} \quad (3.58)$$

$$COP = C1 + C2 \times T_{ig} + C3 \times T_{rr} + C4 \times m_{wg} + C5 \times m_{wr} + C6 \times T_{ig}^2 + C7 \times T_{rr}^2 + C8 \times m_{wg}^2 + C9 \times m_{wr}^2 + C10 \times T_{ig} \times T_{rr} + C11 \times m_{wg} \times m_{wr} + C12 \times T_{ig} \times m_{wg} + C13 \times T_{rr} \times m_{wr} \quad (3.59)$$

3.3.8 Heat exchanger model

1. Return water nodes of the primary side:

Equation 3.60 describes the rate of heat stored in the primary side of is equal to the heat supplied by the primary piping network minus the heat transferred to secondary side.

$$C_{hl} \frac{d(T_{rel})}{dt} = c_w m_{wlp} (T_{mix} - T_{rel}) - q_{ex} \quad (3.60)$$

2. Supply water nodes of the secondary side:

The rate of heat stored in the secondary side is equal to the heat input from the primary side, minus the heat transferred to the secondary side. This is expressed in Equation 3.61

$$C_{h2} \frac{d(T_{spr})}{dt} = q_{ex} - c_w m_{wr} (T_{spr} - T_{rl}) \quad (3.61)$$

Logarithmic mean temperature difference of each heat exchanger is computed from:

$$LMTD = \frac{(T_{exp} - T_{spr}) - (T_{rel} - T_{rl})}{\ln \frac{T_{exp} - T_{spr}}{T_{rel} - T_{rl}}} \quad (3.62)$$

The rate of heat transferred is determined from:

$$q_{ex} = U_{ex} A_{ex} LMTD \quad (3.63)$$

3.3.9 Boiler model

A gas-fired condensing boiler is used in this study. The temperature of supply water of boiler is a function of the capacity of the boiler, the efficiency of boiler, mass flow rate of supply-return water and the rate of fuel consumption. The boiler efficiency is calculated by using the equation given in Li et al (2010). The energy balance equation of the boiler can be described as:

$$C_b \frac{d(T_b)}{dt} = U_f m_{f_{max}} HVEb - m_w c_w (T_b - T_{rb}) \quad (3.64)$$

The return water temperature to the boiler can be described as:

$$T_{rb} = \frac{(T_{rc} m_{wc} + T_{rel} m_{wlp})}{m_{wc} + m_{wlp}} \quad (3.65)$$

3.3.10 Heat losses from the water distribution pipe network

The heat losses from the water distribution loop are evaluated based on the boiler supply water temperature T_b , ground temperature T_g , water flow rate, pipe material, as well as

the insulation property and the total length of pipe. The pipe segments that contribute to the pipe heat losses are: from the boiler to the commercial zone supply; from the commercial zone to the boiler return; from the boiler to the heat exchanger supply; and from the heat exchanger to the boiler return. It is assumed that the heat pump unit and the heat exchanger are located inside the building. Therefore, the pipe heat losses from the ground source heat exchanger, heat pump and heat exchanger are ignored.

3.4 Open loop simulations of the system

All the component models described earlier in sections 3.1 to 3.3 were integrated to develop an overall hybrid hydronic heating system model. The model equations were solved using MATLAB. Open loop simulation runs were made to study the dynamic responses of the system. The open loop test results for the design condition are depicted in Figure 3.4.1.

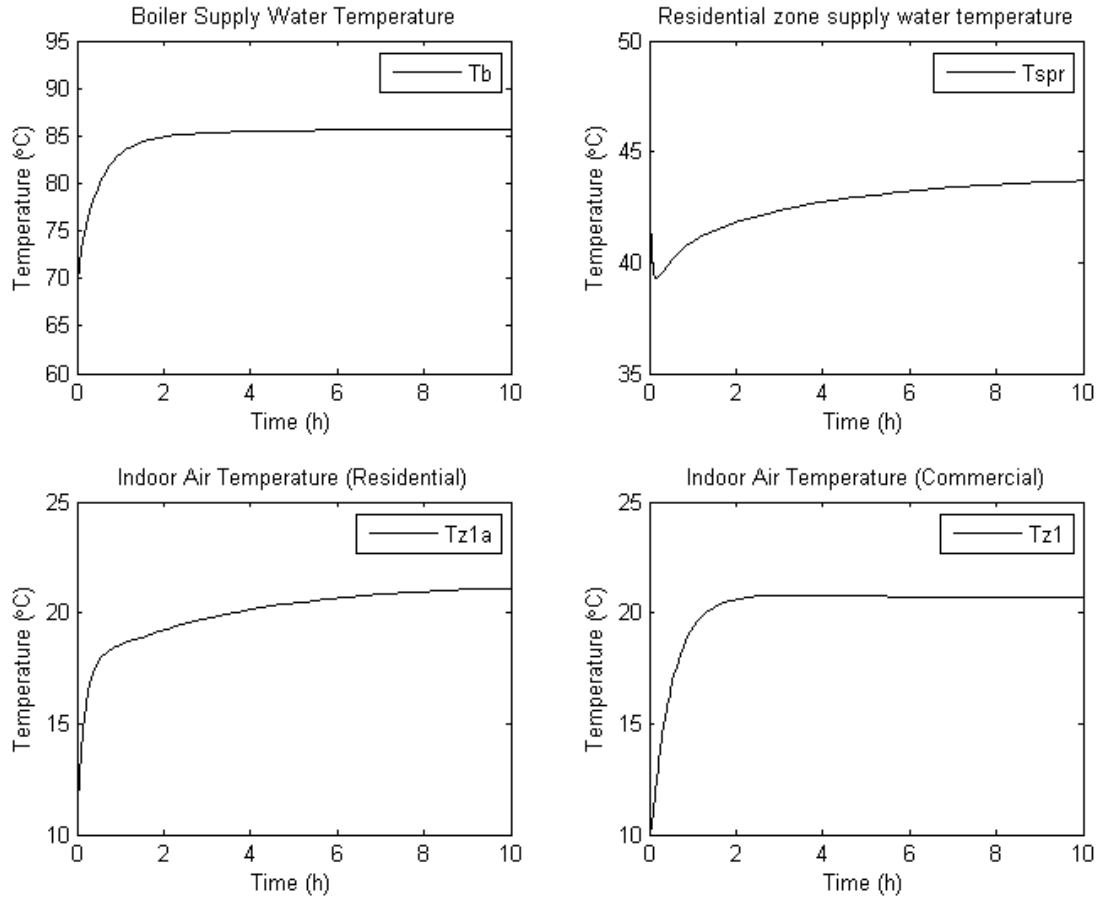


Figure 3.4.1 System open loop test at design condition (-15°C outside air temperature)

The temperature responses at design condition are depicted in Figure 3.4.1. The system was started from arbitrary initial conditions. As shown in the figure, the boiler and the heat exchanger supply temperatures reach nearly steady state in 2 hours and 7 hours, respectively, at their design loads, and the response time is affected by the thermal capacity of components and the loads acting on the system. For the residential zone 1a and commercial zone 1, the response times are 8 hours and 2 hours, respectively, which are indicative of the higher thermal mass of the radiant floor heating system than the baseboard heater system. The overall system responses are not only affected by space

heating loads but due to thermal dynamic effect of the heat pump loop interacting with the ground loop. A ten day responses of the overall system were simulated and the results are depicted in Figure 3.4.2.

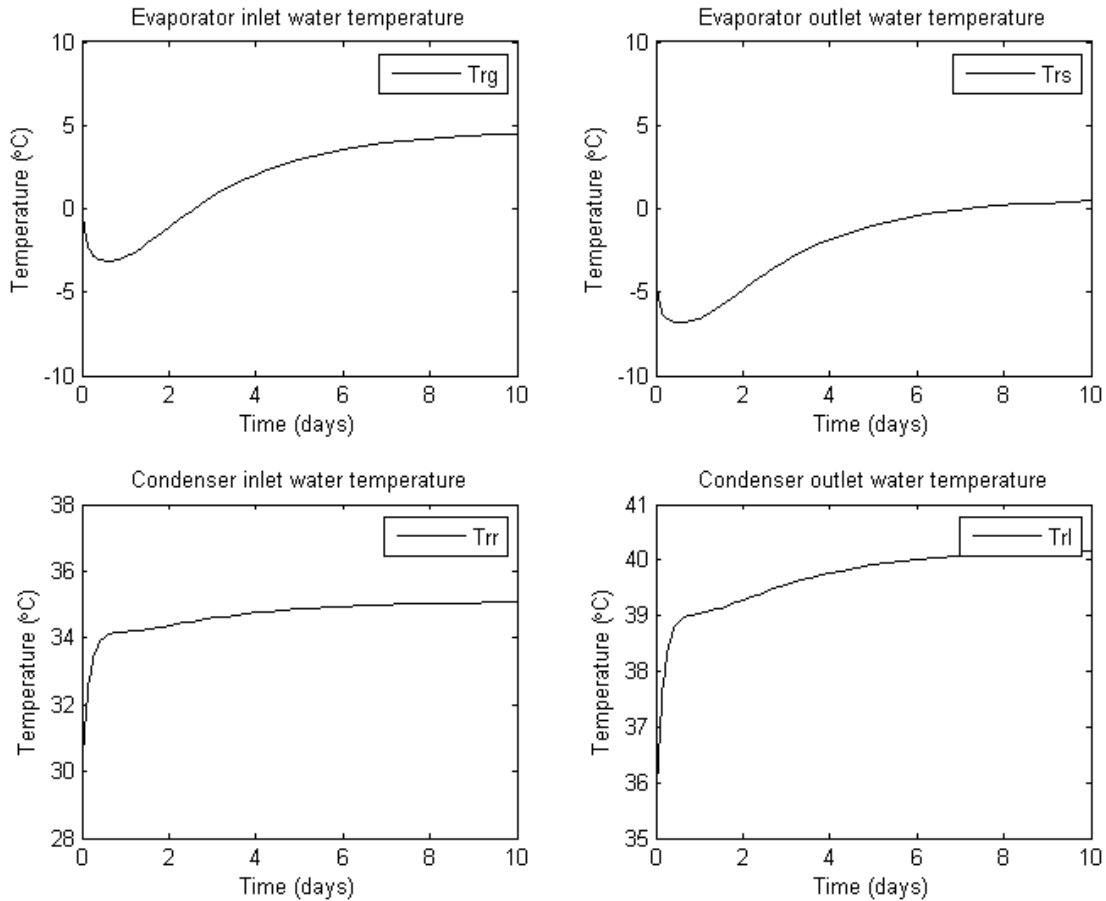


Figure 3.4.2 System open loop test for the heat pump temperature responses at design condition (-15 °C outside air temperature)

By comparing Figure 3.4.1 and 3.4.2, it can be noted that the boiler and zone temperature responses reach steady state much faster than heat pump loop temperatures. This is due to the effect of ground loop thermal interactions while the boiler and zone temperatures responses are impacted by the changers in zone loads. The heat pump-ground loop

temperature responses exhibit much slower variations that reflect large thermal capacity effect of the ground loop.

In order to improve the energy efficiency of the overall system, it would be important to reset the boiler supply water temperature and the supply water from the heat exchanger as a function of loads. To study this aspect, simulation runs were made to determine the functional relationship between boiler water temperature and the outdoor air temperature. Likewise, the heat exchanger supply water temperature as a function of outdoor air temperature was examined. The results are depicted in Figure 3.4.3. In this simulation, the outside air temperature was varied from the design condition at -15°C to the partial load condition at -5°C , and the corresponding boiler supply water temperature and the heat exchanger supply water temperature were determined.

As shown in Figure 3.4.3, the boiler temperature decreased from 87°C to 72°C when the system loads changed from full load to partial load condition. Similarly, it can be stated that the heat exchanger supply water temperature can be regulated between 45°C to 39°C to meet the zone loads of the residential building while the outdoor temperature vary from -15°C to -5°C range.

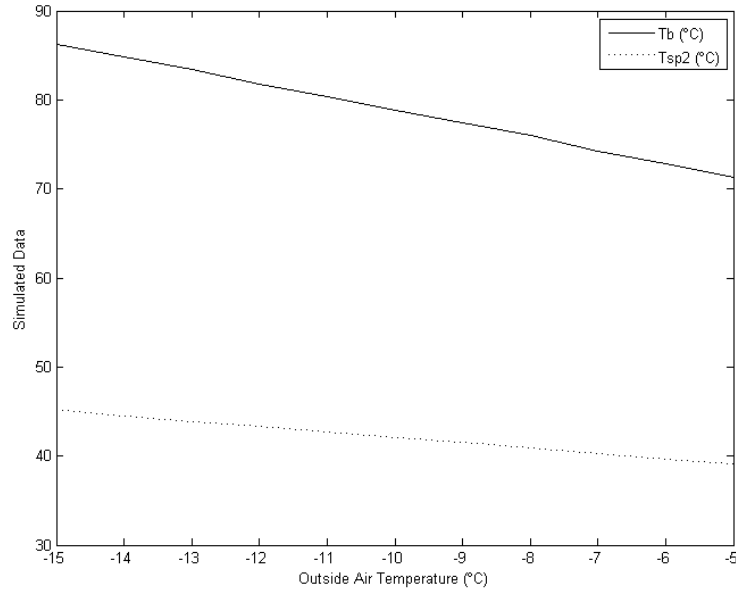


Figure 3.4.3 Supply water temperature of boiler and heat exchanger under different outside air temperature

The entering source water temperature is one of the most important factors to determine the efficiency of a heat pump. To this end, open loop simulation runs were also made to study the impact of entering ground loop water temperature on the COP of the heat pump. The entering source temperature (EST) is related to the temperature of the ground where the ground loop is installed. In terms of space heating application, a higher soil temperature will provide a higher EST and a more efficient heat pump operation. The simulation results presented in Figure 3.4.4 show that the COP increases linearly as the EST increases.

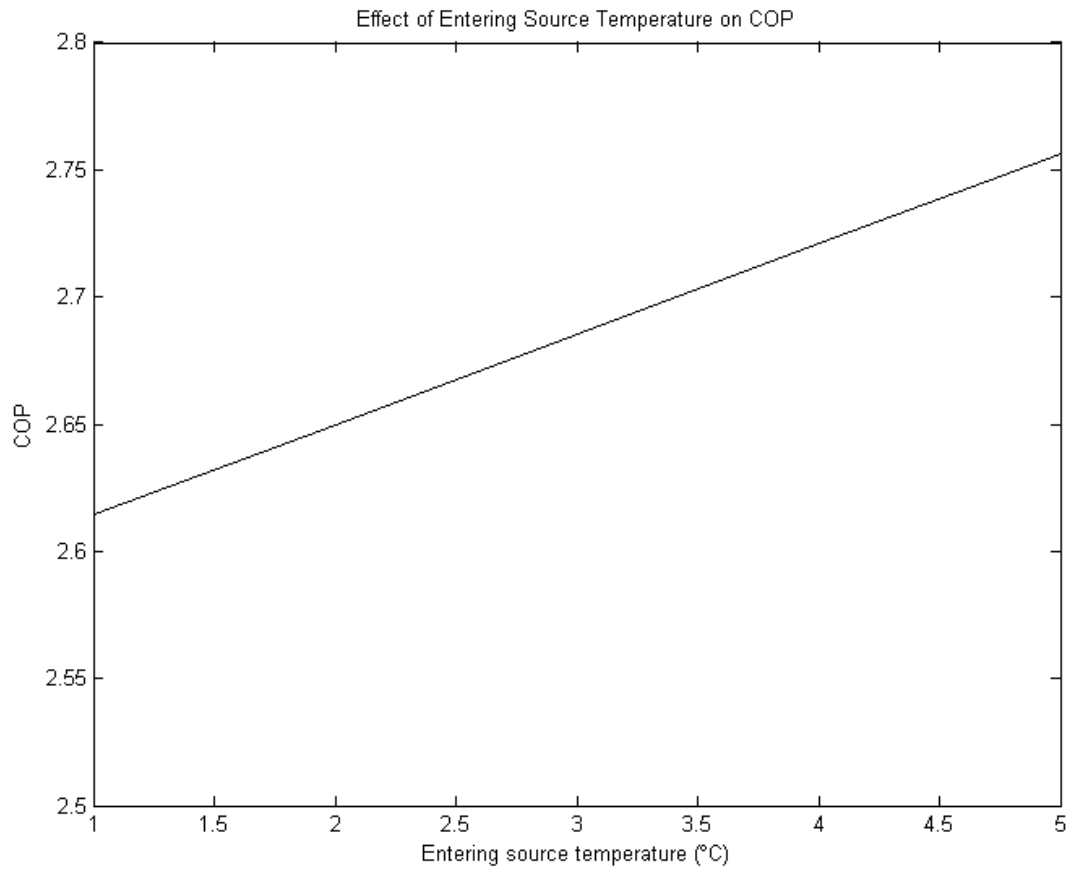


Figure 3.4.4 Effect of entering source temperature on COP

Chapter 4 Proportional-Integral and Adaptive Control of Hybrid Hydronic Heating System

4.1 Introduction

In this chapter, the design and tuning of feedback controllers are explored and the responses of the system subject to disturbances are investigated. The objective is to improve the regulation performance of the control loops of the overall hybrid hydronic heating system. Figure 4.1.1 shows the schematic diagram of a hybrid source hot water heating system supplying space heating via boiler and ground loop heat pump. Also, shown in Figure 4.1.1 are the feedback control loops. There are five loops in the system: (1) boiler control loop (Figure 4.1.2), which controls the boiler fuel supply to maintain the boiler supply water temperature at its set-point; (2) heat exchanger control loop (Figure 4.1.3), which controls the secondary side supply water temperature through the regulation of the primary side water temperature; (3) Heat pump loop (Figure 4.1.4), which controls the condenser side supply water temperature through the compressor power regulation; (4) Commercial zone water loop (Figure 4.1.5), which regulates the water flow rate according to zone air temperature change via a two way zone valve; and (5) Residential zone water loop (Figure 4.1.6), which regulates the supply water flow rate by a three way mixing valve.

The application of two types of control schemes was examined: a conventional fixed gain PI control, and an adaptive gain PI control.

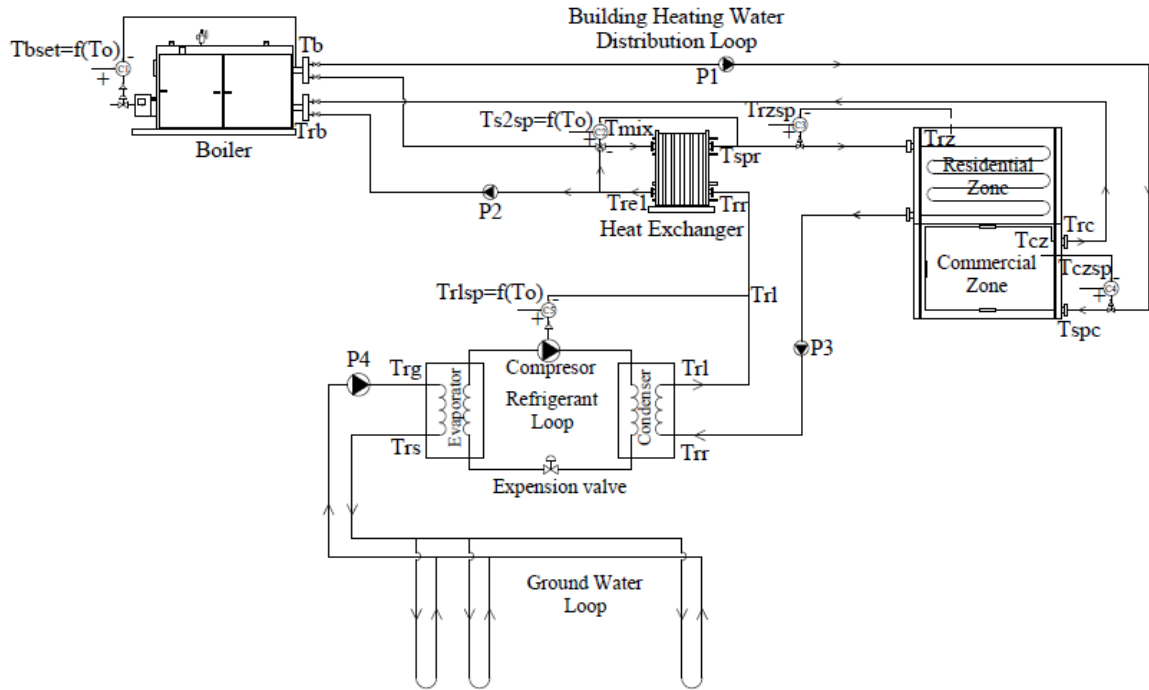


Figure 4.1.1 Schematic diagram of hybrid source hydronic heating system control loop for space heating

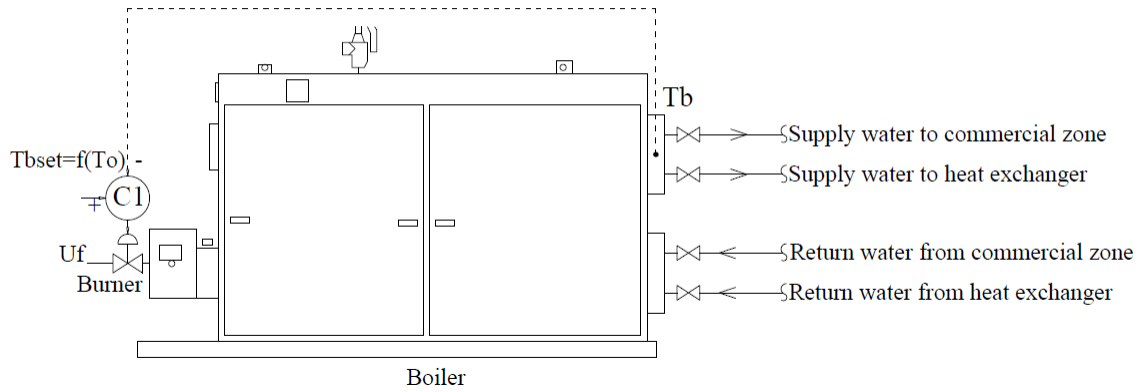


Figure 4.1.2 Boiler control loop

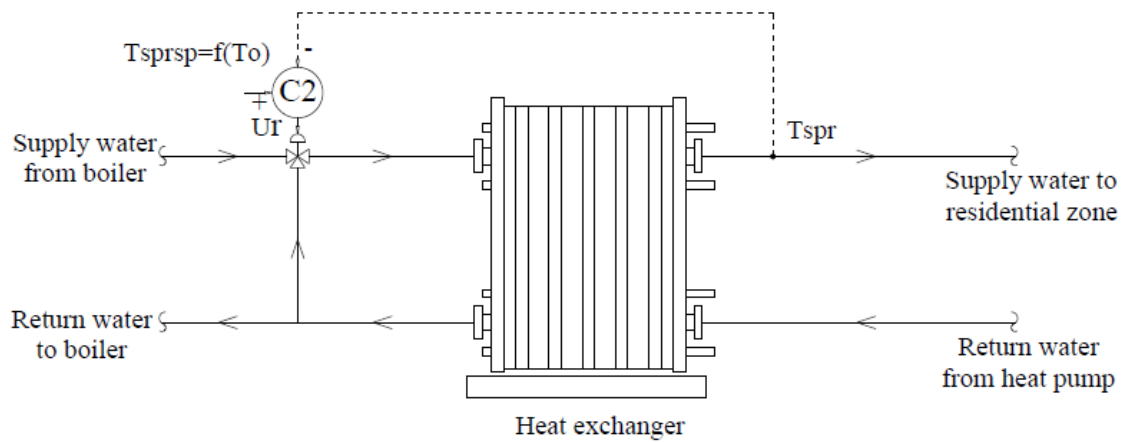


Figure 4.1.3 Heat exchanger control loop

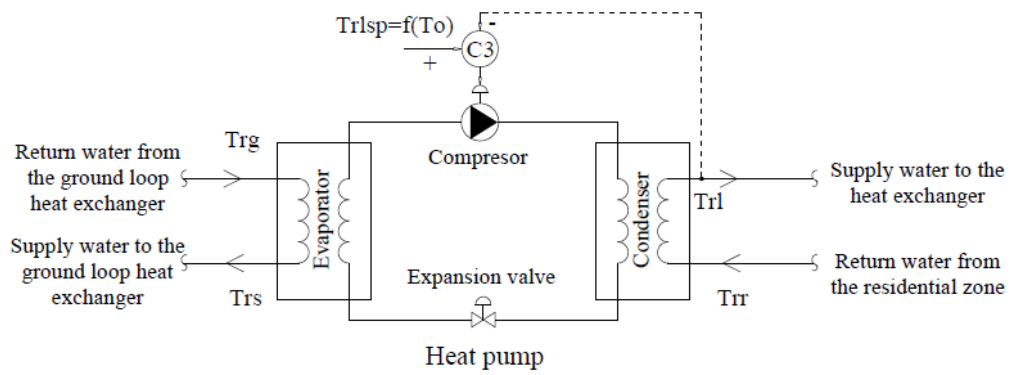


Figure 4.1.4 Heat pump control loop

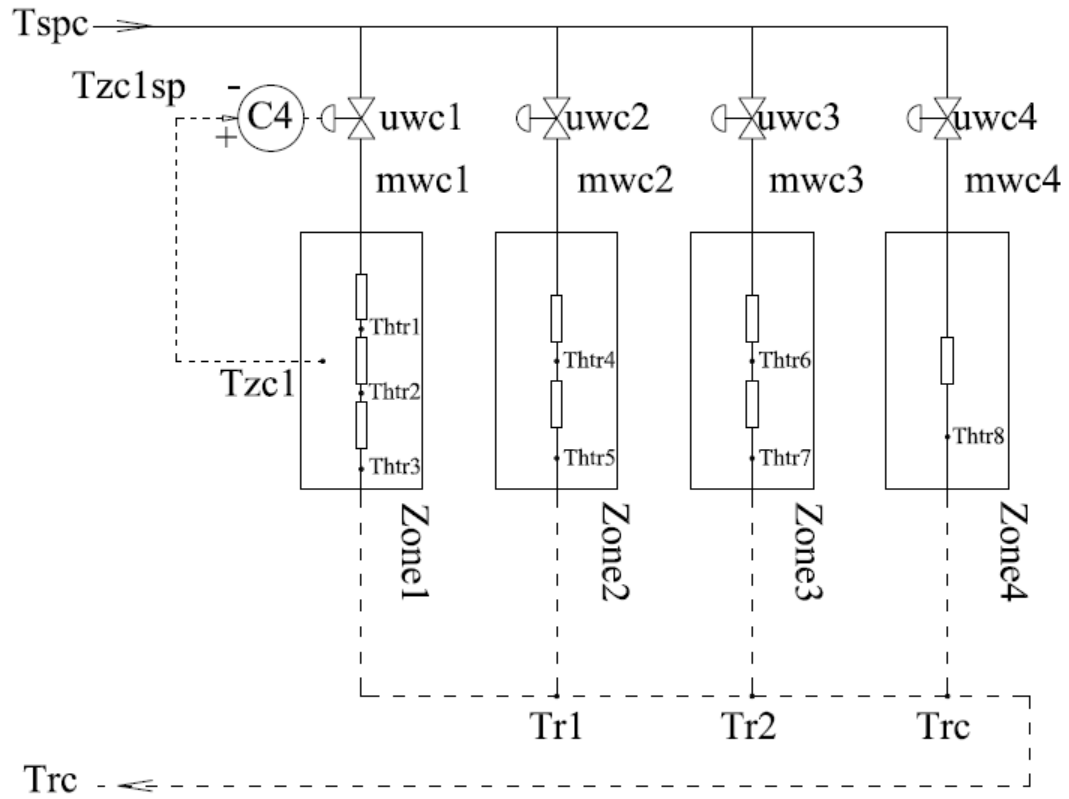


Figure 4.1.5 Commercial zone control loop

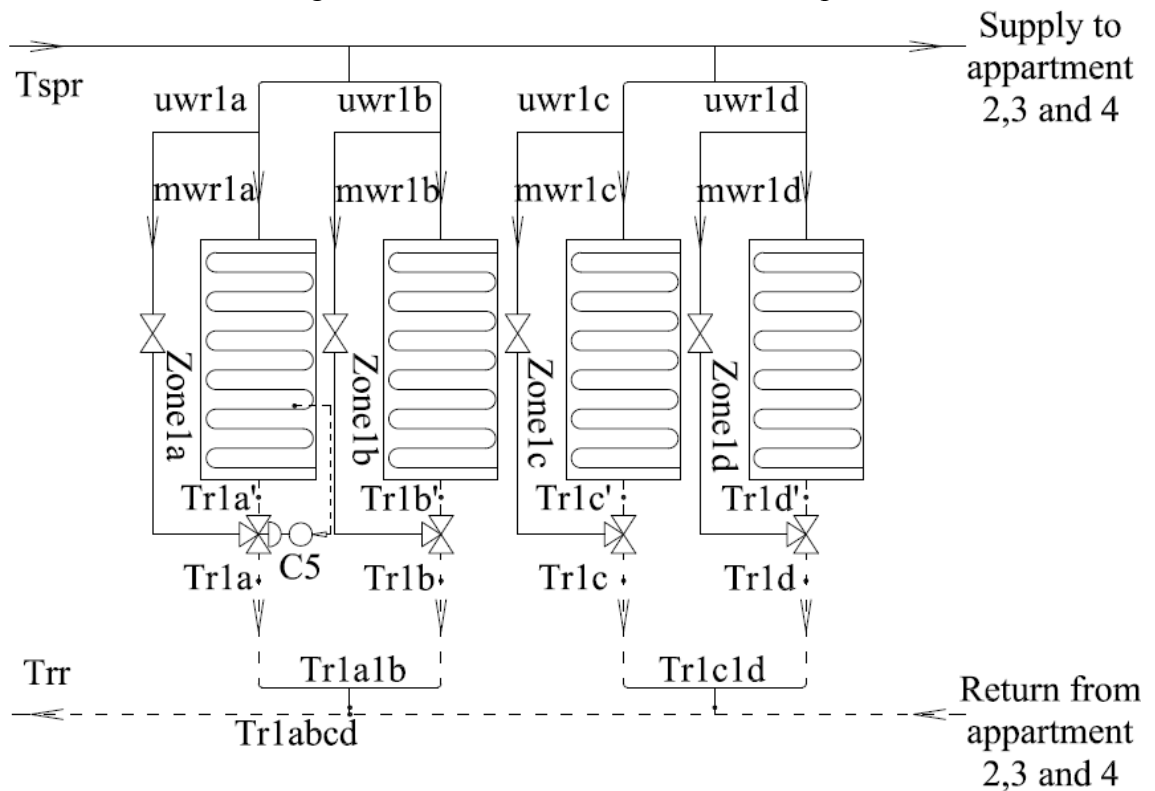


Figure 4.1.6 Residential zone control loop

4.2 The effects of load disturbances on the residential and commercial zones

The zone temperatures are affected by several disturbances such as the outdoor temperature, the thermal dynamic effects of incident or transmitted solar radiation, as well as the internal heat gain. The changes in initial conditions of the model itself can also lead to variations in zone temperature. These disturbances could occur concurrently or in several combinations. Note that most of the HVAC systems are designed at the peak load condition. As such the effects of solar heat gain and internal heat gain are not considered at the design stage. In practice, however, the buildings operate under variable load conditions which are much less than the design load conditions. To maintain zone temperatures at desired set-points under such conditions, proper design and selection of the control system is critical to maintain desirable zone air condition and to avoid unnecessary energy waste.

To carry out the simulation runs, a sinusoidal profile for the outdoor air temperature is assumed, with the mean air temperature -10°C and an amplitude 10°C . The hourly data of solar radiation is considered in both the incident and transmitted form and was modeled by using Hottel's clear sky model. The daily outdoor air temperature profile is shown in Figure 4.2.1.

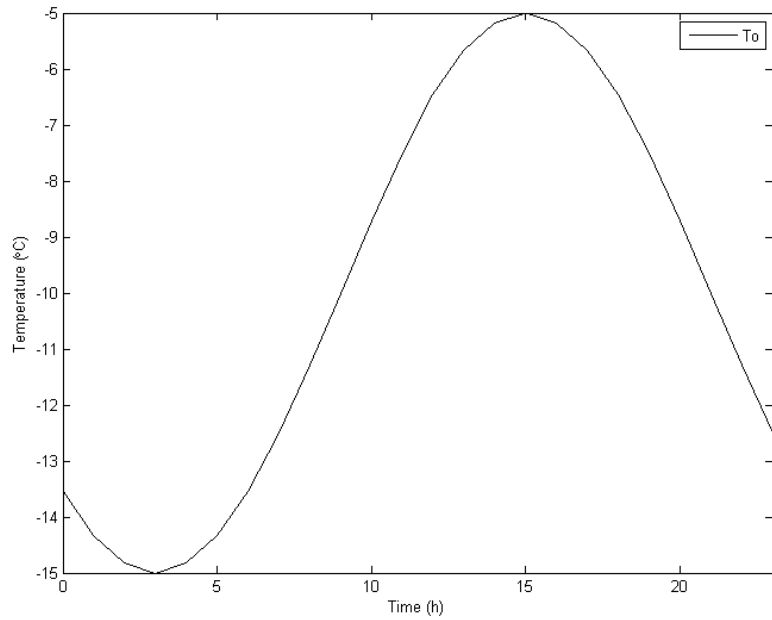


Figure 4.2.1 Outdoor air temperature profile

By applying the above outdoor air temperature profile, the temperature responses of the commercial and residential zones without control were simulated. The results are shown in Figure 4.2.2.

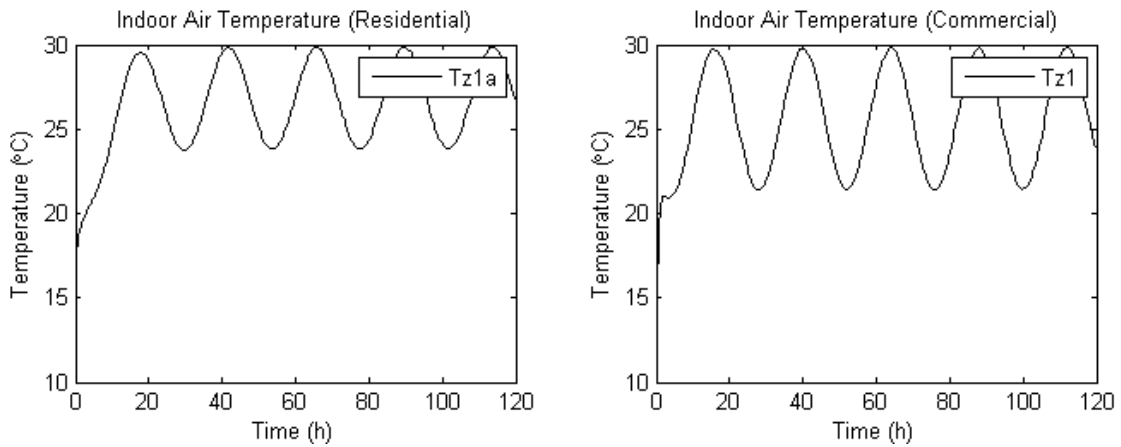


Figure 4.2.2 Residential and commercial zone air temperature responses with no control

As shown in Figure 4.2.2, the residential zone air temperature fluctuates between 24 ° C and 30 ° C, and the commercial zone air temperature fluctuates between 21 ° C and 30 ° C without control. These fluctuations will be amplified if the solar radiation and internal heat gain are also included in the simulation. The results demonstrate that it would be reasonable to expect up to 10 ° C temperature fluctuations in buildings when no control is applied when the system operates under a typical day load conditions.

4.3 Fixed gain PI control of zone air temperatures

A fixed gain PI control strategy for zone temperature control in both residential and commercial zones was studied. A well-tuned PI controller can provide satisfactory temperature regulation performance of the hydronic heating system.

The PI control algorithm can be described as:

$$U(t) = K_p(t)e(t) + K_i(t) \int e(t)dt \quad (4.1)$$

where $e(t) = T_{set} - T_{pv}$, $K_p(t)$ is the proportional gain, $K_i(t)$ is the integral gain, T_{set} is the set-point temperature, T_{pv} is the present value, and $U(t)$ is the control signal.

In the simulations, the set-point temperatures for the residential and commercial zones were assumed to be 21 ° C and 20 ° C, respectively. The set-point water temperatures for the boiler supply is 88.7 ° C, and for the residential and commercial zones are 45 ° C. Temperature responses subject to outside air temperature changes, solar heat flux and internal heat gains for the residential and commercial zones are depicted in Figure 4.3.1. The controller gains used in the simulation runs were obtained by trial-and-error. The

following set of controller gains $k_{p1a} = 2.0$, $k_{i1a} = 0.0022$, $k_{p1} = 0.8$, $k_{i1} = 0.05$ gave acceptable set-point tracking responses.

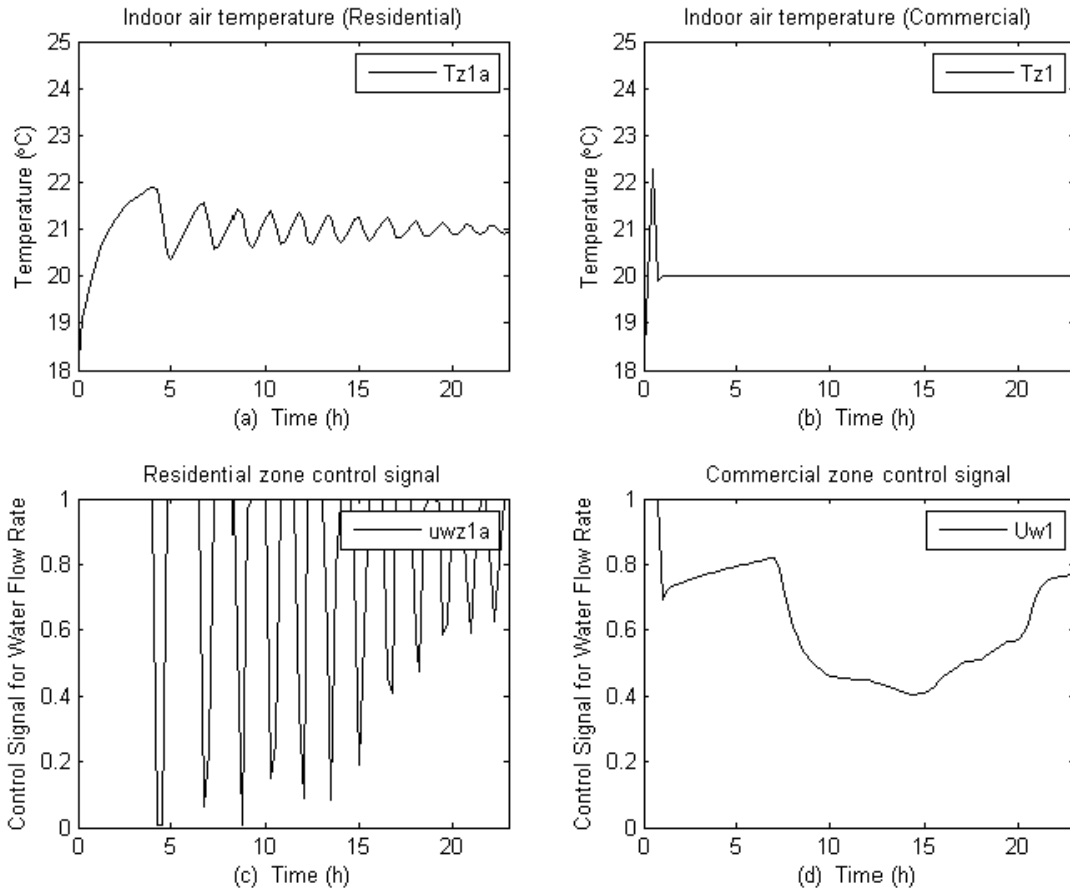


Figure 4.3.1 Validation of the constant gain values of PI controllers for the residential and commercial zone temperature control

The simulation results depicted in Figure 4.3.1 (a) and (b) show that the set-point temperatures for both residential and commercial zones can be maintained, but more noticeable oscillations were found in the residential zone. This is due to the fact that the residential RFH system has significantly higher thermal capacity as such the initial temperature in the zone impacts the control performance. The slow system response to

control input changes of the RFH system also contributes to this sluggish response. Furthermore, due to the fact that the PI controller was designed and tuned based in the most critical operation point, the responses under partial load conditions show noticeable fluctuations. To this end, an adaptive control scheme is proposed to improve the controller performance.

4.4 Simulation results for the adaptive PI control

A well-tuned fixed gain PI controller can provide good disturbance rejection, such as due to changes in initial conditions and ambient air temperature, as well as the thermal dynamic effects of absorbed solar radiation fluxes. Nevertheless, due to nonlinear dynamics of the system and unknown external disturbances, reliance on fixed gain PI controller to achieve good temperature control remains a challenging problem. To this end, an adaptive controller has been designed and implemented to improve control performance of the system. Instead of using trial-and-error approach to find the gains, the adaptive PI control considers both input and output to define and update the gains.

The adaptive gain PI control algorithm was described as:

$$U(t) = \alpha K_{ap}(t)e(t) + \beta K_{ai}(t) \int e(t)dt + k_o(T_{om} - T_o) \quad (4.2)$$

where $K_{ap}(t)$ is the adaptive proportional gain, which is given by:

$$K_{ap}(t) = \frac{a_z(T_{zri} - T_o)}{c_w m_{wr}(T_{spr} - T_{w,i})}, \quad (4.3)$$

a_z is the zone heat loss coefficient, T_{spr} and $T_{w,i}$ are the supply and return water temperature of the zone, T_{zri} and T_o are the zone air temperature and outside air temperature.

$K_{ai}(t)$ is the adaptive integral gain which is reset when the error build up exceeds large value. When the controller is settled and the present value is close to the set-point, an adaptive gain $K_{ai}(t)$ is applied to eliminate the steady-state error. A preview action term $k_o(T_{om} - T_o)$ is also included in the adaptive control algorithm, where k_o is the predictive gain of the outside air temperature, T_{om} is the mean ambient air temperature, and T_o is the present ambient air temperature. α and β are the multiplier of the proportional and integral terms.

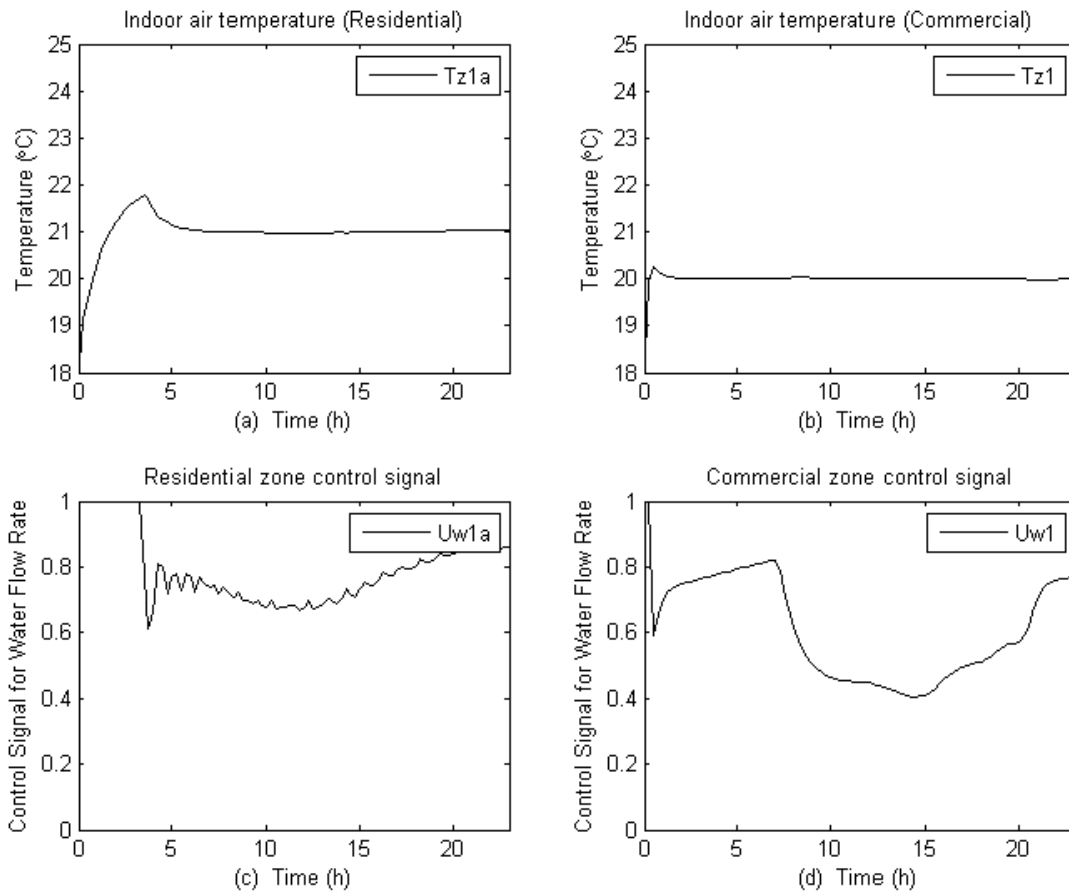


Figure 4.4.1 Responses of the adaptive PI controllers for the residential and commercial zones temperature control

The responses of the adaptively controlled system are shown in Figure 4.4.1. Compared with the constant gain PI controller performance (Figure 4.3.1) under same operating conditions, the adaptive PI control shows better disturbance rejection and higher stability (Figure 4.4.1).

Moreover, when a sudden step change is applied, such as an increase or decrease in set-point temperature of the zone, the controller responds in a stable and smooth manner as shown in Figure 4.4.2. The simulations were conducted at two different outdoor air

temperature profiles (one ranging between -15°C and -5°C to simulate a cold-day; and the other ranging from -5°C to 5°C , representing a mild winter day condition) were applied for this analysis. Zone temperature set-points in buildings were assumed to be 19°C during the first 10 hours, and set forward to 21°C for the remainder of the day.

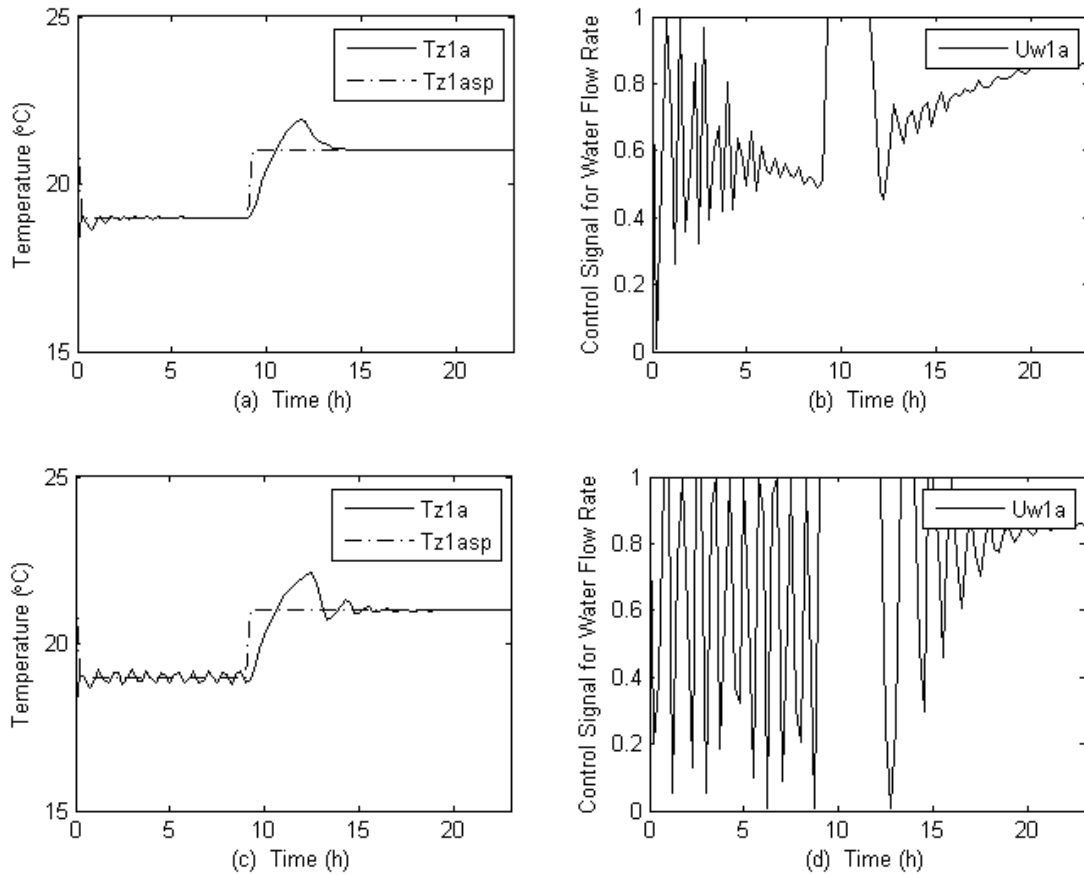


Figure 4.4.2 Comparison of controller responses with adaptive control (a-b) and fixed gain control (c-d) for the residential zone subject to step change in 2°C and a outside air temperature profile from -15°C to -5°C

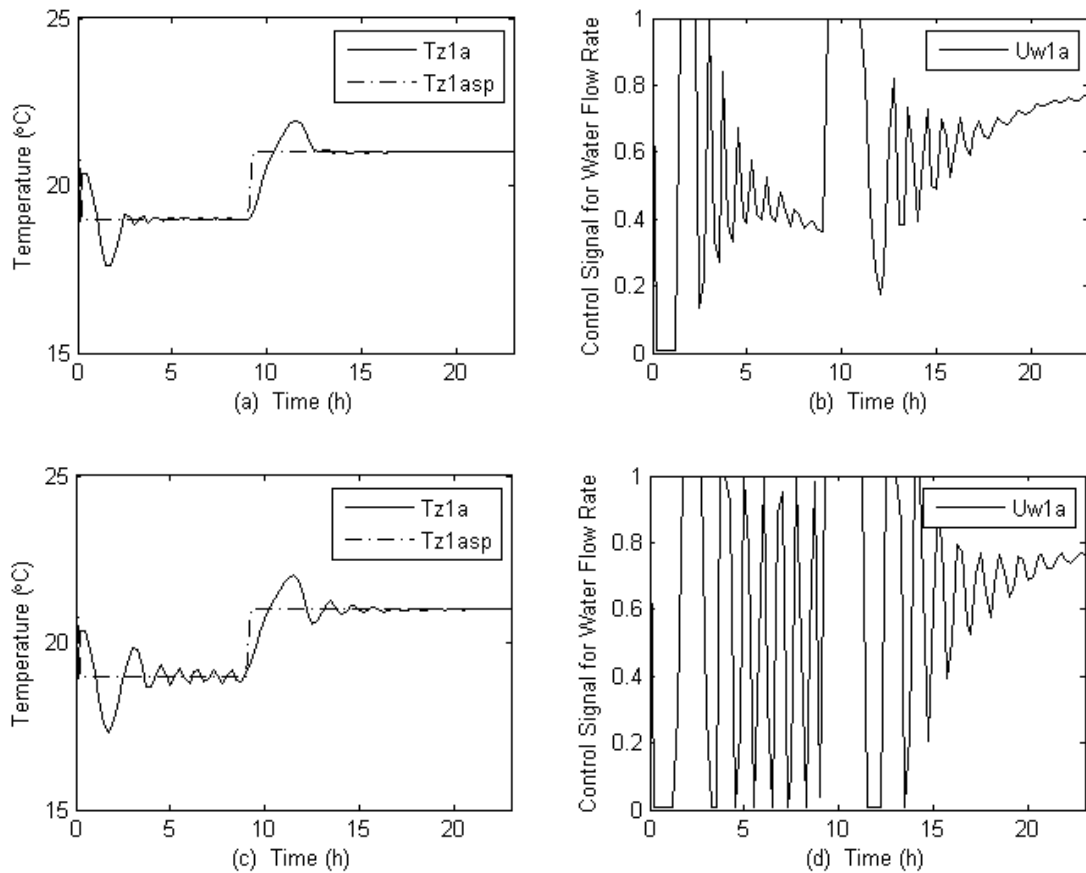


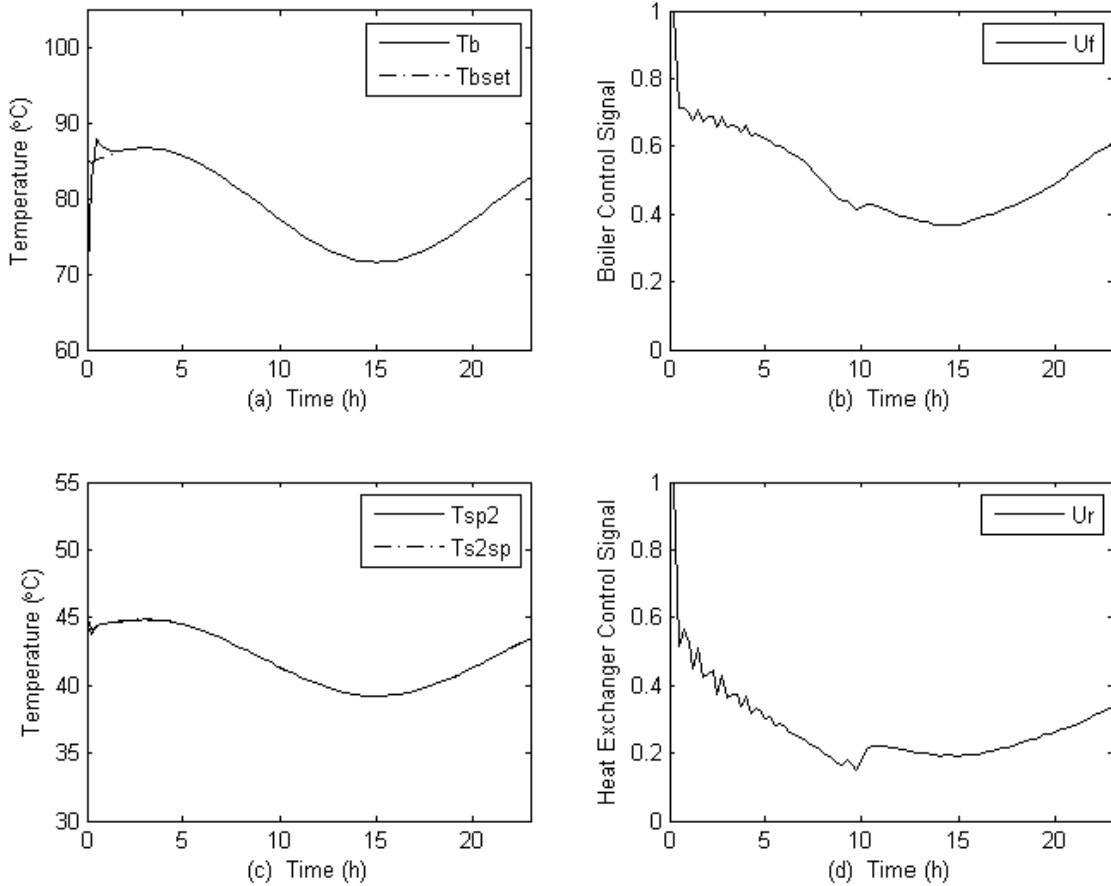
Figure 4.4.3 Comparison of controller responses with adaptive control (a-b) and fixed gain control (c-d) for the residential zone subject to step change in 2°C and a outside air temperature profile from -5°C to 5°C

The manner in which the adaptive controller brings the zone temperatures from a lower set-point to a higher set-point is depicted in Figure 4.4.1 (a), (b) and Figure 4.4.2 (a), (b) for two cases with different outdoor air temperature profiles. Also shown in Figure 4.4.2 (c) (d) and Figure 4.4.2 (c) (d) are the responses obtained from the fixed gain controller. Due to the fact that the controller is designed and tuned for high load condition, under low load conditions when outside air temperature is higher and and/or zone set-point temperature is lower, oscillations in zone temperature may occur because of the nonlinear

dynamics of the systems. A remedy to this problem is to make the controller adaptive with the operating conditions so that during the whole operating range, stable and fast temperature responses of the zone air can be achieved

The responses presented in Figure 4.4.2 and 4.4.3 show that the adaptive controller performance is better than the fixed gain PI controller and responds to change in set-point smoothly.

The adaptive control strategy was further implemented into other control loops, such as the boiler loop, the heat exchanger loop, and the heat pump loop. The performance evaluation of adaptive control for these control loops are shown in Figure 4.4.4.



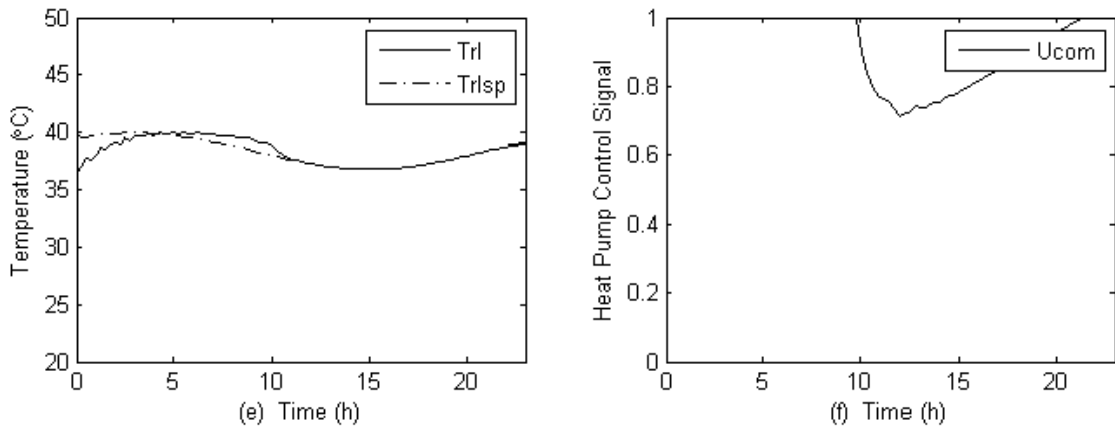


Figure 4.4.4 Temperature responses of the boiler, heat exchanger, and heat pump control loops for adaptive control

Figure 4.4.4 shows the adaptive control responses of the boiler temperature, heat exchanger temperature and the return water temperature through the heat pump loop corresponding to a typical day simulation result. As can be noted, the controller is adapting very well to diurnal load changes that occur during a typical day operation and variable set-points.

Chapter 5 Control Strategies for Improved Energy Efficiency of Hybrid Hydronic Heating System

5.1 Introduction

Several control strategies were investigated to improve the energy efficiency of the hybrid hydronic heating system. Energy simulations runs were conducted under different operating conditions. A conventional fixed set-point PI control was used as the base case control strategy. In this case, supply water temperatures of boiler, heat pump and heat exchanger are pre-determined and kept constant according to the historical performance data. Also, an outdoor reset control strategy was developed in a way that the rate of heat delivery to the building can be adjusted to match the building heat losses. Finally, an optimal set-point control strategy is proposed to minimize the overall energy consumption of the system while maintaining desirable zone air temperature.

5.2 Conventional fixed set-point control strategy

A conventional fixed set-point PI control strategy is presented as the base case. Here, the supply water temperatures of boiler, heat pump and heat exchanger are pre-determined and kept constant. The set-point temperature of boiler supply is 88.7 ° C, and the supply temperatures for both heat exchanger and heat pump were set at 45 ° C. The set-point temperatures for both residential and commercial zones were 21 ° C. Under these

conditions, the zone temperature responses and control valve responses are shown in

Figure 5.2.1.

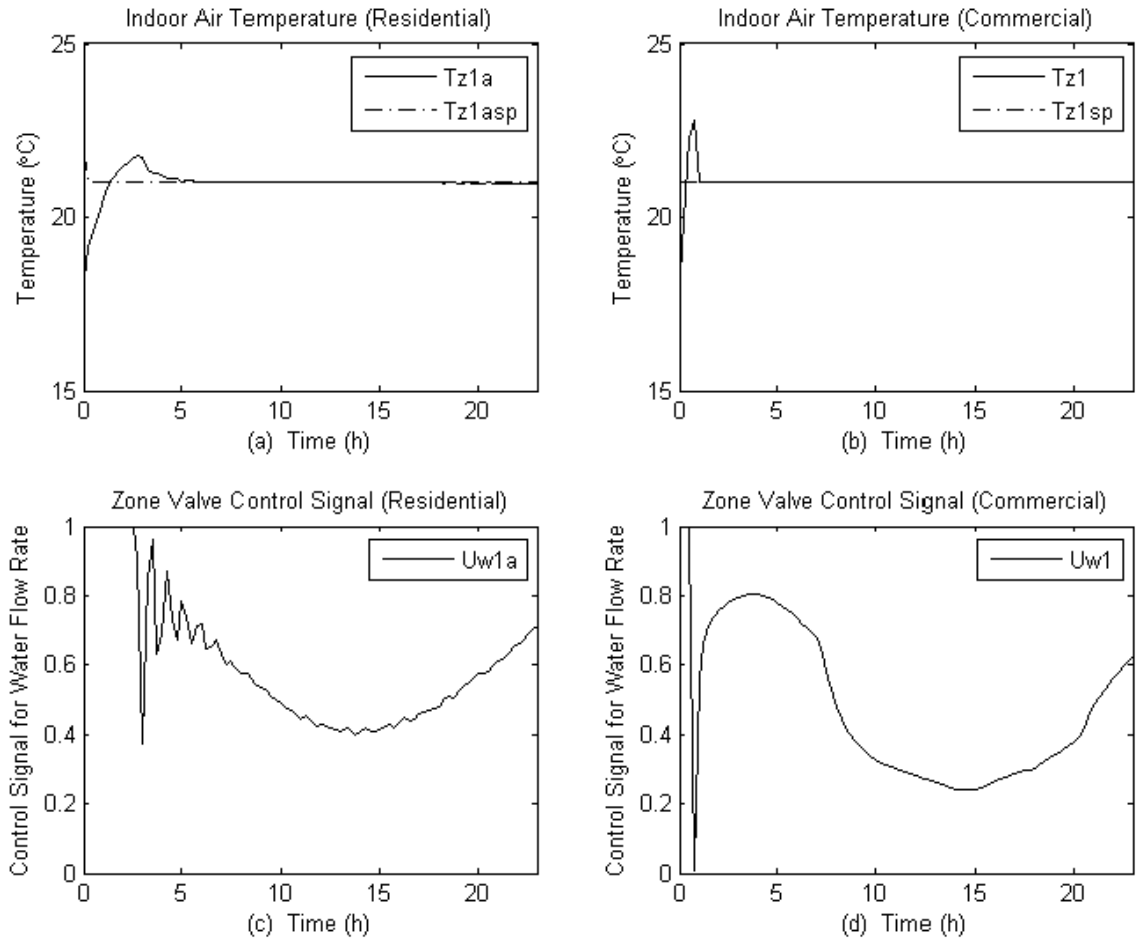


Figure 5.2.1 Output responses of residential and commercial zone (fixed set-point control strategy)

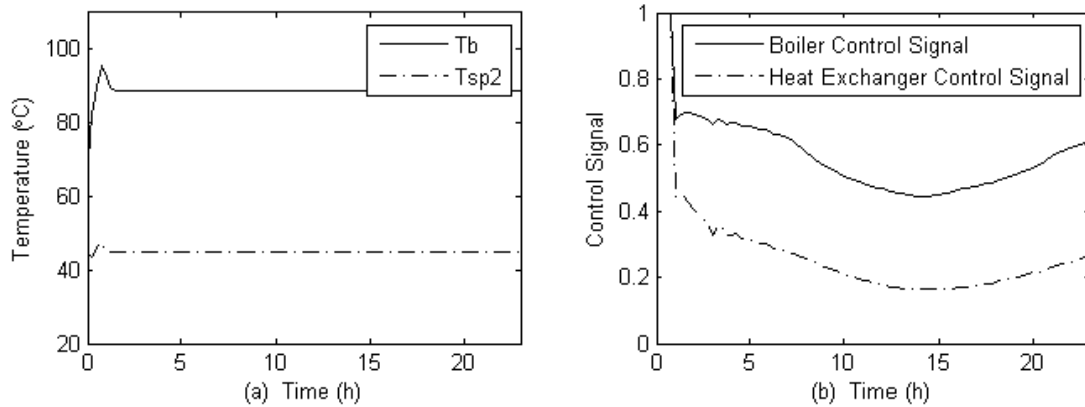


Figure 5.2.2 Output responses of boiler and heat exchanger (fixed set-point control strategy)

The results show that a well tuned PI controller can maintain zone and boiler temperatures at their respective set-point in the presence of disturbances acting on the system.

5.3 Outside air temperature reset control strategy

An outside air temperature reset control strategy is developed to continually adjust the rate of heat delivery to the zone to match the zone heat loads. To simplify the control process, same set-point temperatures for the heat exchanger and the heat pump supply were applied in this simulation. A series of open loop tests were conducted to determine the target set-point water temperature as a function of the outside air temperature. Figure 5.3.1 shows the change of the supply water temperature set-point as a function of the outside air temperature.

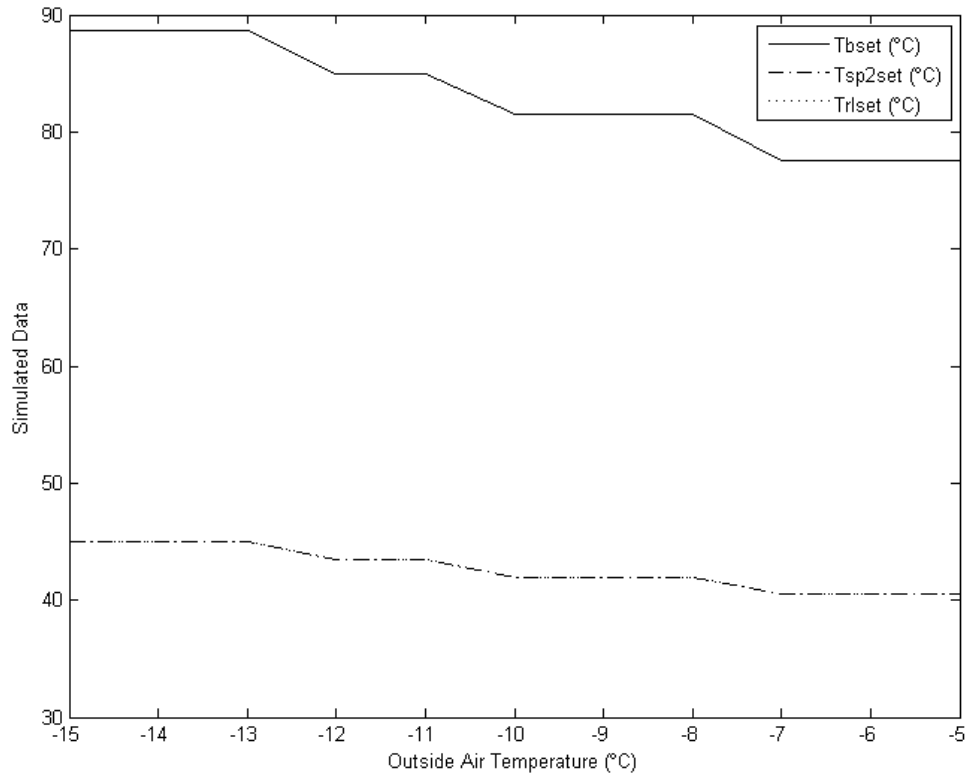


Figure 5.3.1 Outside temperature reset profile of boiler, heat exchanger and heat pump

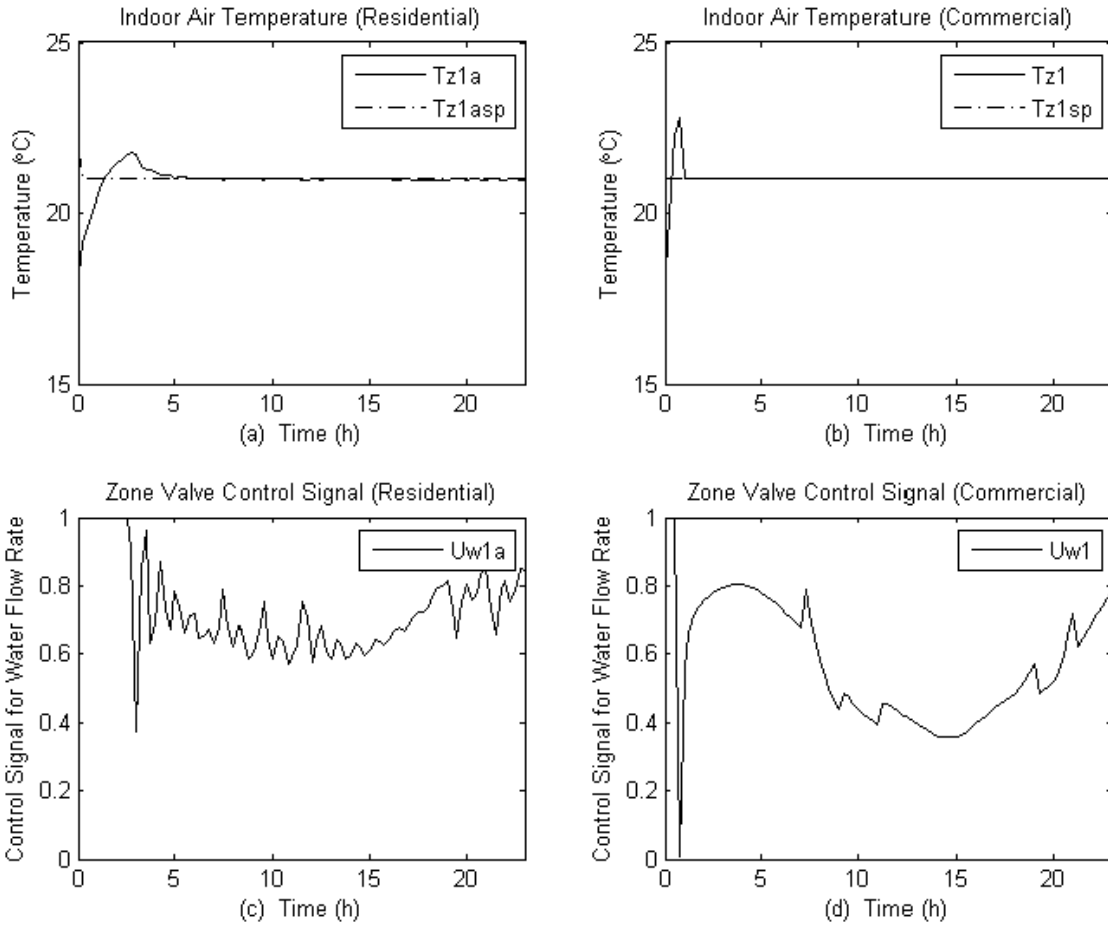


Figure 5.3.2 Output responses of residential and commercial zone (outside air temperature reset control strategy)

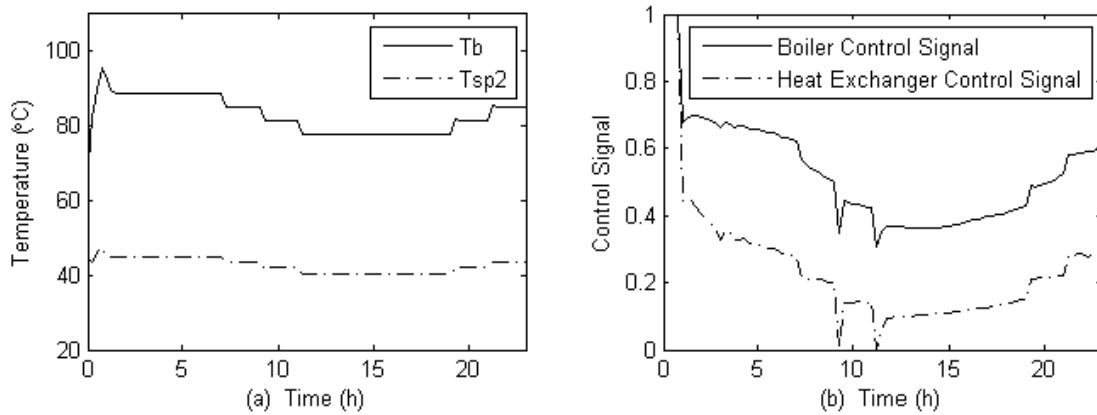


Figure 5.3.3 Output responses of boiler and heat exchanger (outside air temperature reset control strategy)

The outside air temperature is used as the basis for determining an ideal “target” water temperature to be supplied to the system’s heat emitters. As shown in Figure 5.3.2 (a) and (b), both the residential and commercial zones can be maintained at desirable set-points.

It can be noted from Figure 5.3.3 (a) that the boiler temperature is reset throughout the day as a function of outside air temperature. Compared to fixed set-point temperature control strategy (Figure 5.2.2 a), the boiler temperature in the reset control strategy remains lower.

5.4 Optimal set-point control strategy

In order to obtain optimal set-points for the boiler, heat exchanger, and heat pump supply water temperatures, an optimization problem was formulated and solved.

A multi-variable constraint optimization technique for energy optimized operation was applied to determine the steady state optimal set-point temperature. The set-point supply water temperature of boiler, heat exchanger, and heat pump were determined by using a simplified aggregated system model with 25 steady state equations. The aggregated model was compared with the full-order model developed in Chapter 3.

The objective function to be minimized was set up based on three main considerations: (1) the energy input to the boiler and to the heat pump compressor are to be minimized, (2) the zone air temperature should be always maintained close to the set-point, and (3) the upper and lower bounds for each parameter should not be exceeded. To this end, the objective function J was defined as:

$$J = U_f m_{f_{\max}} HVeb + U_{com} E_{com} COP + \gamma(T_{zr,agg} - T_{rset})^2 + \phi(T_{zc,agg} - T_{cset})^2 \quad (5.1)$$

The simplified aggregate model equations, expressed as steady state constraints are shown in the following:

$$\frac{Q_{rad,conv,agg} = A_{winr,agg} U_{win} (T_{zr,agg} - T_o) - A_{wnr,agg} U_w (T_{zr,agg} - T_o) + A_{ceil,agg} U_{ceil} (T_{zr,agg} - T_o) + ACH \times Vol_{agg} \times c_{air} \rho_{air} (T_{zr,agg} - T_o)}{3600} \quad (5.2)$$

$$c_w m_{wr,agg} (T_{spr,agg} - T_{rer,agg}) = 2U_{cond,wc,h,agg} (T_{rer,agg} - T_{c1,agg}) + U_{cond,wc,v,agg} (T_{rer,agg} - T_{c2,agg})$$

$$2U_{cond,wc,h,agg} (T_{rer,agg} - T_{c1,agg}) = U_{cond,cc,v,agg} (T_{c2,agg} - T_{c3,agg}) \quad (5.3)$$

$$U_{cond,wc,v,agg} (T_{rer,agg} - T_{c2,agg}) = 2U_{cond,cc,h,agg} (T_{c2,agg} - T_{c3,agg}) + U_{cond,cflo,v,agg1} (T_{c2,agg} - T_{flo1,agg}) \quad (5.4)$$

$$U_{cond,cflo,v,agg2} (T_{c3,agg} - T_{flo2,agg}) = 2U_{cond,cc,h,agg} (T_{c2,agg} - T_{c3,agg}) + U_{cond,cc,v,agg} (T_{c1,agg} - T_{c3,agg}) \quad (5.5)$$

$$U_{cond,cflo,v,agg1} (T_{c2,agg} - T_{flo1,agg}) = 2U_{cond,flo,h,agg} (T_{flo1,agg} - T_{flo2,agg}) + U_{cond,flo,v,agg} (T_{flo1,agg} - T_{s1,agg}) \quad (5.6)$$

$$U_{cond,flo,v,agg2} (T_{flo2,agg} - T_{s2,agg}) = 2U_{cond,flo,h,agg} (T_{flo1,agg} - T_{flo2,agg}) + U_{cond,cflo,v,agg2} (T_{c3,agg} - T_{flo2,agg}) \quad (5.7)$$

$$T_{s1,agg} = T_{flo1,agg} - \left(\frac{q_{r1,agg}}{U_{cond,flo,v,agg}} \right) - \left(\frac{q_{c1,agg}}{U_{cond,flo,v,agg}} \right) \quad (5.8)$$

$$T_{s2,agg} = T_{flo2,agg} - \left(\frac{q_{r2,agg}}{U_{cond,flo,v,agg2}} \right) - \left(\frac{q_{c2,agg}}{U_{cond,flo,v,agg2}} \right) \quad (5.9)$$

$$c_w m_{wc,agg} (T_{spc,agg} - T_{rec,agg}) = A_{winc,agg} U_{win} (T_{zc,agg} - T_o) + A_{wnc,agg} U_w (T_{zc,agg} - T_o) + \frac{ACH \times Vol_{agg} \times c_{air} \rho_{air} (T_{zc,agg} - T_o)}{3600} \quad (5.10)$$

$$c_w m_{wc,agg} (T_{spc,agg} - T_{rec,agg}) = U_{htr,agg} \left(\frac{T_{spc,agg} + T_{rec,agg}}{2} - T_{zc,agg} \right)^{1+n} \quad (5.11)$$

$$q_{ex} = c_w m_{w1p,agg} (T_{mix,agg} - T_{rel,agg}) \quad (5.12)$$

$$c_w m_{wr,agg} (T_{spr,agg} - T_{rl,agg}) = q_{ex} \quad (5.13)$$

$$q_{ex} = U_{ex} ALMTD \quad (5.14)$$

$$LMTD = \frac{(T_{exp,agg} - T_{spr,agg}) - (T_{rel,agg} - T_{rl,agg})}{\ln \frac{T_{exp,agg} - T_{spr,agg}}{T_{rel,agg} - T_{rl,agg}}} \quad (5.15)$$

$$T_{mix,agg} = \frac{U_r m_{w1p,agg} T_{exp,agg} + (1 - U_r) m_{w1p,agg} m_{w1p,agg}}{U_r m_{w1p,agg} + (1 - U_r) m_{w1p,agg}} \quad (5.16)$$

$$m_{wg,agg} c_w (T_{rg,agg} - T_{rs,agg}) = U_{com} E_{com} (COP - 1) \quad (5.17)$$

$$U_{com} E_{com} COP = m_{wr,agg} c_w (T_{rl,agg} - T_{rer,agg}) \quad (5.18)$$

$$COP = \frac{E_{cond}}{E_{com}} \quad (5.19)$$

$$COP = C1 + C2 \times T_{rg,agg} + C3 \times T_{rer,agg} + C4 \times m_{wg,agg} + C5 \times m_{wr,agg} + C6 \times T_{rg,agg}^2 + C7 \times T_{rer,agg}^2 + C8 \times m_{wg,agg}^2 + C9 \times m_{wr,agg}^2 + C10 \times T_{rg,agg} \times T_{rer,agg} + C11 \times m_{wg,agg} \times m_{wr,agg} + C12 \times T_{rg,agg} \times m_{wg,agg} + C13 \times T_{rer,agg} \times m_{wr,agg} \quad (5.20)$$

$$U_f m_{f,max} HVe_b = m_w c_w (T_{b,agg} - T_{rb,agg}) \quad (5.21)$$

$$T_{rb,agg} = \frac{(T_{rc,agg} m_{wc,agg} + T_{exre,agg} m_{w1p,agg})}{m_{wc,agg} + m_{w1p,agg}} \quad (5.22)$$

$$m_{w1p,agg} c_w (T_{b,agg} - T_{exp,agg}) = U_{loss1} (T_{b,agg} - T_g) \quad (5.23)$$

$$m_{w1p,agg} c_w (T_{rel,agg} - T_{exre,agg}) = U_{loss1} (T_{rel,agg} - T_g) \quad (5.24)$$

$$m_{wc,agg} c_w (T_{b,agg} - T_{spc,agg}) = U_{loss2} (T_{b,agg} - T_g) \quad (5.25)$$

$$m_{wc,agg} c_w (T_{rec,agg} - T_{rc,agg}) = U_{loss2} (T_{rec,agg} - T_g) \quad (5.26)$$

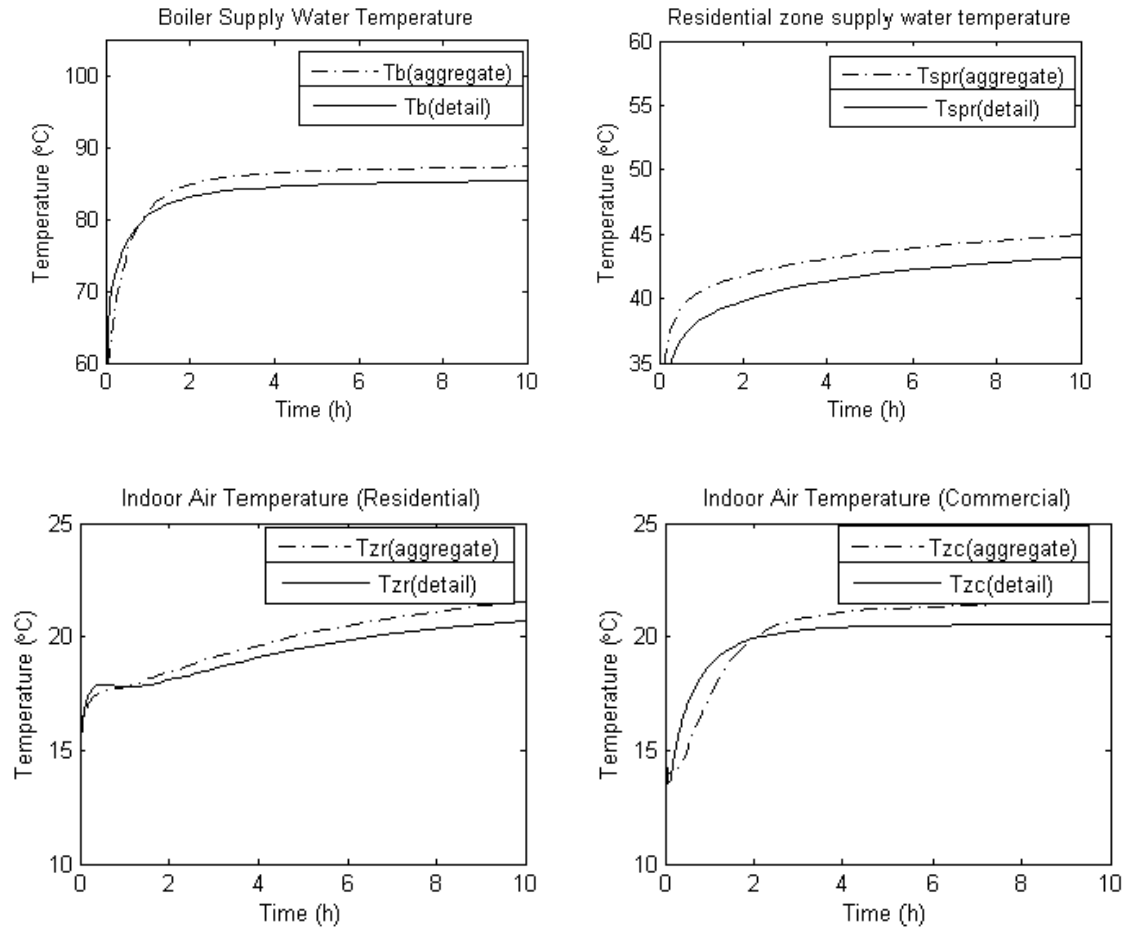


Figure 5.4.1 Comparison between the simplified aggregated model and the detailed full order model

The open loop tests for both simplified aggregated model and detailed full order model were conducted and the results were shown in Figure 5.4.1. The temperature responses

for the boiler, heat exchanger, residential zone, and commercial zone for both cases were plotted. It can be noted that the errors between the two models is not very significant.

The optimization problem was solved by utilizing the f_{mincon} (J) function in MATLAB.

The sensitivity of optimal set-points of boiler, heat exchanger and heat pump to the outside air temperature were studied and shown in Figure 5.4.2.

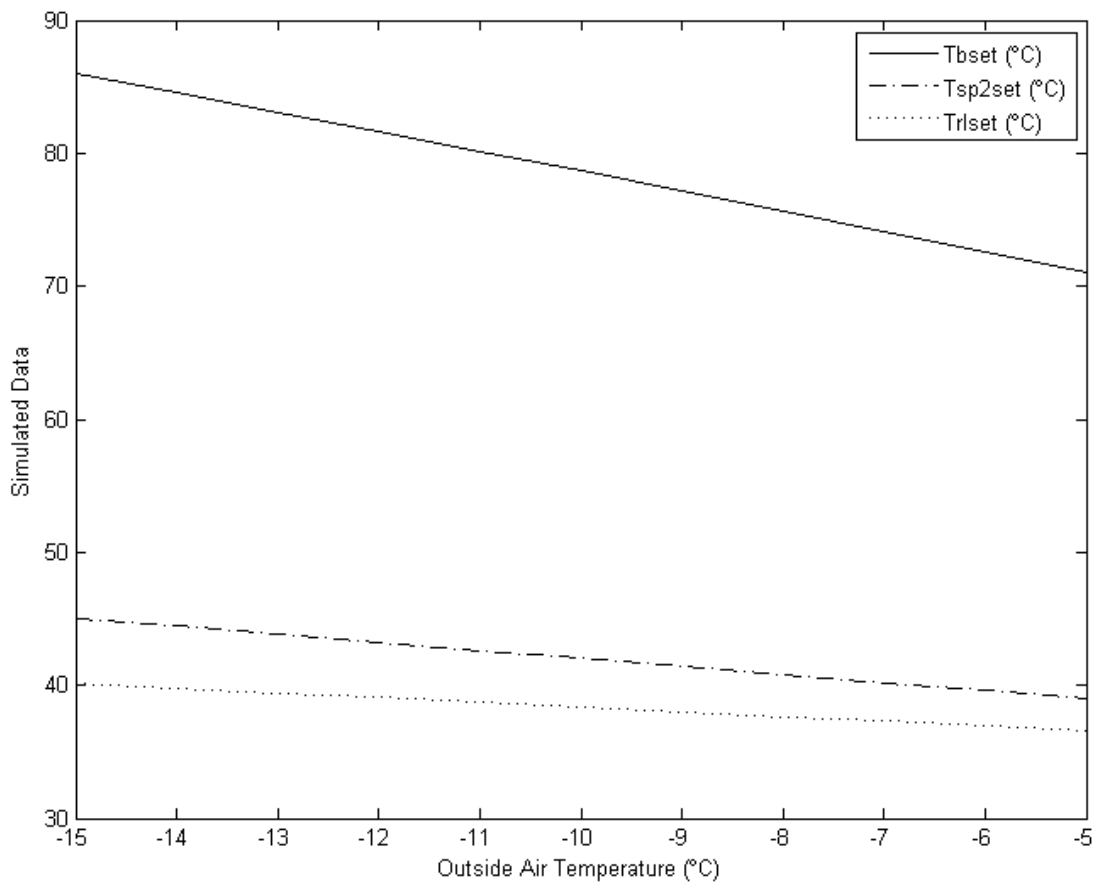


Figure 5.4.2 Optimal set-point temperature profile for boiler, heat exchanger and heat pump

The above figure shows the optimal set-point of boiler, heat exchanger and heat pump, as a function of outside air temperature. The results show that the set-point temperatures

decrease as the outside air temperature increases. The above optimal set-point temperature were implemented on the system by conducting a typical day simulation.

The results are depicted in Figure 5.4.3 and Figure 5.4.4.

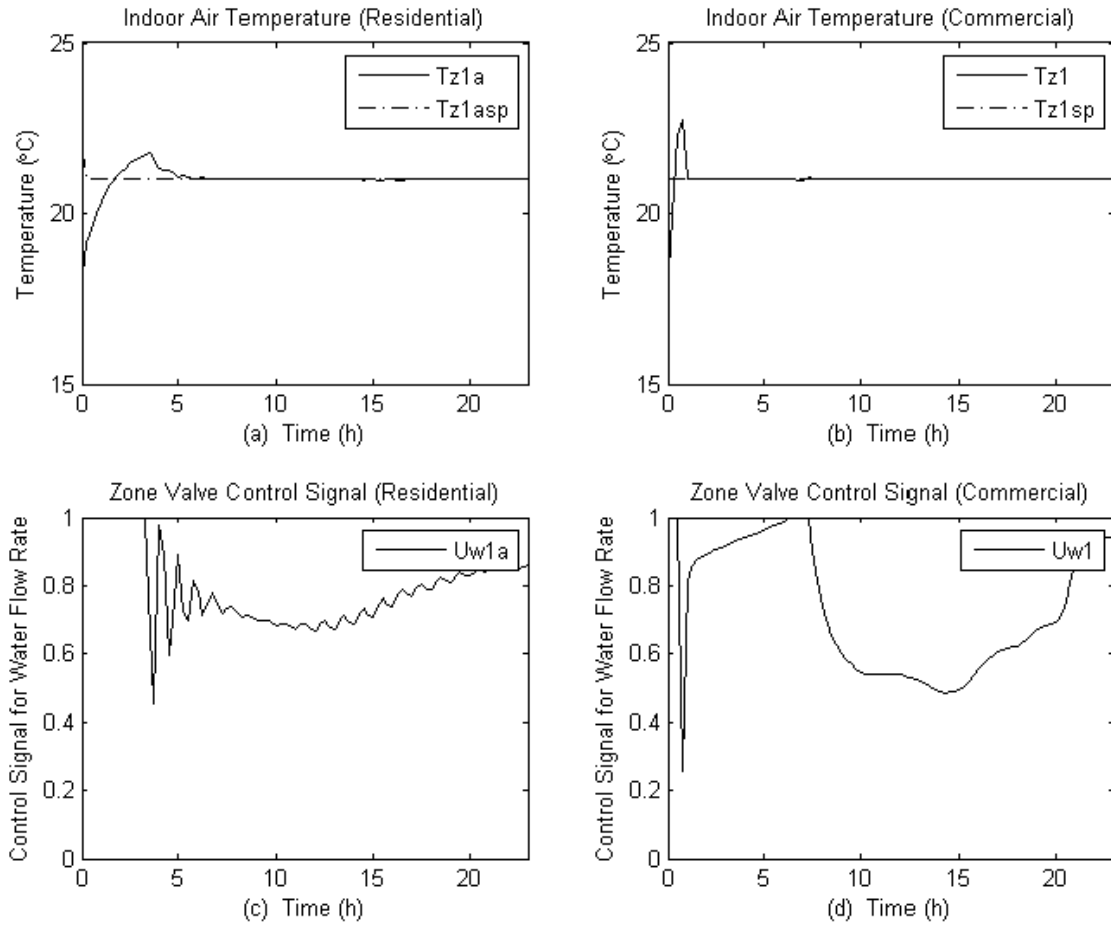


Figure 5.4.3 Output responses of residential and commercial zone (optimal control strategy)

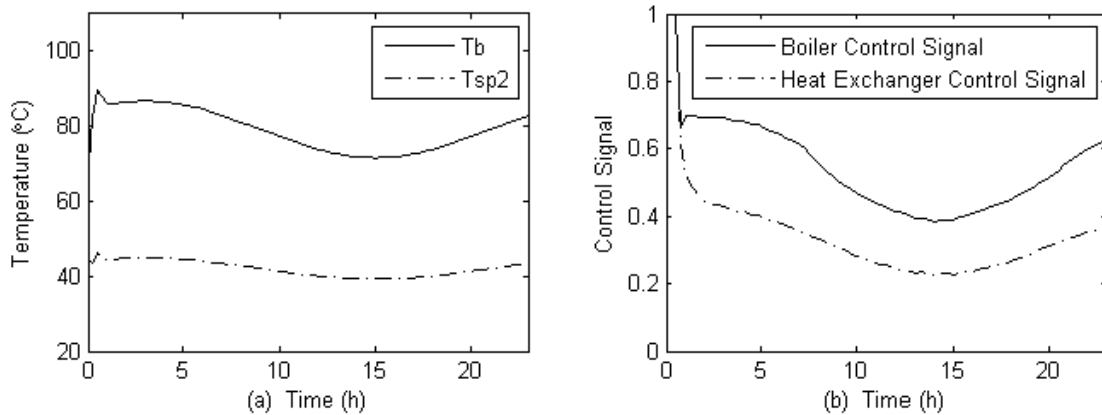


Figure 5.4.4 Output responses of boiler and heat exchanger (optimal control strategy)

Simulation results presented in Figure 5.4.4 reflect continuous change in boiler and heat exchanger temperature which track the optimal set-points smoothly.

5.5 Energy consumption

System-based and control-based energy simulations were conducted. For the purpose of simulation, two different days: a cold day (temperature range -15°C to -5°C) and a mild day (temperature range -5°C to 5°C) were used. Comparison of the energy consumption between all boiler system and hybrid hydronic system were made.

As shown in Table 5.5.1, the implementation of the ground source heat pump system can contribute to 55.4% and 70% of boiler energy savings for the cold day and mild day, as compared with the conventional all boiler system.

Energy simulation of hybrid hydronic system was conducted under three different control strategies and the simulations results are presented in Table 5.5.2. It can be noted from the table that on a cold day (-15°C to -5°C), the energy savings of 4.5% and 6.6%

respectively for the reset control and the optimal control were obtained compared to the base case. Under the mild day conditions (-15°C to -5°C), the heating load demands are lower, and as such more energy saving (19.9% and 22%) were realized by using the reset and optimal control strategies.

The simulation results show that the outside air temperature reset control strategy is an efficient and simple strategy to achieve energy savings. As the supply water temperatures are regulated according to the outside air temperature, less pipe heat losses occur and higher boiler operational efficiency can be achieved. Although the optimal control strategy results in higher energy savings, it is relatively more difficult to implement in real systems.

Daily outdoor air temperature profile (Cold winter day) (-15<T _o <-5)	Conventional all boiler heating system	Hybrid source heating system	Boiler energy saving
Total energy consumption (MJ)	2184.2	2185.1	NA
Energy consumption (commercial zone) (MJ)	1182.4 (Boiler)	1183.5 (Boiler)	NA
Energy consumption (Residential zone) (MJ)	1001.8 (Boiler)	446.7 (Boiler) 554.9 (Heat pump)	55.4%
Daily outdoor air temperature profile (Mild winter day) (-5<T _o <5)	Conventional all boiler heating system	Hybrid source heating system	Boiler energy saving
Total energy consumption (MJ)	1683.1	1684.7	NA
Energy consumption (commercial zone) (MJ)	913.4 (Boiler)	915 (Boiler)	NA
Energy consumption (Residential zone) (MJ)	769.7 (Boiler)	231.5 (Boiler) 538.2 (Heat pump)	70%

Table 5.1 Energy comparison of different operating methods (system based) under high heating low demand and low heating load demand conditions

Daily outdoor air temperature profile (Higher Demand) (-15<T _o <-5)	Conventional fixed set-point PI control	Outdoor air temperature reset control	Optimal set-point PI control
Total energy consumption (MJ)	2185.1	2087	2040.2
Energy consumption (commercial zone) (MJ)	1183.5	1133.3	1099.6
Energy consumption (Residential zone) (MJ)	446.7 (Boiler) 554.9 (Heat pump)	380.6 (Boiler) 573.1 (Heat pump)	468.0 (Boiler) 472.6 (Heat pump)
Energy saving	NA	4.5%	6.6%
Daily outdoor air temperature profile (Lower Demand) (-5<T _o <5)	Conventional fixed set-point PI control	Outdoor air temperature reset control	Optimal set-point PI control
Total energy consumption (MJ)	1684.7	1350	1317
Energy consumption (commercial zone) (MJ)	915	746.5	717.8
Energy consumption (Residential zone) (MJ)	231.5 (Boiler) 538.2 (Heat pump)	80.7 (Boiler) 522.8 (Heat pump)	183.6 (Boiler) 415.6 (Heat pump)
Energy saving	NA	19.9%	22%

Table 5.2 Energy comparison of different operating methods (control based) under high heating low demand and low heating load demand conditions

5.6 Summary

The transient responses and energy simulations for all three control strategies were conducted. With properly selected hot water supply set-point temperatures and well-tuned PI controllers, both the residential and commercial zones can be maintained at desirable conditions. However, supplying the hot water at constant temperature can lead

to higher pipe heat losses and low boiler efficiency at partial load conditions. To this end, an outside air temperature reset strategy was implemented. The supply water temperatures to the zones were regulated according to the outside air temperatures. As such, continual adjustment of heat delivery to the zone was achieved to match the zone heat losses. Moreover, less flow rate fluctuations at the zone level were observed for the reset control. This more stable circulation can ensure that the heat delivered to different parts is even and the potential localized heat sinks can be avoided. Furthermore, a multi-variable constraint optimization technique for energy optimized operation was applied to determine the steady state optimal set-point temperature. In this case, the operational interactions among control loops were taken into consideration. Instead of using same supply water temperature for heat pump and the heat exchanger, a unique temperature profile for the heat pump was determined and used. These measures resulted in further energy savings.

Chapter 6 Conclusions, Contributions and Recommendations for Future Research

6.1 Conclusions and contributions

The development of the dynamic model, the design and simulations of the control strategies and the model-based energy analysis for the hybrid source hydronic heating system have been presented in this study. The conclusions and contributions are stated in the following sections: design and dynamic modeling of the overall HWH system, energy simulations under different operating conditions, and the study of control strategies for the optimized system performance.

6.1.1 Dynamic modeling of the hybrid source hydronic heating system

Dynamic models for each component were first developed and integrated, including the boiler, heat exchanger, ground loop heat pump, ground loop heat exchanger, baseboard heaters, and radiant floor heating pipes. The hybrid hydronic heating system model was used to analyze and simulate the system responses, in terms of the influences of building heating load, zone air temperature variation, circulating water flow rate, as well as other disturbances.

It was found that zone and boiler temperature responses are faster compared to the heat exchanger and heat pump loop temperature because of the large thermal capacity of the

ground loop. For the daily temperature responses of the boiler and zone, the direct effect of the ground loop thermal capacity is less considerable.

6.1.2 Adaptive control of hybrid hydronic system

A conventional fixed gain PI control and an adaptive gain PI control were presented and the simulation results for both controls were investigated. A well-tuned PI controller was found to give good temperature control. However, the dynamic characteristics of RFH system change significantly during operation. The system nonlinearities cause unstable oscillatory behavior in zone temperature, especially during the low load conditions. A fixed set of control gains were shown to be not efficient to handle the multiple time varying processes during the system operation. To this end, an adaptive gain strategy was designed. It was shown that the adaptive control strategy gives good temperature control under variable load conditions compared to the conventional fixed gain control. The responses were smooth and control was stable.

6.1.3 Energy comparison under three different control strategies

Energy simulations of the system under different control strategies were conducted. The fixed set-point strategy was found to contribute to higher energy consumption due to higher pipe heat losses. The reset control strategy, on the other hand, was found to be effective in reducing system energy consumption. The supply water temperature was regulated as a function of the outdoor air temperature, so that the water temperature is

just sufficient to compensate for the zone heat losses. By this way, the boiler energy was saved by 5% (cold winter day) and 20% (mild winter day), respectively, compared to the fixed set-point control strategy. The optimal set-point control strategy resulted in the highest energy saving of 7% (cold winter day) and 22% (mild winter day), respectively. In this case, the interactions and tradeoff under different operating conditions between sources are considered and modeled by a multi-variable constraint objective function optimization technique.

It was also found that the ground loop heat pump system contributes between 50 to 70% of energy to the residential RFH system compared to the all boiler system.

6.2 Recommendations for future research

- 1) Solar radiation incident on the radiant floor surface plays an important role for both the energy and control analysis. Solar energy absorption by the thermal mass of a floor heating system may contribute to a considerable reduction in energy consumption. However, proper predictive control strategy should also be implemented to anticipate the thermal lag effect.
- 2) Dynamic optimal control instead of steady-state optimal control should be studied and implemented in the current system to develop improved control strategies.

References

- [1] Bauer, D., W. Heidemann, and H.-J.G. Diersch, 2011. Transient 3D analysis of borehole heat exchanger modeling. *Geothermics* 40, 250-260.
- [2] Bernier, M.A., P. Pinel, R. Labib, and R. Paillot. 2004. A Multiple-load aggregation Algorithm for Annual Hourly Simulations of GCHP Systems. *HVAC&R Research*.
- [3] Carslaw HS, Jaeger JC. 1946. *Conduction of heat in solids*. Oxford UK: Clarendon
- [4] Cecchini, C., D. Marchal. 1991. A simulation model of refrigerant and air-conditioning equipment based on experimental data. *ASHRAE Transactions* 97(2): 388-393.
- [5] Chae, Y.T, K. H. Lee, J. S. Park. 2011. Improved thermal performance of a hydronic radiant panel heating system by the optimization of tube shapes. *Journal of Zhejiang University (Applied Physics & Engineering)*, 428-437.
- [6] Chen, T.Y. 2002. Application of Adaptive Predictive Control to a Floor Heating System with a Large Thermal lag. *Energy and Buildings*. 34 (2002). Pp.45-51.
- [7] Cho, S.H, and Zaheer-uddin, M, (1999) "An experimental study of multiple parameter switching control for radiant floor heating systems", *Energy, the Int. Journal*, Vol.24, pp. 433-444.
- [8] Daniel E. Fisher and Simon J. Rees, 2005. Modeling Ground Source Heat Pump Systems in a Building Energy Simulation Program (EnergyPlus). Ninth International IBPSA Conference.

- [9] Eskilson, P. 1987. Thermal Analysis of Heat Extraction Boreholes. Doctoral Thesis. University of Lund, Sweden.
- [10] Fatemeh Tahersima, Jakob Stoustrup and Henrik Rasmussen. 2011. Eliminating Oscillations in TRV-Controlled Hydronic Radiators. 2011 50th IEEE Conference on Decision and Control and European Control Conference (CDC-ECC) Orlando, FL, USA, December 12-15, 2011
- [11] Florides. G and S. Kalogirou. 2007. Ground heat exchangers – A review of systems, models and applications. *Renewable Energy* 32 (2007). 2461-2478.
- [12] Ingersoll LR, Plass HJ. Theory of the ground pipe source for the heat pump. *ASHVE Trans* 1948; 54:339–48.
- [13] Ingersoll, L.R. and A.C. Zobel. 1954. Heat conduction with engineering and geological application, 2th ed. McGraw-Hill, New York.
- [14] Jin, Spitler. 2002. A parameter estimation based model of water-to-water heat pumps for use in energy calculation programs. *ASHRAE Transactions* 2002, Vol 108, Part1.
- [15] Kavanaugh SP. 1985. Simulation and experimental verification of vertical ground coupled heat pump systems. Ph.D dissertation. Stillwater, Oklahoma: Oklahoma State University, Stillwater.
- [16] Li L, Zaheer-uddin, M, 2010. Steady State and Dynamic Modeling of an Indirect District Heating System. *Int. Journal of Air-Conditioning and Refrigeration* Vol. 18, No. 1 (2010) 61-75

- [17] Li, S.C 2010. Modeling and control strategies for radiant floor heating systems. Master thesis, Concordia University.
- [18] Liao, Z., Parand. 2002. Develop a Dynamic Model of Gas and Oil Burned Boilers for Optimization of Boiler Control in Central Heating Systems.
- [19] Morrison, A.1997. GS2000 Software. Proceedings of the Third International Heat Pumps in Cold Climates Conference, Wolfville, Nova Scotia, pp. 67-76.
Press
- [20] Sattari. S and B. Farhanieh, 2006. A parametric study on radiant floor heating system performance. Renewable Energy 31, 1617-1626.
- [21] Singh. G, M. Zaheer-uddin, R.V.Patel. 2000. Adaptive control of multivariable thermal processes in HVAC systems. Energy Conversion & Management 41 (2000), 1671-1685.
- [22] Spitler, J.D, S.J.Rees, and C. Yavuzturk. 2000. Recent developments in ground source heat pump system design, modeling and applications. Proceedings of the Dublin 2000 Conference.
- [23] Stefanuk, N.B.M., J.D. Aplevich, and M. Renksizbulut. 1992. Modeling and simulation of a superheat-controlled water-to-water heat pump. ASHRAE Transactions 98(2): 172-184.
- [24] Tang. 2003. Modeling Packaged Heat Pumps in a Quasi-steady State Energy Simulation Program. Master thesis. Oklahoma State University.

- [25] Nam.Y, R. Ooka, and S. Hwang, 2008. Development of a numerical model to predict heat exchange rates for a ground-source heat pump system. *Energy and Buildings* 40, 2133-2140.
- [26] Zaheer-uddin, M, Z.L. Zhang, and S.H. Cho (2001) "Augmented control strategies for radiant floor heating systems", *Int. Journal of Energy Research*, Vol.25.
- [27] Zaheer-uddin, M. 1993. Optimal, Sub-optimal and Adaptive Control Methods for the Design of Temperature Controllers for Intelligent Buildings. *Building and Environment*, Vol. 28, No. 3, pp. 311-322.
- [28] Zaheer-uddin, M., P. Monastiriakos, 1998. Hydronic heating systems: transient modeling, validation and load matching control. *Int. Journal of Energy Research*, Vol. 22, pp. 33-46

Appendices

Appendix-A Design parameters of Hybrid Hydronic Heating System

Symbol	Description	Value or formula
Heating Load Estimation		
T_{od} [° C]	Outside air temperature at design condition	-15
T_{zcd} [° C]	Commercial zone air temperature at design condition	21
T_{zrd} [° C]	Residential zone air temperature at design condition	22
Q_{hc} [W]	Total heating load of commercial zone	14224
Q_{hcz1} [W]	Heating load of commercial zone 1	5715.6
Q_{hcz2} [W]	Heating load of commercial zone 2	2973.7
Q_{hcz3} [W]	Heating load of commercial zone 3	3243.5
Q_{hcz4} [W]	Heating load of commercial zone 4	2291.6
Q_{hr} [W]	Total heating load of residential zone	12788
Q_{hrz1a} [W]	Heating load of residential zone 1a	748.4
Q_{hrz1b} [W]	Heating load of residential zone 1b	1053.3
Q_{hrz1c} [W]	Heating load of residential zone 1c	452.6
Q_{hrz1d} [W]	Heating load of residential zone 1d	942.6
Boiler selection		
Q_{bd} [W]	Boiler capacity	35000
Radiant floor heating system sizing		

T_{rspd} [° C]	Residential zone design supply water temperature	45
T_{rred} [° C]	Residential zone design return water temperature	35
$d_{i,r}$ [m]	Inner diameter of the tube	0.0087
$d_{o,r}$ [m]	Outer diameter of the tube	0.0127
S_t [m]	Interval between tubes	Varies for each zone
t_p [m]	Thickness of the floor slab concrete layer	0.0381
t_c [m]	Thickness of the floor slab covering layer	0.009525
L [m]	Radiant floor pipe length for each control segment	Varies for each zone
Baseboard heater sizing		
T_{cspd} [° C]	Commercial zone design supply water temperature	85
T_{cred} [° C]	Commercial zone design return water temperature	65
n	Factor identified based on heater heat transfer test	0.3
U_{htr1} [W/K]	Thermal conductance of the baseboard heater 1	$U_{htr1} = \frac{0.25 \cdot Q_{hcz1}}{\left(\frac{T_{cspd} + T_{cred}}{2} - T_{czd}\right)^{1+n}}$
U_{htr2} [W/K]	Thermal conductance of the baseboard heater 2	$U_{htr2} = \frac{0.5 \cdot Q_{hcz1}}{\left(\frac{T_{cspd} + T_{cred}}{2} - T_{czd}\right)^{1+n}}$
U_{htr3} [W/K]	Thermal conductance of the baseboard heater 3	$U_{htr3} = \frac{0.25 \cdot Q_{hcz1}}{\left(\frac{T_{cspd} + T_{cred}}{2} - T_{czd}\right)^{1+n}}$
U_{htr4} [W/K]	Thermal conductance of the baseboard heater 4	$U_{htr4} = \frac{0.5 \cdot Q_{hcz2}}{\left(\frac{T_{cspd} + T_{cred}}{2} - T_{czd}\right)^{1+n}}$

U_{hr5} [W/K]	Thermal conductance of the baseboard heater 5	$U_{hr5} = \frac{0.5 \cdot Q_{hc2}}{\left(\frac{T_{cspd} + T_{cred}}{2} - T_{czd}\right)^{1+n}}$
U_{hr6} [W/K]	Thermal conductance of the baseboard heater 6	$U_{hr6} = \frac{0.5 \cdot Q_{hc3}}{\left(\frac{T_{cspd} + T_{cred}}{2} - T_{czd}\right)^{1+n}}$
U_{hr7} [W/K]	Thermal conductance of the baseboard heater 7	$U_{hr7} = \frac{0.5 \cdot Q_{hc3}}{\left(\frac{T_{cspd} + T_{cred}}{2} - T_{czd}\right)^{1+n}}$
U_{hr8} [W/K]	Thermal conductance of the baseboard heater 8	$U_{hr8} = \frac{1.0 \cdot Q_{hc4}}{\left(\frac{T_{cspd} + T_{cred}}{2} - T_{czd}\right)^{1+n}}$
Ground loop heat exchanger sizing		
N1	Number of bores in each series circuit	2
N2	Number of parallel circuit	2
$d_{i,g}$ [m]	Inner diameter of the tube	0.0262
$d_{o,g}$ [m]	Outer diameter of the tube	0.032
Δz [m]	Distance between vertical nodes	2/13.7
$z1$ [m]	Distance between vertical nodes, $z < 10$ m	2
$z2$ [m]	Distance between vertical nodes, $10\text{m} < z < 75\text{m}$	13.7
s [m]	Shank space between two tubes	0.06
L_{bore} [m]	Center to center distance between two boreholes	6
D_{bore} [m]	Borehole diameter	0.13
D_{pbore} [m]	Borehole depth	75
Heat pump selection		
	Heat pump type	Water-to-water heat pump

	Refrigeration type	R410a
E_{com} [W]	Heat pump compressor power	5000
Heat exchanger sizing		
T_{exspd} [° C]	Heat exchanger primary side design supply water temperature	85
T_{exred} [° C]	Heat exchanger primary side design return water temperature	75
$LMTD_d$	Design Log Mean Temperature Difference	$LMTD_d = \frac{(T_{exspd} - T_{rspd}) - (T_{exred} - T_{rred})}{\ln \frac{T_{exspd} - T_{rspd}}{T_{exred} - T_{rred}}}$
U_{ex} [W/(m ² C)]	Heat transfer coefficient of heat exchanger	3000
A_{ex} [m ²]	Heat transfer area of heat exchanger	$A_{ex} = \frac{Q_{hr}}{U_{ex} \cdot LMTD_d}$

HS018 - Performance Data cont.

Heating Capacity

Source		Load Flow-3 GPM						Load Flow-4 GPM						Load Flow-5 GPM							
EST F	Flow GPM	ELT F	LLT F	HC MBTUH	Power kW	HE MBTUH	COP	LST F	LLT F	HC MBTUH	Power kW	HE MBTUH	COP	LST F	LLT F	HC MBTUH	Power kW	HE MBTUH	COP	LST F	
	4	60																			
		80																			
		100																			
		120																			
25		60	69.8	14.2	0.90	11.1	4.62	20.4	67.4	14.3	0.88	11.3	4.76	20.3	65.9	14.4	0.86	11.5	4.91	20.3	
		80	89.4	13.7	1.21	9.6	3.31	21.1	87.1	13.8	1.19	9.7	3.38	21.0	85.7	13.9	1.17	9.9	3.46	20.9	
	5	100	109.1	13.2	1.53	8.0	2.53	21.7	106.8	13.3	1.51	8.1	2.58	21.6	105.5	13.3	1.49	8.3	2.63	21.6	
		120	128.7	12.7	1.84	6.4	2.02	22.4	126.6	12.8	1.82	6.5	2.05	22.3	125.3	12.8	1.80	6.7	2.08	22.3	
		60	70.4	15.1	0.91	12.0	4.86	21.8	68.3	15.2	0.90	12.1	4.96	21.7	66.3	15.2	0.88	12.2	5.06	21.6	
		80	90.0	14.5	1.22	10.4	3.48	22.9	88.0	14.6	1.21	10.5	3.55	22.8	86.0	14.6	1.19	10.6	3.61	22.7	
	3	100	109.6	14.0	1.54	8.7	2.66	24.0	107.7	14.0	1.52	8.8	2.71	23.9	105.8	14.1	1.49	9.0	2.76	23.8	
		120	129.2	13.4	1.85	7.1	2.12	25.1	127.4	13.5	1.83	7.2	2.16	25.0	125.6	13.5	1.80	7.4	2.20	24.9	
		60	70.7	15.5	0.91	12.4	5.02	23.2	68.6	15.6	0.89	12.6	5.14	23.2	66.5	15.7	0.88	12.7	5.26	23.1	
	4	80	90.2	14.9	1.22	10.7	3.58	24.2	88.2	15.0	1.20	10.9	3.66	24.1	86.2	15.0	1.18	11.0	3.75	24.0	
		100	109.8	14.3	1.53	9.0	2.73	25.1	107.9	14.3	1.50	9.2	2.79	25.0	105.9	14.4	1.48	9.3	2.85	24.9	
		120	129.4	13.7	1.85	7.4	2.17	26.0	127.5	13.7	1.81	7.5	2.21	25.9	125.6	13.7	1.78	7.6	2.26	25.8	
		60	70.9	15.9	0.90	12.8	5.18	24.7	68.8	16.1	0.89	13.0	5.32	24.6	66.7	16.2	0.87	13.2	5.46	24.5	
	5	80	90.5	15.2	1.21	11.1	3.68	25.4	88.4	15.3	1.19	11.3	3.78	25.3	86.4	15.4	1.16	11.5	3.89	25.3	
		100	110.0	14.6	1.53	9.4	2.80	26.1	108.0	14.6	1.49	9.5	2.87	26.1	106.0	14.7	1.46	9.7	2.95	26.0	
		120	129.6	13.9	1.84	7.6	2.21	26.9	127.6	13.9	1.80	7.8	2.27	26.8	125.7	13.9	1.75	7.9	2.33	26.7	
		60	73.5	19.7	0.90	16.6	6.46	38.6	70.9	19.8	2.74	10.4	4.71	42.8	68.2	20.0	4.59	4.3	2.97	47.1	
	3	80	93.0	18.9	1.21	14.7	4.58	39.9	90.4	19.0	2.43	10.7	3.48	42.7	87.9	19.1	3.65	6.6	2.37	45.4	
		100	112.4	18.1	1.52	12.9	3.48	41.2	110.0	18.1	2.12	10.9	2.85	42.5	107.5	18.2	2.71	9.0	2.21	43.8	
		120	131.9	17.3	1.84	11.0	2.76	42.4	129.5	17.3	1.80	11.1	2.82	42.3	127.2	17.4	1.77	11.3	2.88	42.2	
		60	73.9	20.2	0.89	17.1	6.62	40.7	71.2	20.4	1.81	14.2	3.31	42.7	68.5	20.6	2.72	11.3	2.22	44.8	
	4	80	93.3	19.3	1.21	15.2	4.69	41.7	90.7	19.5	1.80	13.3	3.16	43.0	88.1	19.6	2.40	11.4	2.40	44.4	
		100	112.7	18.4	1.52	13.2	3.55	42.8	110.2	18.5	1.80	12.4	3.02	43.4	107.7	18.6	2.08	11.5	2.63	44.0	
		120	132.1	17.6	1.83	11.3	2.81	43.8	129.7	17.6	1.80	11.5	2.87	43.7	127.3	17.7	1.76	11.7	2.94	43.6	
		60	74.2	20.7	0.89	17.7	6.83	42.7	71.5	21.0	0.87	18.0	7.12	42.6	68.7	21.2	0.85	18.3	7.41	42.4	
	5	80	93.6	19.8	1.20	15.6	4.82	43.5	90.9	19.9	1.17	15.9	4.99	43.4	88.3	20.1	1.15	16.2	5.17	43.3	
		100	112.9	18.8	1.52	13.6	3.64	44.4	110.4	18.9	1.48	13.9	3.75	44.3	107.8	19.0	1.45	14.1	3.87	44.2	
		120	132.3	17.9	1.83	11.6	2.86	45.2	129.8	17.9	1.79	11.8	2.94	45.1	127.4	18.0	1.75	12.0	3.02	45.1	
		60	76.6	24.2	0.88	21.2	8.06	55.4	73.4	24.5	4.59	8.8	4.46	64.0	70.2	24.7	8.30	-3.6	0.87	72.5	
	3	80	95.9	23.2	1.19	19.1	5.69	56.9	92.8	23.4	3.65	10.9	3.41	62.5	89.7	23.5	6.11	2.7	1.13	68.2	
		100	115.2	22.1	1.51	17.0	4.30	58.3	112.2	22.3	2.72	13.0	2.99	61.1	109.2	22.4	3.93	9.0	1.67	63.8	
		120	134.5	21.1	1.82	14.9	3.40	59.8	131.6	21.2	1.78	15.1	3.48	59.6	128.7	21.2	1.74	15.3	3.57	59.5	
		60	77.1	24.9	0.88	21.8	8.27	58.1	73.8	25.2	2.72	15.9	2.71	62.2	70.5	25.5	4.56	9.9	1.64	66.4	
	4	80	96.3	23.7	1.19	19.6	5.82	59.3	93.1	23.9	2.41	15.7	2.91	62.0	90.0	24.2	3.62	11.8	1.96	64.8	
		100	115.5	22.6	1.51	17.4	4.39	60.5	112.5	22.7	2.09	15.6	3.18	61.8	109.4	22.9	2.68	13.7	2.50	63.1	
		120	134.7	21.5	1.82	15.2	3.45	61.7	131.8	21.5	1.78	15.4	3.54	61.6	128.9	21.6	1.74	15.7	3.64	61.4	
		60	77.5	25.5	0.88	22.5	8.49	60.7	74.2	25.9	0.85	22.9	8.93	60.5	70.8	26.2	0.82	23.4	9.36	60.3	
	5	80	96.7	24.3	1.19	20.2	5.96	61.7	93.5	24.5	1.16	20.6	6.20	61.5	90.2	24.8	1.13	21.0	6.45	61.4	
		100	115.8	23.0	1.51	17.9	4.48	62.6	112.7	23.2	1.47	18.2	4.63	62.5	109.6	23.4	1.43	18.5	4.78	62.4	
		120	135.0	21.8	1.82	15.6	3.51	63.6	132.0	21.9	1.78	15.8	3.61	63.5	129.1	22.0	1.74	16.1	3.70	63.4	
		60	79.6	28.5	0.88	25.5	9.49	72.5	75.6	28.4	0.85	25.5	9.84	72.5	71.6	28.2	0.81	25.4	10.20	72.5	
	3	80	98.6	27.1	1.18	23.0	6.70	74.2	94.9	27.1	1.15	23.1	6.92	74.1	91.1	27.0	1.11	23.2	7.14	74.0	
		100																			
		120																			
		60	80.1	29.2	0.88	26.2	9.72	75.7	76.0	29.0	0.85	26.1	10.05	75.7	71.9	28.8	0.81	26.0	10.40	75.8	
	4	80	99.0	27.7	1.19	23.6	6.84	77.1	95.2	27.6	1.15	23.7	7.05	77.0	91.4	27.6	1.11	23.8	7.28	77.0	
		100																			
		120																			
		60	80.5	29.9	0.88	26.9	9.96	78.9	76.3	29.6	0.85	26.7	10.28	79.0	72.1	29.3	0.81	26.5	10.60	79.1	
	5	80	99.4	28.2	1.19	24.2	6.97	80.0	95.5	28.2	1.15	24.2	7.19	80.0	91.6	28.1	1.11	24.3	7.42	80.0	
		100																			
		120																			

HS025 - Performance Data cont.

Heating Capacity

Source		Load Flow-4 GPM							Load Flow-5.5 GPM							Load Flow-7 GPM						
EST F	Flow GPM	ELT F	LLT F	HC MBTUH	Power kW	HE MBTUH	COP	LST F	LLT F	HC MBTUH	Power kW	HE MBTUH	COP	LST F	LLT F	HC MBTUH	Power kW	HE MBTUH	COP	LST F		
25	5.5	60																				
		80																				
		100																				
		120																				
	7	60	71.0	21.4	1.28	17.0	4.90	20.0	68.1	21.5	1.26	17.2	5.02	19.9	66.4	21.6	1.23	17.4	5.15	19.9		
		80	90.6	20.5	1.70	14.7	3.54	20.7	87.7	20.7	1.67	14.9	3.62	20.6	86.1	20.8	1.65	15.1	3.70	20.5		
		100	110.1	19.7	2.12	12.4	2.72	21.3	107.4	19.8	2.09	12.7	2.77	21.3	105.9	19.9	2.06	12.9	2.83	21.2		
		120	129.7	18.8	2.54	10.1	2.17	22.0	127.1	19.0	2.51	10.4	2.21	21.9	125.6	19.1	2.48	10.6	2.26	21.9		
	4	60	71.4	22.2	1.29	17.8	5.04	20.8	69.1	22.4	1.26	18.1	5.21	20.7	66.7	22.6	1.23	18.4	5.38	20.5		
		80	91.0	21.4	1.71	15.6	3.67	22.0	88.7	21.6	1.68	15.9	3.78	21.8	86.4	21.8	1.64	16.2	3.88	21.7		
		100	110.6	20.6	2.12	13.4	2.84	23.1	108.4	20.8	2.09	13.6	2.91	23.0	106.2	20.9	2.06	13.9	2.98	22.8		
		120	130.2	19.8	2.54	11.1	2.28	24.3	128.1	20.0	2.51	11.4	2.33	24.1	125.9	20.1	2.47	11.7	2.38	24.0		
30	5.5	60	71.8	22.9	1.29	18.4	5.19	22.6	69.3	23.0	1.26	18.7	5.35	22.5	66.8	23.2	1.23	19.0	5.53	22.4		
		80	91.3	21.9	1.71	16.1	3.76	23.5	88.9	22.1	1.68	16.4	3.87	23.4	86.6	22.3	1.64	16.7	3.98	23.3		
		100	110.8	21.0	2.12	13.7	2.90	24.5	108.6	21.2	2.09	14.1	2.97	24.4	106.3	21.4	2.06	14.4	3.05	24.2		
		120	130.3	20.1	2.54	11.4	2.31	25.4	128.2	20.3	2.51	11.7	2.37	25.3	126.0	20.5	2.47	12.1	2.43	25.2		
	7	60	72.1	23.5	1.29	19.1	5.34	24.4	69.6	23.7	1.26	19.3	5.50	24.3	67.0	23.8	1.23	19.6	5.67	24.2		
		80	91.6	22.4	1.71	16.6	3.85	25.1	89.1	22.6	1.68	16.9	3.96	25.0	86.7	22.8	1.64	17.2	4.07	24.9		
		100	111.0	21.4	2.12	14.1	2.95	25.8	108.7	21.6	2.09	14.5	3.03	25.7	106.4	21.9	2.06	14.8	3.12	25.6		
		120	130.5	20.3	2.54	11.6	2.34	26.6	128.3	20.6	2.51	12.1	2.41	26.5	126.2	20.9	2.47	12.5	2.48	26.3		
	4	60	75.2	29.4	1.31	24.9	6.55	37.2	71.9	29.5	1.27	25.1	6.79	37.1	68.7	29.5	1.23	25.3	7.03	37.0		
		80	94.5	28.2	1.74	22.3	4.74	38.5	91.4	28.3	1.69	22.5	4.89	38.4	88.3	28.5	1.65	22.7	5.04	38.3		
		100	113.9	27.0	2.16	19.6	3.65	39.9	111.0	27.1	2.11	19.9	3.75	39.7	108.0	27.2	2.06	20.1	3.85	39.6		
		120	133.3	25.9	2.59	17.0	2.91	41.2	130.5	25.9	2.54	17.3	2.99	41.1	127.7	26.0	2.48	17.5	3.07	41.0		
50	5.5	60	75.7	30.4	1.31	25.9	6.79	39.6	72.3	30.4	1.27	26.1	7.02	39.5	69.0	30.5	1.23	26.3	7.25	39.5		
		80	95.0	29.1	1.74	23.2	4.90	40.7	91.8	29.1	1.69	23.4	5.04	40.6	88.6	29.2	1.65	23.6	5.19	40.6		
		100	114.3	27.7	2.16	20.4	3.76	41.8	111.3	27.8	2.11	20.6	3.86	41.7	108.2	27.9	2.06	20.9	3.96	41.6		
		120	133.6	26.4	2.59	17.6	2.99	42.9	130.7	26.5	2.54	17.9	3.06	42.8	127.8	26.6	2.48	18.2	3.15	42.7		
	7	60	76.2	31.5	1.32	27.0	6.98	42.1	72.7	31.4	1.27	27.1	7.23	42.0	69.2	31.4	1.23	27.2	7.48	42.0		
		80	95.4	30.0	1.74	24.0	5.02	42.9	92.1	30.0	1.69	24.2	5.18	42.9	88.8	30.0	1.65	24.4	5.34	42.8		
		100	114.7	28.5	2.17	21.1	3.83	43.8	111.5	28.5	2.11	21.3	3.95	43.7	108.4	28.6	2.06	21.6	4.06	43.6		
		120	133.9	27.0	2.59	18.1	3.04	44.7	131.0	27.1	2.54	18.4	3.13	44.6	128.0	27.3	2.48	18.8	3.22	44.5		
	4	60	78.9	36.6	1.33	32.1	8.06	53.5	74.8	36.5	1.28	32.1	8.37	53.4	70.7	36.4	1.23	32.2	8.67	53.4		
		80	98.1	35.0	1.77	29.0	5.81	55.0	94.2	35.0	1.71	29.1	6.00	55.0	90.3	34.9	1.65	29.3	6.20	54.9		
		100	117.3	33.5	2.20	25.9	4.45	56.6	113.5	33.4	2.14	26.1	4.59	56.5	109.8	33.4	2.07	26.3	4.73	56.4		
		120	136.4	31.9	2.64	22.9	3.54	58.2	132.9	31.9	2.57	23.1	3.65	58.1	129.4	31.9	2.49	23.4	3.75	57.9		
70	5.5	60	79.6	38.0	1.34	33.4	8.34	56.6	75.3	37.9	1.28	33.5	8.65	56.6	71.1	37.7	1.23	33.5	8.98	56.6		
		80	98.7	36.3	1.77	30.2	6.00	57.9	94.7	36.2	1.71	30.3	6.19	57.9	90.6	36.1	1.65	30.4	6.40	57.8		
		100	117.8	34.5	2.21	27.0	4.58	59.2	114.0	34.5	2.14	27.2	4.72	59.1	110.1	34.4	2.07	27.3	4.87	59.0		
		120	136.9	32.8	2.64	23.7	3.63	60.5	133.3	32.8	2.57	24.0	3.74	60.4	129.6	32.8	2.49	24.3	3.85	60.3		
	7	60	80.3	39.4	1.34	34.8	8.61	59.7	75.9	39.2	1.29	34.8	8.95	59.7	71.5	39.0	1.23	34.8	9.29	59.7		
		80	99.3	37.5	1.77	31.4	6.19	60.7	95.1	37.3	1.71	31.5	6.40	60.7	91.0	37.2	1.65	31.6	6.61	60.7		
		100	118.3	35.5	2.21	28.0	4.72	61.8	114.4	35.5	2.14	28.2	4.86	61.7	110.4	35.4	2.07	28.3	5.01	61.7		
		120	137.3	33.6	2.64	24.6	3.73	62.8	133.6	33.6	2.57	24.8	3.84	62.7	129.9	33.6	2.49	25.1	3.95	62.6		
	4	60	82.7	44.0	1.37	39.3	9.41	69.7	77.7	43.7	1.31	39.2	9.79	69.8	72.8	43.4	1.25	39.1	10.17	69.8		
		80	101.6	41.9	1.80	35.7	6.80	71.6	96.9	41.7	1.73	35.8	7.07	71.6	92.2	41.5	1.66	35.9	7.33	71.5		
		100																				
		120																				
90	5.5	60	83.5	45.5	1.38	40.8	9.66	73.6	78.2	44.8	1.32	40.3	9.96	73.8	73.0	44.1	1.26	39.8	10.30	73.9		
		80	102.3	43.2	1.81	37.0	6.99	75.2	97.4	42.8	1.74	36.8	7.22	75.2	92.5	42.4	1.66	36.7	7.46	75.2		
		100																				
	7	60	84.2	47.0	1.39	42.3	9.91	77.6	78.7	45.9	1.33	41.4	10.16	77.8	73.2	44.8	1.26	40.5	10.42	78.1		
		80	102.9	44.5	1.82	38.3	7.18	78.7	97.8	43.8	1.74	37.9	7.38	78.8	92.7	43.2	1.67	37.5	7.59	79.0		
		100																				
120																						

HS040 - Performance Data cont.

Heating Capacity

Source			Load Flow-5 GPM							Load Flow-7.5 GPM							Load Flow-10 GPM						
EST F	Flow GPM	ELT F	LLT F	HC MBTUH	Power kW	HE MBTUH	COP	LST F	LLT F	HC MBTUH	Power kW	HE MBTUH	COP	LST F	LLT F	HC MBTUH	Power kW	HE MBTUH	COP	LST F			
25	7.5	60																					
		80																					
		100																					
			120																				
		10	60	72.2	29.7	1.83	23.5	4.76	20.2	68.2	29.7	1.78	23.6	4.89	20.1	66.1	29.6	1.72	23.7	5.04	20.1		
	80		91.9	28.8	2.42	20.6	3.50	20.8	87.9	28.8	2.36	20.7	3.58	20.7	85.9	28.7	2.29	20.9	3.67	20.7			
	100		111.5	28.0	3.00	17.7	2.73	21.3	107.7	27.9	2.94	17.9	2.78	21.3	105.7	27.8	2.87	18.0	2.84	21.3			
		5	60	72.7	30.9	1.84	24.6	4.92	19.8	69.5	30.8	1.79	24.7	5.06	19.8	66.3	30.7	1.73	24.8	5.20	19.8		
	80		92.4	30.0	2.42	21.8	3.64	21.0	89.3	30.0	2.36	21.9	3.73	21.0	86.2	29.9	2.30	22.0	3.81	20.9			
	100		112.0	29.2	2.99	19.0	2.85	22.2	109.0	29.1	2.93	19.1	2.91	22.1	106.0	29.0	2.86	19.3	2.97	22.1			
		7.5	60	73.3	32.3	1.84	26.0	5.14	22.1	70.0	32.2	1.78	26.1	5.29	22.1	66.6	32.2	1.73	26.3	5.46	22.0		
	80		92.8	31.0	2.43	22.7	3.74	23.1	89.6	31.0	2.36	23.0	3.85	23.0	86.4	31.1	2.29	23.2	3.97	22.9			
100	112.3		29.8	3.02	19.5	2.90	24.0	109.2	29.9	2.94	19.9	2.98	23.9	106.2	30.0	2.86	20.2	3.07	23.9				
	10	60	73.9	33.6	1.84	27.3	5.35	24.4	70.4	33.6	1.78	27.5	5.54	24.3	66.9	33.6	1.72	27.7	5.72	24.3			
80		93.2	32.0	2.44	23.7	3.85	25.1	89.9	32.1	2.37	24.1	3.99	25.0	86.6	32.2	2.29	24.4	4.12	25.0				
100		112.6	30.5	3.04	20.1	2.94	25.9	109.5	30.7	2.95	20.6	3.05	25.8	106.4	30.9	2.86	21.1	3.16	25.6				
	5	60	76.9	41.1	1.88	34.7	6.37	35.7	72.7	40.8	1.81	34.7	6.61	35.7	68.4	40.6	1.74	34.6	6.84	35.7			
80		96.3	39.5	2.47	31.1	4.67	37.2	92.2	39.3	2.39	31.1	4.82	37.2	88.1	39.1	2.30	31.2	4.97	37.1				
100		115.6	37.9	3.06	27.4	3.61	38.7	111.7	37.7	2.96	27.6	3.72	38.6	107.8	37.6	2.87	27.8	3.84	38.5				
	7.5	60	77.7	43.0	1.86	36.6	6.77	38.9	73.2	42.7	1.80	36.5	6.95	38.9	68.7	42.3	1.74	36.4	7.15	38.9			
80		96.9	41.1	2.46	32.7	4.89	40.1	92.7	40.9	2.38	32.7	5.03	40.0	88.4	40.7	2.30	32.8	5.18	40.0				
100		116.1	39.1	3.06	28.7	3.75	41.3	112.1	39.1	2.97	29.0	3.86	41.2	108.0	39.0	2.87	29.2	3.98	41.1				
	10	60	78.5	44.9	1.84	38.6	7.14	42.0	73.8	44.5	1.79	38.4	7.29	42.1	69.1	44.1	1.74	38.2	7.43	42.1			
80		97.6	42.6	2.45	34.3	5.08	42.9	93.1	42.5	2.38	34.3	5.23	42.9	88.7	42.3	2.30	34.4	5.37	42.9				
100		116.7	40.4	3.07	30.0	3.85	43.8	112.5	40.4	2.97	30.3	3.99	43.8	108.3	40.4	2.87	30.6	4.13	43.7				
	5	60	81.2	51.3	1.92	44.7	7.83	51.5	75.8	50.9	1.83	44.6	8.16	51.6	70.4	50.4	1.74	44.5	8.49	51.7			
80		100.2	48.9	2.52	40.3	5.69	53.4	95.1	48.6	2.42	40.4	5.91	53.4	90.0	48.3	2.31	40.4	6.13	53.3				
100		119.2	46.6	3.12	35.9	4.37	55.2	114.4	46.4	3.00	36.1	4.54	55.1	109.5	46.2	2.88	36.4	4.70	55.0				
	7.5	60	82.1	53.7	1.88	47.3	8.37	55.6	76.5	53.1	1.81	46.9	8.58	55.7	70.8	52.5	1.75	46.5	8.82	55.8			
80		101.1	51.1	2.49	42.6	6.00	57.1	95.7	50.7	2.40	42.5	6.18	57.1	90.4	50.3	2.31	42.4	6.38	57.1				
100		120.0	48.5	3.11	37.9	4.57	58.5	115.0	48.3	2.99	38.1	4.73	58.4	109.9	48.1	2.88	38.3	4.90	58.4				
	10	60	83.1	56.1	1.84	49.8	8.93	59.7	77.2	55.4	1.80	49.2	9.04	59.9	71.3	54.6	1.75	48.6	9.14	60.0			
80		102.0	53.2	2.47	44.8	6.32	60.8	96.4	52.8	2.39	44.6	6.47	60.8	90.8	52.3	2.31	44.4	6.62	60.8				
100		120.8	50.4	3.09	39.8	4.77	61.8	115.5	50.2	2.99	40.0	4.93	61.8	110.3	50.0	2.88	40.2	5.09	61.7				
	5	60	85.4	61.5	1.99	54.7	9.05	67.4	78.5	59.0	1.88	52.5	9.20	68.3	71.6	56.4	1.77	50.4	9.34	69.2			
80		104.5	59.4	2.56	50.7	6.79	69.1	97.8	56.7	2.44	48.3	6.80	70.1	91.1	53.9	2.32	46.0	6.80	71.0				
100																							
	7.5	60	86.2	63.7	2.01	56.8	9.30	72.6	79.0	60.4	1.89	53.9	9.37	73.5	71.8	57.1	1.77	51.0	9.44	74.3			
80		105.5	61.9	2.58	53.1	7.03	73.8	98.4	58.3	2.45	49.9	6.97	74.7	91.3	54.7	2.33	46.8	6.90	75.6				
100		124.8	60.1	3.15	49.3	5.59	75.0	117.8	56.2	3.01	45.9	5.47	76.0	110.8	52.4	2.88	42.6	5.33	76.9				
	10	60	87.1	65.8	2.02	58.9	9.54	77.9	79.5	61.8	1.90	55.3	9.55	78.6	71.9	57.7	1.77	51.7	9.55	79.3			
80		106.5	64.3	2.59	55.4	7.27	78.6	99.0	59.9	2.46	51.5	7.13	79.4	91.5	55.6	2.33	47.6	7.00	80.2				
100		125.9	62.7	3.16	51.9	5.82	79.3	118.4	58.1	3.02	47.8	5.62	80.2	111.0	53.4	2.88	43.6	5.43	81.0				
		120																					

HS050 - Performance Data cont.

Heating Capacity

Source			Load Flow-8 GPM							Load Flow-11.5 GPM							Load Flow-15 GPM						
EST F	Flow GPM	ELT F	LLT F	HC MBTUH	Power kW	HE MBTUH	COP	LST F	LLT F	HC MBTUH	Power kW	HE MBTUH	COP	LST F	LLT F	HC MBTUH	Power kW	HE MBTUH	COP	LST F			
25	11.5	60																					
		80																					
		100																					
		120																					
	15	60	71.3	43.9	2.50	35.4	5.15	20.1	67.9	44.0	2.50	35.4	5.16	20.1	66.0	44.0	2.49	35.5	5.18	20.1			
		80	91.0	42.6	3.41	31.0	3.66	20.7	87.6	42.6	3.37	31.1	3.71	20.7	85.9	42.6	3.33	31.3	3.75	20.7			
		100	110.6	41.3	4.32	26.6	2.80	21.3	107.4	41.3	4.25	26.8	2.85	21.3	105.7	41.3	4.17	27.0	4.20	21.3			
		120	130.3	40.0	5.23	22.2	2.24	22.0	127.2	40.0	5.12	22.5	2.29	21.9	125.5	39.9	5.01	22.8	2.33	21.9			
	8	60	71.8	45.7	2.36	37.6	5.67	20.3	69.0	45.8	2.43	37.5	5.53	20.3	66.3	45.8	2.49	37.3	5.39	20.4			
		80	91.4	44.4	3.31	33.1	3.92	21.5	88.8	44.4	3.33	33.0	3.91	21.5	86.1	44.4	3.34	33.0	3.89	21.5			
		100	111.1	43.0	4.27	28.5	2.96	22.7	108.5	43.0	4.23	28.6	2.98	22.6	105.9	43.0	4.19	28.7	3.01	22.6			
		120	130.7	41.7	5.22	23.9	2.34	23.8	128.2	41.7	5.13	24.1	2.38	23.8	125.7	41.6	5.04	24.4	2.42	23.7			
30	11.5	60	72.2	47.2	2.50	38.6	5.53	22.4	69.3	47.2	2.49	38.7	5.56	22.4	66.5	47.3	2.48	38.8	5.59	22.4			
		80	91.7	45.5	3.41	33.9	3.92	23.4	89.0	45.6	3.37	34.1	3.96	23.3	86.3	45.6	3.33	34.2	4.01	23.3			
		100	111.3	43.9	4.31	29.2	2.98	24.3	108.7	43.9	4.25	29.4	3.03	24.2	106.0	43.9	4.18	29.6	3.08	24.2			
		120	130.9	42.3	5.22	24.5	2.37	25.2	128.4	42.3	5.13	24.8	2.42	25.1	125.8	42.2	5.03	25.0	2.46	25.1			
	15	60	72.5	48.6	2.64	39.6	5.39	24.6	69.6	48.7	2.56	40.0	5.59	24.5	66.7	48.8	2.47	40.4	5.79	24.5			
		80	92.0	46.7	3.50	34.8	3.91	25.2	89.2	46.8	3.41	35.1	4.02	25.2	86.4	46.8	3.32	35.5	4.13	25.1			
		100	111.5	44.8	4.36	29.9	3.01	25.9	108.9	44.8	4.27	30.2	3.08	25.8	106.2	44.8	4.17	30.6	3.15	25.8			
		120	131.1	42.9	5.22	25.1	2.41	26.6	128.5	42.9	5.12	25.4	2.45	26.5	125.9	42.8	5.02	25.7	2.50	26.5			
	8	60	75.1	58.8	2.56	50.0	6.65	37.1	71.6	58.6	2.54	50.0	6.72	37.1	68.0	58.5	2.52	49.9	6.80	37.1			
		80	94.5	56.3	3.47	44.4	4.71	38.5	91.1	56.2	3.42	44.6	4.80	38.5	87.7	56.2	3.36	44.7	4.88	38.5			
		100	113.9	53.9	4.39	38.9	3.58	40.0	110.6	53.8	4.30	39.2	3.66	39.9	107.4	53.8	4.21	39.4	3.74	39.8			
		120	133.2	51.4	5.30	33.3	2.83	41.4	130.2	51.4	5.18	33.7	2.91	41.3	127.1	51.5	5.06	34.2	2.98	41.2			
50	11.5	60	75.7	61.0	2.64	52.0	6.78	39.8	72.0	60.8	2.58	52.0	6.91	39.9	68.3	60.5	2.51	51.9	7.06	39.9			
		80	95.0	58.1	3.53	46.1	4.83	41.0	91.5	57.9	3.44	46.2	4.93	41.0	87.9	57.8	3.36	46.3	5.04	41.0			
		100	114.2	55.2	4.41	40.2	3.67	42.1	110.9	55.1	4.31	40.4	3.75	42.1	107.6	55.0	4.21	40.6	3.83	42.0			
		120	133.5	52.4	5.30	34.3	2.89	43.3	130.3	52.3	5.18	34.6	2.96	43.2	127.2	52.3	5.06	35.0	3.03	43.1			
	15	60	76.3	63.3	2.72	54.0	6.79	42.6	72.4	62.9	2.61	54.0	7.03	42.6	68.6	62.5	2.51	53.9	7.27	42.6			
		80	95.4	59.9	3.58	47.7	4.89	43.4	91.8	59.6	3.47	47.8	5.03	43.4	88.2	59.4	3.36	47.9	5.17	43.4			
		100	114.6	56.6	4.44	41.5	3.72	44.3	111.2	56.4	4.32	41.7	3.82	44.3	107.7	56.2	4.20	41.9	3.91	44.2			
		120	133.7	53.3	5.30	35.2	2.94	45.2	130.5	53.2	5.18	35.5	3.01	45.1	127.3	53.1	5.05	35.8	3.07	45.1			
	8	60	78.5	71.8	2.76	62.4	7.62	53.9	74.1	71.5	2.65	62.5	7.92	53.9	69.8	71.2	2.54	62.5	8.21	53.9			
		80	97.6	68.2	3.63	55.8	5.50	55.6	93.5	68.1	3.51	56.1	5.69	55.5	89.3	67.9	3.39	56.3	5.87	55.5			
		100	116.7	64.7	4.51	49.3	4.20	57.3	112.8	64.6	4.37	49.7	4.34	57.2	108.9	64.6	4.23	50.2	4.47	57.1			
		120	135.7	61.1	5.38	42.7	3.33	59.0	132.1	61.2	5.23	43.4	3.43	58.8	128.4	61.3	5.08	44.0	3.54	58.7			
70	11.5	60	79.3	74.9	2.78	65.4	7.90	57.3	74.7	74.3	2.66	65.2	8.18	57.3	70.1	73.7	2.55	65.0	8.48	57.3			
		80	98.2	70.7	3.64	58.3	5.69	58.6	93.9	70.3	3.52	58.3	5.86	58.6	89.6	69.9	3.39	58.3	6.04	58.6			
		100	117.2	66.6	4.51	51.2	4.32	60.0	113.1	66.3	4.37	51.4	4.44	59.9	109.1	66.1	4.24	51.6	4.57	59.9			
		120	136.1	62.4	5.38	44.0	3.40	61.4	132.3	62.4	5.23	44.5	3.49	61.3	128.6	62.3	5.08	45.0	3.59	61.2			
	15	60	80.1	77.9	2.79	68.4	8.18	60.6	75.3	77.1	2.67	67.9	8.47	60.7	70.5	76.2	2.55	67.5	8.76	60.7			
		80	98.9	73.2	3.65	60.7	5.87	61.7	94.4	72.5	3.52	60.5	6.04	61.7	89.9	71.9	3.39	60.3	6.21	61.7			
		100	117.6	68.4	4.52	53.0	4.44	62.7	113.5	68.0	4.38	53.1	4.56	62.7	109.3	67.6	4.24	53.1	4.68	62.7			
		120	136.4	63.7	5.38	45.3	3.47	63.8	132.6	63.5	5.23	45.7	3.56	63.7	128.7	63.3	5.08	46.0	3.65	63.7			
	8	60	81.9	84.9	2.85	75.2	8.73	70.6	76.5	82.8	3.51	70.8	7.21	71.7	71.1	80.7	4.16	66.5	5.68	72.9			
		80	100.6	80.1	3.71	67.4	6.32	72.6	95.6	78.7	4.09	64.8	5.70	73.3	90.6	77.4	4.47	62.2	5.08	74.0			
		100	119.4	75.2	4.58	59.6	4.82	74.6	114.8	74.7	4.68	58.7	4.68	74.9	110.2	74.1	4.77	57.8	4.55	75.1			
		120																					
90	11.5	60	82.3	86.6	2.86	76.9	8.89	74.9	76.8	84.1	3.12	73.5	7.91	75.6	71.2	81.6	3.38	70.1	7.08	76.4			
		80	101.1	81.8	3.72	69.0	6.43	76.5	95.9	80.2	3.84	67.1	6.12	76.9	90.8	78.6	3.95	65.1	5.83	77.3			
		100	119.8	76.9	4.59	61.2	4.91	78.0	115.1	76.2	4.56	60.7	4.90	78.1	110.4	75.5	4.52	60.1	4.90	78.3			
		120																					
	15	60	82.8	88.3	2.86	78.5	9.05	79.2	77.0	85.4	2.73	76.1	9.19	79.5	71.3	82.5	2.59	73.7	9.33	79.9			
		80	101.5	83.4	3.73	70.7	6.55	80.3	96.2	81.6	3.58	69.3	6.68	80.5	91.0	79.7	3.43	68.0	6.81	80.7			
		100	120.2	78.6	4.61	62.8	5.00	81.4	115.4	77.7	4.44	62.6	5.14	81.4	110.6	76.9	4.26	62.3	5.28	81.4			
		120																					

HS060 - Performance Data cont.

Heating Capacity

Source		Load Flow-9 GPM							Load Flow-13.5 GPM							Load Flow-18 GPM						
EST F	Flow GPM	ELT F	LLT F	HC MBTUH	Power kW	HE MBTUH	COP	LST F	LLT F	HC MBTUH	Power kW	HE MBTUH	COP	LST F	LLT F	HC MBTUH	Power kW	HE MBTUH	COP	LST F		
	60																					
	80																					
	100																					
	120																					
25	60	71.1	48.3	2.93	38.3	4.83	20.6	67.4	48.6	2.86	38.8	4.98	20.6	65.6	48.9	2.79	39.4	5.14	20.5			
	80	90.8	47.3	3.93	33.9	3.53	21.1	87.3	47.6	3.85	34.4	3.62	21.1	85.5	47.8	3.76	35.0	3.72	21.0			
	100	110.6	46.3	4.93	29.5	2.75	21.6	107.1	46.5	4.83	30.0	2.82	21.6	105.4	46.8	4.74	30.6	2.89	21.5			
	120	130.4	45.3	5.93	25.1	2.24	22.1	126.9	45.5	5.82	25.6	2.29	22.1	125.2	45.7	5.71	26.2	2.35	22.0			
	60	71.5	50.1	2.94	40.1	4.99	20.8	68.7	50.5	2.87	40.7	5.17	20.7	65.8	50.9	2.79	41.4	5.35	20.5			
	80	91.3	49.3	3.95	35.9	3.66	21.8	88.5	49.7	3.86	36.5	3.77	21.6	85.7	50.0	3.77	37.1	3.89	21.5			
	100	111.1	48.6	4.95	31.7	2.87	22.7	108.4	48.8	4.85	32.3	2.95	22.6	105.6	49.0	4.74	32.8	3.03	22.5			
	120	131.0	47.8	5.96	27.5	2.35	23.7	128.2	48.0	5.84	28.0	2.41	23.6	125.5	48.1	5.72	28.6	2.46	23.5			
	60	71.9	52.1	3.0	42.0	5.17	22.9	68.9	51.8	2.87	42.0	5.29	22.9	65.9	51.6	2.8	42.0	5.41	22.8			
	80	91.7	50.9	4.0	37.4	3.77	23.7	88.7	50.8	3.86	37.6	3.86	23.6	85.8	50.7	3.8	37.8	3.95	23.5			
	100	111.4	49.7	5.0	32.8	2.94	24.4	108.6	49.8	4.84	33.2	3.01	24.3	105.7	49.8	4.7	33.7	3.08	24.3			
	120	131.1	48.6	6.0	28.2	2.39	25.2	128.4	48.8	5.83	28.9	2.45	25.1	125.6	49.0	5.7	29.5	2.51	25.0			
	60	72.4	54.1	2.97	44.0	5.34	25.0	69.2	53.2	2.88	43.3	5.41	25.0	66.0	52.2	2.79	42.7	5.48	25.1			
	80	92.0	52.5	3.96	39.0	3.88	25.5	89.0	52.0	3.86	38.8	3.95	25.6	85.9	51.4	3.76	38.6	4.01	25.6			
	100	111.7	50.9	4.96	34.0	3.01	26.1	108.7	50.8	4.84	34.2	3.07	26.1	105.8	50.6	4.72	34.5	3.14	26.1			
	120	131.3	49.3	5.95	29.0	2.43	26.7	128.5	49.6	5.82	29.7	2.50	26.6	125.7	49.8	5.69	30.4	2.56	26.5			
	60	75.1	66.0	3.0	55.7	6.34	37.2	71.4	66.2	2.92	56.2	6.62	37.1	67.6	66.3	2.8	56.7	6.90	37.0			
	80	94.6	63.9	4.0	50.2	4.66	38.5	91.0	64.1	3.89	50.8	4.83	38.4	87.4	64.3	3.8	51.4	4.99	38.2			
	100	114.1	61.7	5.0	44.7	3.63	39.8	110.6	62.0	4.86	45.4	3.74	39.6	107.1	62.3	4.7	46.1	3.86	39.4			
	120	133.7	59.6	6.0	39.3	2.93	41.0	130.3	60.0	5.83	40.1	3.02	40.8	126.9	60.3	5.7	40.9	3.11	40.6			
	60	75.8	68.8	3.1	58.4	6.61	40.1	71.8	68.5	2.93	58.5	6.84	40.1	67.8	68.2	2.8	58.5	7.09	40.0			
	80	95.2	66.2	4.0	52.5	4.81	41.1	91.4	66.1	3.90	52.8	4.96	41.0	87.6	66.1	3.8	53.2	5.13	41.0			
	100	114.6	63.7	5.0	46.6	3.72	42.1	111.0	63.8	4.87	47.2	3.84	42.0	107.3	64.0	4.7	47.8	3.96	41.9			
	120	134.0	61.1	6.0	40.6	2.98	43.1	130.5	61.5	5.85	41.5	3.08	42.9	127.1	61.9	5.7	42.4	3.18	42.8			
	60	76.4	71.6	3.1	61.1	6.79	43.0	72.2	70.8	2.95	60.7	7.01	43.0	68.0	70.0	2.8	60.4	7.24	43.1			
	80	95.7	68.6	4.1	54.7	4.93	43.7	91.7	68.2	3.92	54.8	5.09	43.7	87.8	67.8	3.8	54.9	5.25	43.7			
	100	115.0	65.6	5.1	48.4	3.79	44.5	111.3	65.6	4.89	48.9	3.92	44.4	107.5	65.6	4.7	49.4	4.06	44.3			
	120	134.3	62.6	6.0	42.0	3.03	45.2	130.8	63.0	5.87	43.0	3.15	45.1	127.3	63.4	5.7	44.0	3.26	45.0			
	60	78.8	81.9	3.12	71.3	7.69	53.7	74.1	81.8	2.98	71.6	8.07	53.6	69.4	81.7	2.83	72.0	8.46	53.5			
	80	98.0	78.4	4.06	64.5	5.65	55.2	93.5	78.5	3.92	65.1	5.88	55.1	89.0	78.6	3.78	65.7	6.10	54.9			
	100	117.2	74.9	5.01	57.8	4.38	56.8	112.9	75.2	4.87	58.6	4.54	56.6	108.7	75.6	4.72	59.4	4.69	56.4			
	120	136.4	71.4	5.95	51.1	3.52	58.3	132.3	72.0	5.81	52.1	3.63	58.1	128.3	72.5	5.67	53.1	3.75	57.8			
	60	79.6	85.5	3.1	74.8	7.97	57.4	74.6	85.1	3.00	74.9	8.33	57.3	69.7	84.8	2.8	75.0	8.73	57.3			
	80	98.7	81.6	4.1	67.5	5.81	58.6	94.0	81.5	3.95	68.0	6.04	58.5	89.3	81.4	3.8	68.5	6.29	58.4			
	100	117.8	77.6	5.1	60.3	4.48	59.8	113.4	77.8	4.91	61.1	4.65	59.6	108.9	78.1	4.7	61.9	4.83	59.5			
	120	136.9	73.7	6.0	53.0	3.57	61.0	132.7	74.2	5.86	54.2	3.71	60.8	128.6	74.8	5.7	55.4	3.86	60.6			
	60	80.4	89.1	3.17	78.3	8.24	61.0	75.2	88.5	3.02	78.2	8.62	61.0	70.1	87.8	2.86	78.0	8.99	61.1			
	80	99.4	84.7	4.16	70.5	5.97	61.9	94.5	84.5	3.98	70.9	6.23	61.9	89.6	84.2	3.80	71.2	6.49	61.8			
	100	118.4	80.3	5.14	62.7	4.57	62.8	113.8	80.5	4.95	63.6	4.77	62.7	109.2	80.6	4.75	64.4	4.98	62.6			
	120	137.4	75.9	6.13	55.0	3.63	63.7	133.1	76.5	5.91	56.3	3.80	63.6	128.8	77.0	5.69	57.6	3.96	63.4			
	60	82.4	97.7	3.26	86.6	8.78	70.2	76.5	95.2	3.09	84.7	9.04	70.6	70.6	92.7	2.92	82.7	9.30	71.0			
	80	101.4	93.2	4.25	78.7	6.42	72.0	95.9	91.9	4.06	78.0	6.65	72.1	90.4	90.5	3.86	77.4	6.87	72.3			
	100																					
	120																					
	60	82.8	99.7	3.3	88.4	8.89	74.9	76.8	96.7	3.11	86.1	9.12	75.3	70.7	93.7	2.9	83.7	9.37	75.7			
	80	101.8	95.3	4.3	80.6	6.52	76.3	96.2	93.5	4.08	79.6	6.72	76.4	90.5	91.8	3.9	78.6	6.94	76.6			
	100	120.8	90.9	5.3	72.8	5.04	77.6	115.6	90.4	5.05	73.1	5.24	77.5	110.3	89.9	4.8	73.4	5.46	77.5			
	120																					
	60	83.3	101.6	3.31	90.3	8.99	79.7	77.1	98.2	3.13	87.5	9.22	80.0	70.8	94.7	2.94	84.7	9.44	80.3			
	80	102.3	97.3	4.31	82.6	6.61	80.5	96.5	95.2	4.10	81.2	6.81	80.7	90.7	93.1	3.89	79.8	7.00	80.9			
	100	121.3	93.0	5.31	74.9	5.13	81.4	115.9	92.2	5.08	74.9	5.33	81.4	110.5	91.4	4.85	74.9	5.53	81.4			
	120																					

HS075 - Performance Data cont.

Heating Capacity

Source			Load Flow-10 GPM							Load Flow-14.5 GPM							Load Flow-19 GPM						
EST F	Flow GPM	ELT F	LLT F	HC MBTUH	Power kW	HE MBTUH	COP	LST F	LLT F	HC MBTUH	Power kW	HE MBTUH	COP	LST F	LLT F	HC MBTUH	Power kW	HE MBTUH	COP	LST F			
	14.5	60																					
		80																					
		100																					
		120																					
25		60	72.1	58.8	3.90	45.5	4.42	20.1	68.4	58.9	3.78	46.0	4.57	20.0	66.4	59.0	3.66	46.5	4.72	19.95			
		80	91.8	57.4	5.11	40.0	3.29	20.7	88.2	57.5	4.97	40.6	3.39	20.6	86.2	57.6	4.82	41.1	3.50	20.5			
	19	100	111.6	56.1	6.32	34.5	2.60	21.3	108.0	56.1	6.15	35.1	2.67	21.2	106.1	56.1	5.98	35.7	2.75	21.1			
		120	131.3	54.7	7.53	29.0	2.13	21.9	127.8	54.7	7.34	29.7	2.18	21.8	125.9	54.7	7.14	30.3	2.24	21.7			
		60	72.6	61.1	3.90	47.8	4.59	20.1	69.6	61.2	3.79	48.3	4.74	20.0	66.7	61.3	3.68	48.7	4.88	20.0			
		80	92.3	59.7	5.12	42.3	3.42	21.3	89.4	59.8	4.99	42.8	3.52	21.2	86.5	59.9	4.85	43.3	3.61	21.1			
	10	100	112.0	58.4	6.35	36.7	2.69	22.4	109.2	58.4	6.19	37.3	2.77	22.3	106.3	58.4	6.03	37.9	2.84	22.2			
		120	131.8	57.0	7.57	31.2	2.21	23.6	129.0	57.0	7.39	31.8	2.26	23.4	126.2	57.0	7.20	32.4	2.32	23.3			
		60	73.1	63.5	3.9	50.1	4.74	22.2	70.0	63.6	3.82	50.5	4.88	22.2	66.9	63.7	3.7	51.0	5.03	22.1			
	14.5	80	92.7	61.7	5.2	44.1	3.51	23.2	89.7	61.8	5.02	44.6	3.60	23.1	86.7	61.9	4.9	45.2	3.71	23.0			
		100	112.4	59.9	6.4	38.1	2.75	24.1	109.4	60.0	6.23	38.7	2.82	24.0	106.5	60.1	6.1	39.4	2.90	23.9			
		120	132.0	58.2	7.6	32.1	2.24	25.0	129.2	58.2	7.43	32.8	2.29	24.9	126.3	58.3	7.2	33.5	2.36	24.8			
		60	73.6	65.8	3.95	52.3	4.88	24.3	70.4	65.9	3.84	52.8	5.03	24.3	67.2	66.0	3.73	53.3	5.18	24.2			
		80	93.1	63.6	5.19	45.9	3.59	25.0	90.0	63.7	5.05	46.5	3.70	25.0	86.9	63.8	4.92	47.1	3.80	24.9			
	19	100	112.7	61.5	6.43	39.5	2.80	25.7	109.7	61.6	6.27	40.2	2.88	25.6	106.7	61.7	6.10	40.8	2.96	25.6			
		120	132.2	59.3	7.67	33.1	2.27	26.4	129.3	59.4	7.48	33.9	2.33	26.3	126.5	59.5	7.29	34.6	2.39	26.2			
		60	76.7	81.0	4.2	66.7	5.60	36.2	72.7	81.0	4.02	67.3	5.85	36.1	68.8	81.0	3.9	67.8	6.10	36.0			
		80	96.1	78.2	5.4	59.6	4.17	37.7	92.3	78.2	5.24	60.3	4.34	37.6	88.5	78.3	5.1	61.0	4.50	37.4			
	10	100	115.5	75.3	6.7	52.5	3.28	39.2	111.9	75.4	6.46	53.3	3.39	39.0	108.2	75.5	6.3	54.2	3.51	38.8			
		120	134.9	72.5	7.9	45.4	2.66	40.6	131.4	72.6	7.69	46.4	2.75	40.4	127.9	72.8	7.5	47.3	2.84	40.2			
		60	77.4	84.5	4.2	70.1	5.86	39.1	73.3	84.4	4.07	70.5	6.08	39.1	69.2	84.3	3.9	71.0	6.32	39.0			
	14.5	80	96.7	81.1	5.5	62.4	4.35	40.3	92.8	81.1	5.29	63.1	4.50	40.2	88.8	81.2	5.1	63.7	4.66	40.1			
		100	116.0	77.7	6.7	54.8	3.39	41.5	112.2	77.9	6.51	55.7	3.51	41.4	108.5	78.0	6.3	56.5	3.63	41.2			
		120	135.3	74.4	8.0	47.2	2.74	42.7	131.7	74.6	7.73	48.2	2.83	42.5	128.1	74.8	7.5	49.3	2.93	42.3			
		60	78.1	87.9	4.3	73.4	5.98	42.0	73.8	87.8	4.11	73.8	6.19	42.0	69.5	87.7	4.0	74.1	6.40	42.0			
		80	97.3	84.0	5.5	65.2	4.42	42.9	93.2	84.1	5.33	65.9	4.58	42.9	89.1	84.1	5.2	66.5	4.74	42.8			
	19	100	116.5	80.2	6.8	57.1	3.44	43.8	112.6	80.3	6.55	58.0	3.57	43.7	108.7	80.5	6.3	58.9	3.69	43.6			
		120	135.7	76.3	8.0	48.9	2.77	44.7	132.0	76.6	7.77	50.1	2.87	44.6	128.3	76.9	7.5	51.2	2.98	44.4			
		60	80.8	100.9	4.48	85.6	6.60	52.3	75.9	100.8	4.26	86.3	6.96	52.2	70.9	100.7	4.03	86.9	7.32	52.1			
		80	99.9	96.6	5.74	77.0	4.93	54.1	95.2	96.6	5.50	77.8	5.16	54.0	90.5	96.6	5.26	78.7	5.39	53.8			
	10	100	119.0	92.2	7.00	68.3	3.86	55.9	114.5	92.4	6.74	69.4	4.02	55.7	110.0	92.6	6.48	70.4	4.18	55.5			
		120	138.1	87.9	8.26	59.7	3.12	57.7	133.9	88.2	7.99	60.9	3.24	57.4	129.6	88.5	7.71	62.2	3.36	57.2			
		60	81.7	105.5	4.5	90.0	6.84	56.0	76.6	105.2	4.32	90.5	7.14	56.0	71.4	105.0	4.1	91.0	7.48	55.9			
	14.5	80	100.7	100.5	5.8	80.8	5.09	57.5	95.8	100.5	5.55	81.5	5.30	57.4	90.9	100.5	5.3	82.3	5.53	57.2			
		100	119.7	95.6	7.0	71.5	3.97	58.9	115.1	95.7	6.79	72.6	4.13	58.7	110.4	95.9	6.5	73.7	4.31	58.6			
		120	138.7	90.6	8.3	62.2	3.19	60.3	134.3	91.0	8.02	63.6	3.32	60.1	129.9	91.4	7.7	65.0	3.46	59.9			
		60	82.7	110.0	4.55	94.5	7.08	59.7	77.3	109.7	4.38	94.7	7.35	59.7	71.9	109.3	4.20	95.0	7.62	59.7			
	19	80	101.5	104.4	5.82	84.6	5.26	60.8	96.4	104.4	5.60	85.2	5.47	60.7	91.3	104.3	5.39	85.9	5.67	60.7			
		100	120.4	98.9	7.09	74.7	4.09	61.9	115.6	99.1	6.83	75.8	4.26	61.8	110.8	99.3	6.57	76.9	4.43	61.7			
		120	139.2	93.3	8.36	64.8	3.27	63.0	134.7	93.8	8.06	66.3	3.42	62.8	130.2	94.3	7.76	67.8	3.56	62.6			
		60	84.8	120.1	4.74	103.9	7.42	68.6	78.6	117.4	4.45	102.2	7.75	68.9	72.4	114.6	4.16	100.4	8.07	69.3			
	10	80	103.7	114.9	6.02	94.4	5.59	70.5	97.9	113.2	5.71	93.7	5.82	70.7	92.1	111.5	5.39	93.1	6.06	70.8			
		100																					
		120																					
		60	85.3	122.8	4.77	106.5	7.55	73.4	79.0	119.5	4.49	104.2	7.80	73.7	72.6	116.2	4.22	101.8	8.08	74.0			
	14.5	80	104.2	117.6	6.07	96.8	5.67	74.9	98.3	115.4	5.76	95.8	5.88	75.0	92.3	113.3	5.44	94.7	6.10	75.2			
		100	123.2	112.4	7.38	87.2	4.46	76.4	117.6	111.4	7.02	87.4	4.65	76.4	112.0	110.4	6.67	87.7	4.85	76.3			
		120																					
		60	85.9	125.4	4.79	109.1	7.67	78.2	79.3	121.6	4.53	106.1	7.88	78.5	72.8	117.8	4.27	103.2	8.08	78.8			
	19	80	104.8	120.2	6.13	99.3	5.75	79.2	98.6	117.7	5.81	97.9	5.95	79.4	92.5	115.2	5.49	96.4	6.15	79.5			
		100	123.7	115.0	7.46	89.5	4.51	80.3	118.0	113.8	7.08	89.6	4.72	80.3	112.2	112.5	6.70	89.7	4.92	80.3			
		120																					

